ISSN: 2224-2007
E-ISSN: 2707-7365

MIJST

MIST International Journal of Science and Technology

A Peer Reviewed Online Open Access Journal

Volume 10
June 2022

Military Institute of Science and Technology (MIST)
https://mijst.mist.ac.bd/mijst
Previously known as:
MIST Journal of Science and Technology

MIJST

MIST International Journal of Science and Technology

Volume 10

June 2022

EDITORIAL BOARD

Assoc. Prof. Lt Col Khondaker Sakil Ahmed, PhD, PEng, CEng
MIST, Bangladesh

Prof. Sergej Hloch
Technical University of Košice, Slovakia

Prof. Mohamed H. M. Hassan
Alexandria University, Egypt

Prof. Xiaolin Wang
University of Tasmania, Australia

Prof. Md. Mahbubur Rahman
MIST, Bangladesh

Prof. Muhammad Mustafizur Rahman
Wichita State University, USA

Prof. Santanu Bandyopadhyay
Indian Institute of Technology (IIT) Bombay, India

Prof. Yan-Hui Feng
University of Science and Technology Beijing, China

Brig Gen A K M Nazrul Islam, PhD
MIST, Bangladesh

Prof. Stanislaw Legutko
Poznan University of Technology, Poland

Prof. Nakorn Tippayawong
Chiangmai University, Thailand

Prof. Katarina Monkova
Technical University of Košice, Slovakia & Tomas Bata University in Zlín, Czech Republic

Asst. Prof. Tariq Mahbub
MIST, Bangladesh

Prof. Elsadig Mahdi Ahmad Saad
Qatar University, Qatar

Prof. Himadri Chattopadhyay
Jadavpur University, India

Prof. Yingai Jin
Jilin University, China

Prof. M A Taher Ali
MIST, Bangladesh

Prof. Changheui Jang
Korea Advanced Institute of Science and Technology (KAIST), South Korea

Prof. Tanvir Farouk
University of South Carolina, USA

Prof. Abdul Hasib Chowdhury
BUET, Bangladesh

Assoc. Prof. Lt Col Osman Md Amin, PhD, Engrs
MIST, Bangladesh

Prof. Simon Watkins
RMIT University, Australia

Prof. Ataur Rahman
International Islamic University Malaysia, Malaysia

Prof. Somnath Chattopadhyaya
Indian Institute of Technology (IIT) Dhanbad, India

Assoc. Prof. Major Kazi Shamima Akter, PhD, Engrs
MIST, Bangladesh

Prof. Kaori Nagai
Nihon University, Japan

Prof. Alessandro Ruggiero
University of Salerno, Italy

Prof. Azam Ali
University of Otago, New Zealand

Assoc. Prof. Md. Sazzad Hossain
MIST, Bangladesh

Prof. Mohammed Quddus
Imperial College, UK

Prof. Anupam Basu
Indian Institute of Technology (IIT) Kharagpur, India

Prof. Muhammad H. Rashid
Florida Polytechnic University, USA

Prof. Md Enamul Hoque
MIST, Bangladesh

Prof. Naoya Umeda
Osaka University, Japan

Prof. Md Abdul Jabbar
University of Dhaka, Bangladesh

Prof. Soumyen Bandyopadhyay
Liverpool University, UK

Asst. Prof. Muammer Din Arif
MIST, Bangladesh

Prof. A.B.M. Harun-ur Rashid
BUET, Bangladesh

Prof. Shahjada Tarafder
BUET, Bangladesh

Prof. Mohammed Abdul Basith
BUET, Bangladesh

Prof. AKM Badrul Alam
MIST, Bangladesh

Prof. Stephen Butt
Memorial University of Newfoundland, Canada

Prof. Cheol-Gi Kim
Daegu Gyeongbuk Institute of Science & Technology, South Korea

Prof. Kawamura Yasumi
Yokohama National University, Japan

Assoc. Prof. Lt Col Brajalal Sinha, PhD, AEC
MIST, Bangladesh

Assoc. Prof. Lt Col Palash Kumar Sarker, PhD, Sigs
MIST, Bangladesh

Dr. Debasish Sarker
Bangladesh Army University of Science and Technology, Bangladesh

Prof. Nahrizul Adib Bin Kadri
University of Malaya, Malaysia

Lt Col Mirza Md Lutful Habib, SUP, psc, Engrs
General Staff Officer First Grade, R&D Wing, MIST, Bangladesh

Assoc. Prof. Maj Md. Manwarul Haq
MIST, Bangladesh

Md Moslem Uddin
Chief Librarian, MIST, Bangladesh

ADVISORY BOARD MEMBERS

Prof. Chanchal Roy
University of Saskatchewan, Canada

Prof. Mahmud Ashraf
Deakin University, Australia

Prof. Daili Feng
University of Science and Technology Beijing, China

Assoc. Prof. A. K. M. Najmul Islam
LUT University, Finland

Prof. Arnab Roy
Indian Institute of Technology (IIT) Kharagpur, India

Prof. Ahmad Faris Ismail
International Islamic University Malaysia (IIUM), Malaysia

Dr. Bhuiyan Shameem Mahmood Ebna Hai
Helmut Schmidt University, Germany

Prof. Md Shahidul Islam
Khulna University of Engineering & Technology, Bangladesh

Prof. Reza Nakahie Jazar
RMIT University, Australia

Prof. Md Azizur Rahman
Texas A&M University, Qatar

Prof. Bashir Ahmmad Arima
Yamagata University, Japan

Prof. Kobayashi Kensei
Yokohama National University, Japan

Prof. Mohammad Kaykobad
BUET, Bangladesh

Prof. Sunil S. Chirayath
Texas A&M University, USA

Prof. Md Hadiuzzaman
BUET, Bangladesh

Prof. Rezaul Karim Begg
Victoria University, Australia

DISCLAIMER

The analysis, opinions, and conclusions expressed or implied in this Journal are those of the authors and do not necessarily represent the views of the MIST, Bangladesh Armed Forces, or any other agencies of Bangladesh Government. Statements of fact or opinion appearing in MIJST Journal are solely those of the authors and do not imply endorsement by the editors or publisher.

ISSN: 2224-2007
E-ISSN: 2707-7365

QUERIES ON SUBMISSION

For any query on submission the author(s) should contact: MIST, Mirpur Cantonment, Dhaka-1216, Bangladesh; Tel: 88 02 8034194, FAX: 88 02 9011311, email: *mijst@mist.ac.bd*. For detailed information on submission of articles, the author(s) should refer to the Call for Papers and About MIJST at the back cover of the MIJST Journal. Authors must browse MIJST website through the journal link (*https://mijst.mist.ac.bd/mijst*) for electronic submission of their manuscripts.

PUBLISHER

Military Institute of Science and Technology (MIST), Dhaka, Bangladesh

DESIGN AND PRINTING

Research and Development Wing
Military Institute of Science and Technology (MIST)
Dhaka, Bangladesh

FOREWORD

Bismillahir Rahmanir Rahim

MIST is striving hard over the years to achieve regional and global ranking through its various actions aiming at excelling in academic quality, building sustainable research & publication capabilities, and developing meaningful collaboration with the industries and research organizations at home and abroad. I am happy to note that MIJST - the Flagship journal of MIST is putting its signature as a quality platform for researchers from all over the world for sharing research ideas. As a mark of its contribution MIJST has already been recognized by a number of reputed journal databases locally and internally. With the latest inclusion of a good number of distinguished scholars and scientists in the areas of science, technology, and engineering as the Journal's Editorial and Advisory Board members, MIJST is now focusing on its ultimate mission of getting enlisted in Scopus and WoS, which I believe is a matter of time for the journal to achieve.

I have the distinct pleasure to congratulate the entire Editorial Team of the journal for their hard work in the timely publication of the June 2022 issue of the journal. I would like to thank from the bottom of my heart all the authors of this issue for their meaningful contributions to MIJST. Sincere appreciations are due to all the reviewers of this issue for providing invaluable suggestions and comments aiming at maintaining a high quality of the journal. Very special thanks to the National and the International Advisory Board Members for their invaluable suggestions and guidance aiming at achieving global recognition of MIJST.

I wish continued success of MIJST!

Major General Md Wahid-Uz-Zaman, BSP, ndc, aowc, psc, te
Commandant, MIST, Bangladesh
Chief Patron, MIJST, Bangladesh

EDITORIAL

The June issue, 2022 has been published on schedule. I express my gratitude and thanks to the authors, reviewers, editors, and the production team for making this happen.

In the editor's note of the December 2021 Issue, I briefly mentioned that there was a makeup of the new Editorial and Advisory Board members representing 22 countries from across the world. I am very pleased to inform you that the editorial and advisory board members have expressed their full support and commitments at a joint meeting held in February 2022 to go ahead with the roadmap for obtaining the Journal's indexation in SCOPUS, Web of Science (WoS), Emerging Source Citation Indexing (ESCI) by Thomson Reuters/Clarivate Analytics, and Directory of Open Access Journals (DOAJ) within the set timeframe. Currently, the MIST International Journal of Science and Technology (MIJST) is indexed through Google Scholar, DOI Crossref., Microsoft Academic Search, Semantic Scholar, Publons, Creative Common, BanglaJOL, and Open Journal system.

My fervent request to you all is to submit your scholarly unpublished, original, and innovative contributions from any branch of science, engineering, technology, and related fields to our Journal. To ensure quality, originality, and innovation, all submitted contributions go through a double-blind peer-review process with effective feedback.

The current (June 2022) issue incorporates six original research articles dealing with the characterization of recycled ceramic and glass powder, dispatch optimization of hybrid microgrid, built-in DBSCAN functions in data science programming languages, cascaded fuzzy logic for adaptive cruise control, energy harvesting circuit for low-power Internet of Thing (IoT) applications, and characterization of cement manufactured in a fast-developing nation. All six articles deal with real-world problems.

I with all my heart thank the Journal team members including the Chief Patron, Executive Editor, Associate Editors, Section Editors, Reviewers, Editorial and Advisory Board Members, Proof-readers, and web production Consultant for their hard work and passion for the journal.

My ardent request to you all is to promote the MIST International Journal of Science and Technology (MIJST) among your colleagues, research scholars, research students, and library liaison officers.

As always, I cordially welcome your valued feedback, suggestion, and advice for the advancement of this journal. Please feel free to contact me via telephone +61 3 99256103 and/or email: firoz.alam@rmit.edu.au or mijst@mist.ac.bd.

Sincerely,

Prof. Dr. Firoz Alam
Editor in Chief

INDEX

MIJST
MIST International Journal of Science and Technology

Characterization of Mechanical Properties of Concrete Recycled Ceramic and Glass Powder Exposed to Elevated Temperatures

Tanvir Mustafy[1*], Md. Maruf Hasan[2], Nayeem Ahmed Shuvo[3], and Joarder Md Sarwar Mujib[4]

[1,2,3,4]Department of Civil Engineering, Military Institute of Science and Technology, Dhaka, Bangladesh
[1]Department of Civil Engineering, University of Alberta, Canada

emails: [1]*mustafy@ualberta.ca;* [2]*marufhasan85611@gmail.com;* [3]*nayeemahmedshuvo@gmail.com; and* [4]*maj.sarwar@ce.mist.ac.bd*

ARTICLE INFO

Article History:

Received: 24th March 2022
Revised: 08th May 2022
Accepted: 08th May 2022
Published online: 26th June 2022

Keywords:

Ceramic recycled aggregate
Glass recycled aggregate
Volumetric replacement of sand

ABSTRACT

Systematic reuse of industrial debris is a crucial component that helps shape the sustainable construction system and green technology. The effective optimization of waste ceramic and glass fines into concrete mixes, as partial replacements of natural sand by volume, has been used in this study to explore the mechanical properties of ceramic recycled aggregate (CRA) and glass recycled aggregate (GRA) concrete at higher temperatures. The study comprises 17 types of concrete mixtures comprised of normal concrete (NC) along with 8 different mixes from both GRA and CRA concrete. In both types of GRA and CRA concrete, the sand replacement (by volume) ratios are similar. This paper highlights NC along with the volumetric replacements of sand as 5%, 10%, 15%, 20%, 25%, 30%, 35%, and 40% in other mixes. A total of 306 cylinders were made whereas 18 cylinders for NC and each group (GRA and CRA) included n=18 cylinders. Selected temperatures were 25°C, 100°C, 200°C, 400°C, 600°C, and 800°C to determine the overall mechanical and chemical alterations in NC and recycled concrete. The study reveals that increasing the addition of recycled glass and ceramic fines improves the overall compressive strength, and tensile strength compared to normal concrete. Higher replacement of ceramic and glass fines reduces the cracks and enhances the durability of concrete. In addition, more strength reduction was noticed in NC with increasing temperatures, while the reduction rate was slower in both GRA and CRA concrete. Furthermore, the study expounds that, by exploiting the ceramic and glass wastes (as fines) into concrete would result in two-way environmental advantages. One is, it would reduce the hazardous ceramic and glass landfills while the other is, it would minimize the frequency of sand mining.

1. INTRODUCTION

Researchers all around the globe were urged to explore for and use more sustainable resources in response to the growing interest in sustainable development. Industrial ceramic and glass debris inclusion in the concrete could be the alternative choices for achieving sustainability in construction systems worldwide, thus removing hazardous waste from the environment. About 22 billion tons of ceramic waste powder (CWP) are produced and disposed to the environment (El-Dieb, Taha, & Abu-Eishah, 2019). It has been approximated that around 30% of ceramic waste is produced from the ceramic industry every day (Al Bakri *et al*., 2013). Annually, the ceramic industry of India produces 100 million tons of ceramic and it contributes 15-30% of the ceramic waste to the environment (Raval, Patel, & Pitroda, 2013, Mujib *et al*., 2022). The total quantity of glass garbage created in the European Union in 2014 was close to 18.5 million tons. A large proportion of glass debris is deposited daily and every year, almost 10 million tons of glass garbage are produced throughout the world (Salem, Khedawi, Baker, & Abendeh, 2017). According to the United Nations, the annual volume of garbage created throughout the world is 200 million tons, with glass waste accounting for 7% (Rashid et al., 2018; Topçu & Canbaz, 2004). Materials such as crushed glass or crushed concrete,

which are claimed to be potential sources of environmental hazard, could be incorporated with concrete to check the fire resistivity.

Recycled ceramic wastes have been found to have a favourable influence on compressive strength, capillary absorption, alkali-silica response, freeze-thaw durability, and impermeability in tests using ceramic wastes in concrete mixtures (M. C. Bignozzi & Saccani, 2012; de Brito, Pereira, & Correia, 2005; Higashiyama, Yamauchi, Sappakittipakorn, Sano, & Takahashi, 2013; Lopez, Llamas, Juan, Moran, & Guerra, 2007; César Medina, de Rojas, & Frías, 2013; Pacheco-Torgal & Jalali, 2010; Senthamarai, Manoharan, & Gobinath, 2011, Mustafy *et al.*, 2020). Portland concrete and fly ash concrete compositions with earthenware fine recycled ceramic aggregate have increased compressive strength(Torkittikul & Chaipanich, 2010). The pozzolanic activity of recycled coarse sanitary ware ceramic aggregate boosted concrete samples' compressive strength (C. Medina, Sánchez de Rojas, & Frías, 2012). Concrete with both coarse and fine sanitary ware aggregate has greater compressive strength and is more resistant to temperature increases (Halicka, Ogrodnik, & Zegardlo, 2013). They found that the aggregate in sanitary ware was mostly made up of SiO_2 (65.80 percent), Al2O3 (22.20%), with traces of K_2O (3.50%), and Na_2O. (1.25%). A blend of waste ceramic powder (WCP) and alkali-activated mortars demonstrate a considerable improvement in concrete construction resistance capability up to 950°C (Huseien et al., 2018). The most common oxides found in ceramic aggregate made from an electoral insulator are SiO2 (70.90%), Al_2O_3(21.10%), and traces of K_2O (3.57%) and Na_2O (1.47%) (Higashiyama, Sappakittipakorn, Mizukoshi, & Takahashi, 2014). Due to the probable pozzolanic effect of ceramic waste, they found that using fine ceramic aggregate based on electrical insulators increases compressive strength.

Container-derived recycled glass has been utilized as fine aggregate in concrete (Corinaldesi, Gnappi, Moriconi, & Montenero, 2005; de Castro & de Brito, 2013; Jin, Meyer, & Baxter, 2000; Shao, Lefort, Moras, & Rodriguez, 2000). Crushed waste glass materials, as a 30% replacement of sand, were found to provide greater compressive strength than conventional concrete (Adaway & Wang, 2015). Because of the near-zero porosity and non-hydrophilic character of glass, incorporating it into mortar and concrete has several advantages, including greater workability, improved resistance to chloride ion penetration, and reduced drying shrinkage (Chen, Chang, Wang, & Huang, 2011; Topcu & Canbaz, 2004). The molten crushed glass fills the inner voids in concrete (above 600°C) and thus major contributions to the water sorptivity and porosity (Ling, Poon, & Kou, 2012). The larger the amount of waste glass used to replace aggregates, the longer the initial and final setting durations. At temperatures above 150°C, concrete containing 10% waste glass as an aggregate has better compressive strength than regular concrete (Terro, 2006). The main disadvantage is the poor bonding between the smooth glass surface and the cement hydration products (Al-Sibahy & Edwards, 2012; Park, Lee, & Kim, 2004), as well as the possibility of detrimental expansion owing to the alkali-silica reaction (ASR), which occurs slowly between silica-rich glass aggregate and alkali in the cement paste. The latter issue, on the other hand, can be addressed by using mineral additions having pozzolanic properties (Liu, 2011). In addition, certain research investigations on the usage of recycled glass (RG) as a pozzolanic material for cement substitution were done (Federico & Chidiac, 2009; Oliveira, de Brito, & Veiga, 2015). RG must be crushed into a powder with a particle size of fewer than 150 μm in order to initiate the pozzolanic reactivity (Y.-c. Guo, Zhang, Chen, & Xie, 2014; Schwarz, Cam, & Neithalath, 2008; Shi, Wu, Riefler, & Wang, 2005, Mustafy & Ahsan, 2010).

High temperatures experienced in fires can exacerbate the component loss of bearing capacity, significantly erode mechanical qualities, jeopardize building structural safety, and potentially cause building collapse (Holan, Novak, Müller, & Štefan, 2020; L.-J. Li, Xie, Liu, Guo, & Deng, 2011; M. Li, Qian, & Sun, 2004; W. Li, Wang, & Han, 2019). Material changes such as cracking pattern, deformation, and discoloration must be visually noticed for this purpose, and non-destructive tests and core tests must be performed to quantify the concrete's deterioration degree, such as strength decrease and counterbalance (Colombo & Felicetti, 2007; Dilek, 2005; Dos Santos, Branco, & de Brito, 2002; Lee, Choi, Hong, & Engineering, 2009). At 400°C, the concrete's residual compressive strength appears to drop by 60%, and at 800°C, it is below 10% (Lee et al., 2009). Throughout the fire episode, temperatures in buildings may reach 1100°C and even 1350°C in tunnels, causing significant damage to concrete structures (38, 2007; Hager, 2013). Furthermore, according to a literature review, concrete loses around 25% of its compressive strength when heated to 300°C, and about 75% when heated to 600°C (G. Khoury, 1992; Lankard, Birkimer, Fondriest, & Snyder, 1971). When heated to 300 °C, normal strength concrete (NSC) generally loses 10 to 20% of its initial compressive strength, and 60 to 75% when heated to 600°C. In a similar way, elastic modulus falls. At temperatures below 450°C, increased rates of strength loss, up to 40% of initial strength, were recorded for high strength concrete (HSC) (Phan & Carino, 2000). Concrete turns pink or red at temperatures ranging from 300°C to 600°C, whitish-grey at temperatures ranging from 600°C to 900°C, and brownish yellow color at temperatures ranging from 900°C to 1000°C (Lee et al., 2009). We can determine the extent of compressive strength deterioration by monitoring the color shift because the concrete's color value changes as temperature rises (Georgali & Tsakiridis, 2005; Short, Purkiss, & Guise, 2001). The structural performance of reinforced concrete construction, which accounts for a substantial fraction of structures, is damaged during a building fire, structural deformation rises, and load-carrying capacity decreases (Dong, Cao, Bian, & Zhang, 2014).

Dissociation of $Ca(OH)_2$ at 300ºC-400°C, large and rapid creep, generally resulting in failure at 600°C, dissociation of $CaCO_3$ at 700°C, ceramic binding and total water loss at

800°C, and melting at 1200-1350°C were evaluated (G. A. J. P. i. s. e. Khoury & materials, 2000; Sarker, Kelly, & Yao, 2014). It was observed that, between 500 and 600°C, Ca(OH)2 dehydrates (Heikal, 2000). It has been investigated the effects of chilling on concrete (G. A. Khoury, Grainger, & Sullivan, 1986). Cooling strains (shrinkage) were discovered to be a result of the aggregate cement interaction, which causes cracking, and were unrelated to the concrete's age, initial moisture content, or heating rate. Spalling of concrete was effectively exhibited to be declined from 22% to less than 1% when polypropylene fibers (3 kg/m^3) were utilized in the concrete (Ali, Nadjai, Silcock, & Abu-Tair, 2004).

The post-fire performance regimes of concrete structures using alkali-activated fly ash cement have been exhibited to be severely dropped at successively higher temperatures i.e. 600°C to 700°C (Fernández-Jiménez, Pastor, Martín, & Palomo, 2010). Concrete incorporated with pozzolanic components such as metakaolin, inflated strength up to 200°C and sustained greater strengths up to 400°C than fly-ash, silica fume, and standard Ordinary Portland Cement (OPC) concrete (Poon, Azhar, Anson, & Wong, 2003). The effect of elevated temperature heat and strain rate on the residual strength of ternary blended concrete containing fly ash and silica fume was investigated (Z. Li, Xu, & Bai, 2012). After the fire episode of 400°C on concrete, there was a significant loss of strength whereas all of the high-strength-concretes (HSC) quickly deteriorated at 400°C. There have been numerous investigations pivoting on the fire performance of concrete components. After 10 minutes at 800°C, it was observed that a 25% loss in compressive strength of 25 mm cube metakaolin-based geopolymer paste specimens (D. L. Y. Kong, Sanjayan, & Sagoe-Crentsil, 2005). The strength of a fly ash-based geopolymer paste increased by 6% following exposure to the heat of 800°C (D. L. Kong, Sanjayan, & Sagoe-Crentsil, 2007).

Metallic fiber reinforced concrete, when exposed to fire episodes, they have a favourable effect, enhancing energy absorption and minimizing cracking (Bednář, Wald, Vodička, & Kohoutková, 2013; Fike & Kodur, 2011; Kim & Lee, 2015). Because of the physical and mechanical qualities of polypropylene fibers, concrete reinforced with them has less permeability and capillary porosity, which prevents the pores in the concrete from becoming blocked. These gains are made possible by using the appropriate amount of polypropylene, which is 0.7 kg/m^3 (Kakooei, Akil, Jamshidi, & Rouhi, 2012; López-Buendía, Romero-Sánchez, Climent, & Guillem, 2013; Ramezanianpour, Esmaeili, Ghahari, & Najafi, 2013; Serrano, Cobo, Prieto, & de las Nieves González, 2016). The inclusion of polypropylene (PP) fibers in high and ultra-high-strength autoclaved mortars is a promising discovery that preserves practically all compressive strength properties without spalling up to 600°C temperature, even with a high silica fume concentration (Aydın, Yazıcı, & Baradan, 2008).

In addition, another study found that replacement of 10-30% of fine aggregate with crumb rubber reduced concrete unit weight and increased thermal and acoustic insulation (Sukontasukkul & Wiwatpattanapong, 2009). Furthermore, the inclusion of rubber increased the standard concrete's durability and deformation ability. Rubber crumbs have also been proven to successfully lower the danger of explosive spalling and the pace of concrete strength loss following exposure to high temperatures (Hernández-Olivares & Barluenga, 2004; Laperre et al., 2011). This is because rubber crumbs, when burned after being exposed to certain temperatures, can allow water vapor to escape from concrete, protecting the concrete skeleton from inflammable spalling. The continual water loss of the hydrated cement paste in the 105–850°C range and crystalline change from α-quartz to β-quartz in the 500–650°C range are both responsible for the rising strength degradation rate over 200°C (Bengar, Shahmansouri, Sabet, Kabirifar, & Tam, 2020).

In retrospect, there have been a few studies carried out with waste glass or waste ceramic incorporated with concrete, especially, in partial volumetric replacement of sand. There were separate studies with waste recycled glass or ceramics but no trace of a combined study. In this comprehensive study, variable amounts of crushed ceramic recycled aggregates (CRA) and crushed glass recycled aggregates (GRA) substituted with fine aggregates (sand) were employed to disclose the total residual structural strength of concrete in contrast to conventional normal concrete (NC) after preheating to various temperatures such as 100°C, 200°C, 400°C, 600°C, and 800°C. The Physico-chemical and mechanical behavior have been explored to divulge the thermal complexion of recycled concrete with waste glass and ceramic fines.

2. RESEARCH SIGNIFICANCE

Structural integrity and safety, serviceability, and design competency, regardless of structure type, have been a word of major importance in many scientific studies and technological developments across the world. Environmental exposure of glass and ceramic debris has been proved to be perilous. So, it calls for an attention to remove debris from the environment, more precisely, the use of CRA and GRA in concrete might be a useful research program since these materials possess enough structural strength to function as an electrical and thermal insulator during a fire. Because of the CRA and GRA's high melting point, greater durability and mechanical stability at elevated temperatures, such as 800°C, 900°C, or even more, it entails a larger region of interest and significance. The pre-firing and post-firing compressive strength of concrete blended with glass and ceramic fines replaced by sand must be determined, which is one of the core themes of this article. It also entails investigating the overall alterations in elastic modulus, tensile behaviors, and various mechanical properties of the heated candidate specimens made with different sand replacements. This study shows that glass recycled aggregate (GRA) and ceramic recycled aggregate (CRA) may be utilized as a fine aggregate substitute in concrete (up to 40%) for structural purposes. To the best of the authors' knowledge, this is the first combined study to look at the effect of altering the replacement amount of sand with recycled glass and ceramic fines with the goal of finding the top limit of its usefulness as a sustainable and lasting

construction material without any prior treatment.

3. DETAILS OF THE EXPERIMENT

A. Materials and Mixtures

A pictorial representation of the constituent materials used in the study has been depicted in Figure 1.

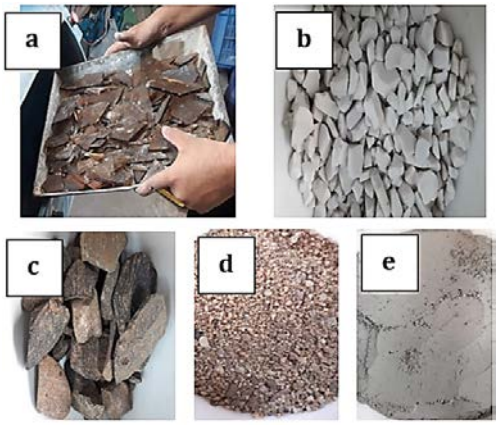

Figure 1: Types of aggregates (a) Crushed Glass (b) Crushed Ceramic (c) Coarse Aggregate (d) Fine Aggregate (e) Ordinary Portland Cement

i. Physical Properties of Aggregate

Several physical properties of natural coarse aggregate, natural fine aggregate, glass recycled aggregate, and ceramic recycled aggregate have been discussed in Table 1.

ii. Fine Aggregate (FA)

In this experiment, a locally available well-graded natural sand with a nominal maximum grain size of 4.75 mm was selected. ASTM C136-14 (A ASTM, 2014) is used for sand sieve analysis and gradation and a standard ASTM C29/29M-17a (17a, 2017) is used to determine the unit weight of FA. Furthermore, sand's specific gravity and water absorption capacity are determined using ASTM C128-15 (ASTM ASTM, 2015).

iii. Coarse Aggregate (CA)

The fraction of the naturally found stone coarse aggregates was kept within the range of 4.75-20mm whereas the maximum size was 19mm. The CA is sieved and graded according to ASTM C136-14 (A ASTM, 2014), while the unit weight is calculated using ASTM C29/29M-17a (17a, 2017). ASTM C127-15 (ASTM ASTM, 2015) is used to determine the CA's specific gravity and water absorption capacity.

Table 1
Physical Properties of aggregates

Variables	NCA	NFA	GRA	CRA
Apparent specific gravity	2.73	2.7	2.7	2.65
Bulk specific gravity (SSD)	2.71	2.6	2.6	2.45
Bulk specific gravity (OD)	2.7	2.46	2.46	2.34
Absorption capacity (%)	0.46	3.5	3	5
Fineness modulus	6.51	2.8	2.7	2.65
Loose unit weight (kg/m^3)	1477.02	1489	1489	1465
Compact unit weight (kg/m^3)	1525.57	1633	1633	1610
% of voids (Loose)	45.1	38.3	37.5	35.7
% of voids (Compact)	43.3	33	33.7	32.9
Abrasion value (%)	14.58	-	32	33.5

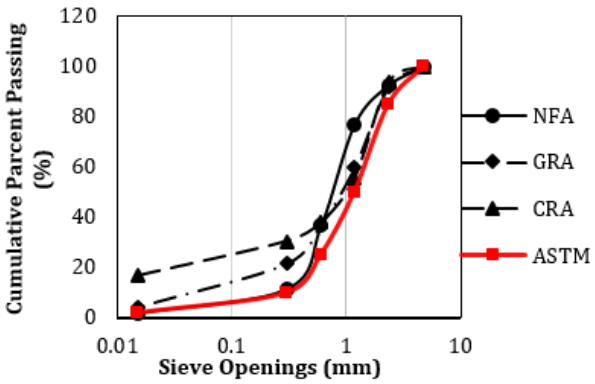

Figure 2: Particle size distribution of aggregates

In addition, the abrasion test is carried out in accordance with ASTM C131-14 (C131/131M, 2014). The particle size distribution of NCA, NFA, GRA, CRA, and ASTM standard is represented in Figure 2.

iv. Cement

As a binding material, Ordinary Portland Cement (OPC) of grade 52.5 was used to carry out the research. From Table 2, the setting time test of the cement paste was performed according to ASTM C191-18a (C191-18a, 2018). In order to govern the normal consistency of OPC cement, ASTM C187-16 (Standard, 2016) code was followed.

Table 2
Properties of Ordinary Portland Cement (52.5 grade)

Specific gravity (g/cm^3)	3.15
Initial setting time (min)	82
Final setting time (min)	229
Consistency (%)	31.5

v. Recycled Ceramic Fines (RCF)

When applied to concrete constructions as a partial replacement of sand, ceramics display enormous structural strength as well as suitable hardness. The waste ceramics were collected from the nearby ceramic factory and later, they were crushed via LA machine and also by manual hammer crushing. Sieve analysis of waste ceramics was conducted to discover the fineness modulus. With a density of 2-6 gms/cm^3, inorganic, metallic, or non-metallic crystalline ceramics with both ionic and covalent bonding have high melting points ranging from 1000°C-1600°C or even higher. The paper (Effting, Folgueras, Güths, & Alarcon, 2010) studied the chemical analysis of ceramics is discussed in Table 3.

Table 3
Chemical components of ceramic

Chemical components (%)	Ceramic powder (%)	Residue (%)
SiO_2	63.36	64.20
Al_2O_3	18.20	18.32
Fe_2O_3	2.77	0.65
CaO	1.74	1.09
Na_2O	0.34	1.95
K_2O	3.87	1.84
MnO	0.02	0.06
TiO_2	0.80	0.26
MgO	2.04	6.63
P_2O_5	0.05	0.06
PF	6.80	4.96

vi. Recycled Glass Fines (RGF)

Recycled glass as a partial substitute for fine aggregate (sand) has superior temperature resistance and melting point (1200-1600°C or more). The waste glass materials were collected from a local glass company to conduct the study. Employing an L.A. machine and manual mechanical hammer, waste glasses were crushed. Mechanical sieving was carried out to determine the fineness modulus and it was almost closer to sand's fineness modulus. The chemical composition of glass materials has been discussed in (M. Bignozzi, Saccani, Barbieri, & Lancellotti, 2015), especially those collected from different sources as depicted in Table 4.

B. Mix Proportions

Nine (09) different mixes of concrete cylinders were meant to be investigated at pre-firing and post-firing stages to reveal the physical and chemical alterations. Concrete mixes of different types have been displayed via specimen identification represented in Table 5 . Initially, M40 or 40 MPa target benchmark was set for determining the compressive strengths of the specimens after 28 days of curing episode at 19±2°C. After mechanical sieving, the fineness modulus of NCA (6.51), NFA (2.8), GRA (2.70), and CRA (2.65) were calculated. Throughout the entire study, the water-cement (w/c=0.42) ratio was kept constant and the density of Ordinary Portland Cement was observed 435kg/m^3 to maintain the uniformity in subsequent trials and tests. The term "uniformity" is mentioned to describe that, the volumetric alterations would occur in NFA, CRA, and GRA only while, there would be no change in cement, NCA, and water content.

Table 4
Chemical composition of glass

Chemical Components	Soda lime glass	Fluorescent lamps	Funnel glass	Crystal glass
SiO_2	70.40	68.47	56.11	58.64
Al_2O_3	2.06	2.26	3.02	0.02
TiO_2	<0.01[a]	<0.01[a]	0.08	<0.01[a]
Fe_2O_3	<0.01[a]	0.08	0.09	0.21
CaO	11.30	5.13	2.56	0.12
MgO	1.47	2.98	1.86	0.29
Sb_2O_3	<0.01[a]	0.08	0.17	0.22
ZnO	<0.01[a]	<0.01[a]	0.14	1.18
BaO	0.12	0.95	2.20	<0.01[a]
K_2O	1.21	1.61	10.01	7.21
Na_2O	13.4	17.65	5.46	4.67
PbO	<0.01[a]	0.79	18.34	27.43
Na_2Oeq[b]	13.90	18.55	12.97	8.95

[a] *Data below the instrument detection limit*
[b] *Amount of (Na_2O+K_2O) expressed as soda equivalent content*

Table 5
Identification of concrete specimens

Identification: $(GRA)_xF_z$ & $(CRA)_yF_z$	Description
NC	Normal concrete
GRA	Glass Recycled Aggregate
CRA	Ceramic Recycled Aggregate
F	Fine aggregate (sand)
x	% of GRA replacement against sand
y	% of CRA replacement against sand
z	% of existing fine aggregate (sand)

Table 6
Mix Ratio of ingredients for normal concrete (per cubic meter of concrete)

Concrete strength (MPa)	NCA (Kg)	NFA (Kg)	Cement (Kg)	Water (Kg)	W/C Ratio
40	993.7	693.5	435	182.7	0.42

From the statistics expressed in Table 6, for 1m^3 of concrete, a combination of the unit contents of NCA, and NFA were measured successively 993.7kg and 695kg. Similarly, the quantities of cement and water were found consecutively 435kg and 182.5kg to design 1m^3 of concrete. Only NFA, GRA, and CRA were altered volumetrically in the subsequent trials.

Referring to Table 1, the bulk specific gravities of the materials were found somewhat different. In order to determine the mechanical properties of concrete with recycled ceramic and glass fines, volumetric partial

alterations of natural sand (NFA) with GRA and CRA have been maintained. Volumetric partial replacements of NFA with GRA and CRA were kept 0%, 5%, 10%, 15%, 20%, 25%, 30%, 35%, and 40% throughout the study. In addition, Table 7 reveals the mix proportioning of various aggregates with respect to the concrete volume of $1m^3$. A 25°C temperature was taken into consideration as normal room temperature as the pre-firing stage and post-firing stages were 100°C, 200°C, 400°C, 600°C, and 800°C.

C. Concrete Specimens

To reveal the physical and chemical identities after 28 days of curing episode, a total of 306 cylinders were cast. Out of 306 cylinders, 18 cylinders were of conventional concrete while 288 cylinders were of CRA (144) and GRA (144) which are presented in Table 7. The dimensions of used molds were uniform in sizes of 100 mm by 200 mm.

Table 7
Aggregates' mix proportion per $1m^3$ of concrete volume

	Batch code	Proportions of fine aggregate (%)			NCA (kg/m^3)	NFA (kg/m^3)	Replaced NFA (kg/m^3)	Cement (kg/m^3)	Water (kg/m^3)
		NFA	GRA	CRA					
1	$(GRA)_0F_{100}$	100	0	-	993.7	693.5	0	435	182.7
2	$(GRA)_5F_{95}$	95	5	-	993.7	658.83	34.67	435	182.7
3	$(GRA)_{10}F_{90}$	90	10	-	993.7	624.15	69.35	435	182.7
4	$(GRA)_{15}F_{85}$	85	15	-	993.7	589.48	104.02	435	182.7
5	$(GRA)_{20}F_{80}$	80	20	-	993.7	554.8	138.7	435	182.7
6	$(GRA)_{25}F_{75}$	75	25	-	993.7	520.13	173.37	435	182.7
7	$(GRA)_{30}F_{70}$	70	30	-	993.7	485.45	208.05	435	182.7
8	$(GRA)_{35}F_{65}$	65	35	-	993.7	450.78	242.72	435	182.7
9	$(GRA)_{40}F_{60}$	60	40	-	993.7	416.1	277.4	435	182.7
10	$(CRA)_5F_{95}$	95	-	5	993.7	660.25	34.75	435	182.7
11	$(CRA)_{10}F_{90}$	90	-	10	993.7	625.5	69.5	435	182.7
12	$(CRA)_{15}F_{85}$	85	-	15	993.7	590.75	104.25	435	182.7
13	$(CRA)_{20}F_{80}$	80	-	20	993.7	556	139	435	182.7
14	$(CRA)_{25}F_{75}$	75	-	25	993.7	521.25	173.75	435	182.7
15	$(CRA)_{30}F_{70}$	70	-	30	993.7	486.5	208.5	435	182.7
16	$(CRA)_{35}F_{65}$	65	-	35	993.7	451.75	243.25	435	182.7
17	$(CRA)_{40}F_{60}$	60	-	40	993.7	417	278	435	182.7

Table 8
Mix proportioning of concrete cylinders at elevated temperatures

Temperatures	25°C	100°C	200°C	400°C	600°C	800°C	
% Replacement							Total
0	3	3	3	3	3	3	18
	GRA+CRA						
5	3+3	3+3	3+3	3+3	3+3	3+3	36
10	3+3	3+3	3+3	3+3	3+3	3+3	36
15	3+3	3+3	3+3	3+3	3+3	3+3	36
20	3+3	3+3	3+3	3+3	3+3	3+3	36
25	3+3	3+3	3+3	3+3	3+3	3+3	36
30	3+3	3+3	3+3	3+3	3+3	3+3	36
35	3+3	3+3	3+3	3+3	3+3	3+3	36
40	3+3	3+3	3+3	3+3	3+3	3+3	36
						Total cylinders	306

D. Experimental Program

After the initial mix design, associated materials were collected whereas waste glasses and ceramics were crushed in a Los Angeles (L.A.) machine to bring the crushed materials into as finer forms as natural sand. Sieve analyses of NCA, NFA, GRA, and CRA were then carried out and materials were arranged as per the replacement ratio of recycled glass and ceramic fines against natural sand using a weighing scale. The final mixing of the materials was accumulated into a mechanical mixer machine maintaining an appropriate w/c ratio (0.42). After each mix, the slump value of newly prepared concrete was

measured according to ASTM C143-15(Standard, 2015). The specimens were first cured in a damp environment for 24 hours before being demolded and stored in a continuous state under fresh water at a regulated laboratory temperature of 19±2°C before being tested. ASTM C39-18(C39, 2018) is used to perform the 28-days compressive strength test. The splitting tensile strength of the concrete cylinders was also investigated after 28 days in accordance with ASTM C496-17(Concrete & Aggregates, 2017). Initially, at the pre-firing stage, the compressive strength of 51 cylinders where 3 of normal concrete (0% sand replacement) and 24 cylinders from both GRA and CRA was calculated at room temperature of 25°. A conventional gas furnace was used in this study to facilitate the firing episode of normal concrete cylinders. The time duration of each heating stage was 1 hour for 100°C, 200°C, 400°C, 600°C, and 800°C at an average rate of 8-9°C/min. There were 3 normal concrete cylinders in every heating temperature, while 24 cylinders from both batches of GRA and CRA. Concrete specimens were then cooled down at room temperature and then the specimens were taken to measure compressive strength.

4. RESULTS AND DISCUSSION

A. Monitoring of Change in the Microstructures at Elevated Temperature

By opening the door when the interior temperature of the conventional gas furnace reached the desired temperature, the circumstances that happened during the heating process were seen and recorded in a data-logger connected laptop associated with 3 thermocouples.

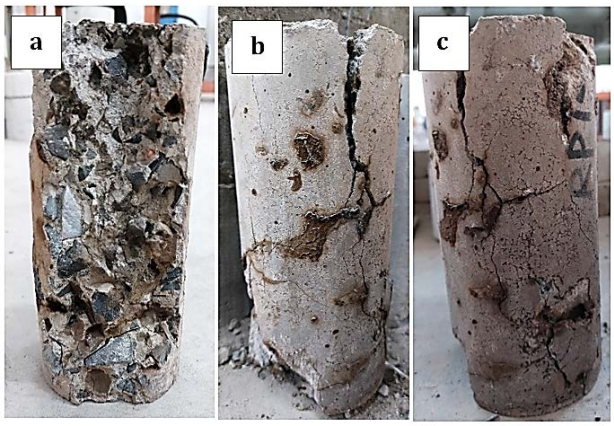

Figure 3: Concrete failures at 800°C (a) NC, (b) GRA (35%), and (c) CRA (35%)

Hardened concrete expands when the temperature increases and finally shrinks due to the loss of water as a form of water vapor. Pictorial illustration from Figure 3 specified the explosive spalling with several larger cracks that appeared on the surface of the concrete when it was 800°C.

i. Analysis of Change in the Microstructure of Normal Concrete

Up to 100°C, no significant alterations except water vapor in normal concrete were detected. When it is recorded at 200°C, some negligible micro-cracks, which were hardly visible were observed and slightly different than the observations made in the literatures (X. Li, Li, Onofrei, Ballivy, & Khayat, 1999; Lin, Lin, & Powers-Couche, 1996). At 400°C, micro-cracks began to expose their intensity evenly over the concrete surface which has been also found similar in previous studies (Arioz, 2007; Aydın & Baradan, 2007; Biolzi, Cattaneo, & Rosati, 2008; Handoo, Agarwal, & Agarwal, 2002; Hossain, 2006; Lau & Anson, 2006; Matesová, Bonen, & Shah, 2006; Peng, Chan, Yan, Liu, & Yi, 2005; Wang, Wu, & Wang, 2005). Comparatively larger cracks (1.5-3.5mm) were visible when the temperature reached 600°C. At temperatures exceeding 600°C, certain minerals in rocks, such as quartz, dissolve or transform. This occurs because concrete undergoes an allotropic transition with a large volume change at 573°C(Zega & Di Maio, 2009, Mujib *et al.*, 2022). At 800°C, explosive cracking with concrete spalling at the edges was observed in conventional concrete which is displayed in Figure 3(a). Thermal expansion, concrete shrinkage while drying, and water evaporation at high temperatures all contributed to cracking(Son, Hajirasouliha, & Pilakoutas, 2011).

ii. Analysis of Change in the Microstructure of GRA Concrete

No significant effect due to temperature increment in GRA_{35} concretes was noticed up to 400°C. Micro-cracks that appeared in GRA_{35} concrete after heating to 400°C were less intense than normal conventional concrete. Fewer cracks occur in GRA_{35} concrete since glass possesses impermeability, superior flow nature, and higher strength exposure to elevated temperatures which is also supported by the previous study (Terro, 2006). Cracks become significant over the surface of GRA_{35} concrete with some minor spalling when heated up to 600°C. Explosive cracking appeared with less concrete spalling than normal concrete along the edges when GRA_{35} experienced heating up to 800°C. This happened since glass normally melts at temperature not less than 700°C, when heated up to 800°C, slowly glass fines turn into a state of liquid and re-solidified when concrete is cooled down (M.-Z. Guo, Chen, Ling, & Poon, 2015).

iii. Analysis of Change in the Microstructure of CRA Concrete

Fewer cracks and spalling were noticed in CRA_{35} than in NC and GRA_{35} when the temperature was in the range of 25°C to 600°C. The visual observation of the appeared results pointed out that explosive patterns and micro-cracks were more significant in GRA than CRA concrete even after heating episodes up to 800°C. After heating to 800°C, less spalling along the edges of the cylinder of CRA was noticed but it was slightly more in GRA concrete. This is due to the higher melting point of ceramic, and better internal cohesiveness of ceramic fines with concrete mortar, which in return helped CRA concrete retain the bond in concrete enduring higher temperatures.

In addition, as temperature increases, more abrupt alterations and failures are found in NC relative to the recycled concretes. Furthermore, superiority over NC was found due to the better internal cohesion among the particles, rough geometric surfaces of crushed glass and ceramic fines, and superior physical and chemical properties of glass and ceramic particles

B. Observation of Concrete Rheology and Consistency

The rheological identity of fresh concrete is determined by the consistency parameter, precisely the conventional slump test, which is illustrated in the Figure 4**.** In comparison to the other 16 concrete mixtures, the normal concrete has a greater slump value of 112 mm. This suggests that the combination of normal concrete is the most workable for the specimens under investigation. Initially, up to 15% replacement in both GRA and CRA, it distinctly provides the slightly higher workability of concrete made with GRA than CRA. When the replacement is 5% in both concrete mixes, GRA_5 concrete is found to be 3.85% higher than CRA_5 concrete. With the increasing replacement trend in concrete mixes, GRA_{15} is noticed 0.97% greater than CRA_{15}. Up to 15% sand replacement in concrete, the graphical illustration depicts the comparatively higher water demand propensity in GRA than CRA concrete due to the greater surface area of glass fines. It clearly indicates that the consistency of both recycled concretes is declining with incrementing replacement rate.

Due to the non-uniform texture, higher particle roughness, and angular shape of the glass and ceramic fines compared to natural fine sand, the inclusion of glass or ceramic fines reduces the workability of concrete. A similar result was obtained in the previous study (Ismail & Al-Hashmi, 2008). However, a higher slump value is observed in the successive mixes of CRA_{20} to CRA_{40}. For CRA_{40}, the slump value is recorded 101 mm which is 3.06% higher than GRA_{40}. More inclusion of recycled ceramic and glass fines as partial replacement of sand creates greater interlocking in concrete due to higher absorption rate and roughness of the surface.

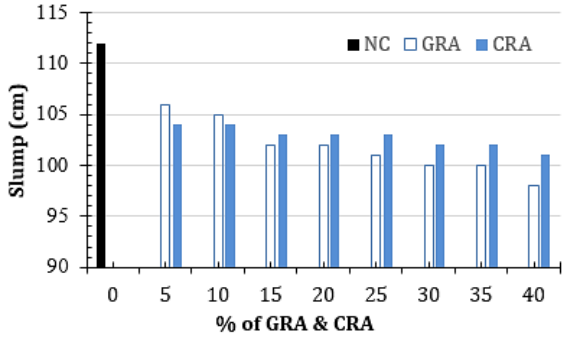

Figure 4: Slump value of varying concrete mixtures

The slump value of normal concrete mix is 112 mm, while the mean slump value for all the mix proportions was observed at approximately 102.60 mm for GRA and 102.75 mm for CRA.

C. Compressive Strength

The compressive strength of concrete samples, after a curing episode of 28 days, changed instantly after a 1-hour heating interval. Evaluation of fire resistivity of recycled concrete with crushed glass and ceramic fines relative to normal concrete is delineated in Figure 5 and Figure 6. At 25°C, the compressive strength of NC is seen 33.86 MPa, however, for CRA_5, CRA_{30}, and CRA_{40}, the readings showed successively 34.4 MPa (1.6% increment), 43.16 MPa (27.47% increment), and 50 MPa (47.67% increment) in comparison with NC. Simultaneously, the strength readings of GRA_5, GRA_{30}, and GRA_{40} at 25°C were consecutively 32.8 MPa (3.23% reduction), and 45.64 MPa (34.79% increment), and 47.18 MPa (39.34% increment) relative to NC. The highest replacements in concrete combinations, such as CRA_{40} and GRA_{40}, also observe the extreme decline of strengths along with concrete spalling as the heating episode lasts for 1 hour. The graphical trend illustrates that the strength reduction is 55.11% for NC when the temperature jumps up from 25°C to 600°C, while it is recorded 49.08% for CRA_{30} and 44.98% for GRA_{30} in a similar fashion.

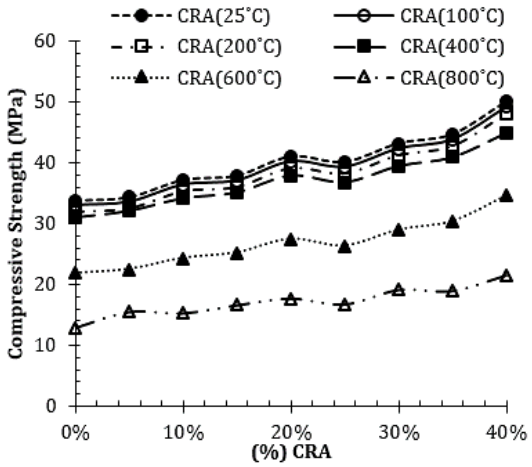

Figure 5: Compressive strength at different temperatures (CRA)

The function of compressive strength of recycled concretes demonstrates that with the increasing replacement of sand with CRA and GRA, strength increases positively. Due to the irregular geometric shape of crushed glass and ceramic, smooth interlocking and inter-particle cohesiveness in concrete mortar escalate (Özkan & Yüksel, 2008; Westerholm, Lagerblad, Silfwerbrand, & Forssberg, 2008, Mujib *et al.*, 2022). At 800°C, the compressive strength of NC is observed 12.93 MPa, while it is 19.11 MPa and 19.82 MPa consecutively for CRA_{30} (47.80% increment) and GRA_{30} (53.28% increment). The highest level of sand replacement (40%) in CRA concrete provides better strength than GRA concrete at 800°C. The increase in strength for CRA_{40} concrete is 66.20% greater than NC but for GRA_{40}, it is 61.41% greater than NC.

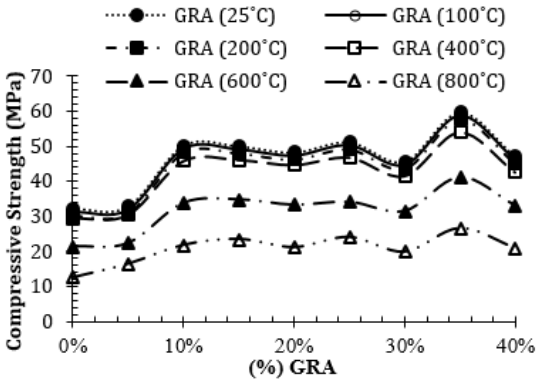

Figure 6: Compressive strength at different temperatures (GRA)

D. Splitting Tensile Strength

In accordance with ACI 318-14(ACI, 2014), the findings of splitting tensile strengths at 28 days for various concrete mixtures are displayed in Figure 7**.** According to ACI 318-14 the equation of mean splitting tensile strength is provided below.

$$f_{ctm,sp} = 0.556\sqrt{f'_c} \quad (1)$$

where f'_c is compressive strength in MPa and $f_{ctm,sp}$ is mean splitting tensile strength in MPa.

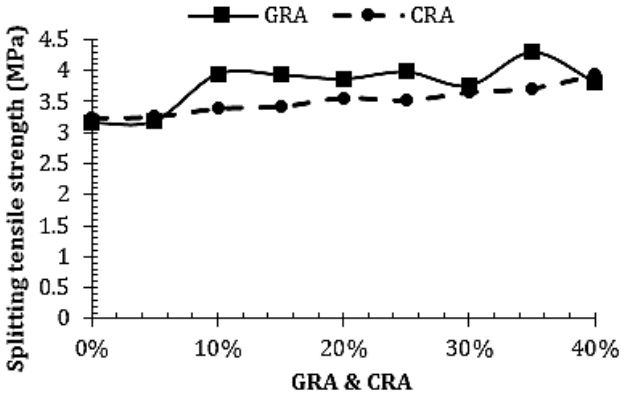

Figure 7: Splitting tensile strength of GRA and CRA concrete

It has been observed that at room temperature (25°C), normal concretes' splitting tensile strength was found 3.15 MPa, while it is noticed 3.18 MPa for GRA_5 and 3.26 MPa for CRA_5 with an increment of successively 0.95% and 3.49% in comparison with normal concrete. The trend depicts that the splitting tensile strength of GRA is consistently higher than CRA. The least difference in strength is noticed when the replacement is 30% for both. The greatest increment is noticed for GRA_{35} and it is 4.21 MPa with a raise of 36.19% against NC. In addition, when the replacement is increased to 40% for both GRA and CRA, the highest increase is seen in CRA_{40} with a 24.76% while it is 20.95% for GRA_{40}.

Despite the abrupt changes, the splitting tensile strength of concrete increases as the amount of recycled glass and recycled ceramic in the concrete mixture increase due to its high tensile capacity. This might be due to the existence of recycled glass and ceramic fines along the fracture plane before it splits, which provides a strong profile of the aggregate-cement paste link.

E. Variations in Poisson's Ratio

While investigating the mechanical properties of recycled concretes along with normal concrete, which is presented in Table 9, average Poisson's ratios of candidate concrete cylinders have been observed. There is an increment of 4.74% in Poisson's ratio in GRA_5 and 11.86% in CRA_5 were found compared to the Poisson's ratio of 0.253 for NC. It defines the soft and smooth nature of recycled glass and ceramic fines with a superior quality of energy absorption to normal concrete. Furthermore, when the maximum volumetric replacement (40%) was taken into consideration, the Poisson's ratio of CRA_{40} exhibited a 47.16% increment compared to the Poisson's ratio of GRA_{40} (0.229). Ceramic fines effectively exhibited cracking by forming a strong, internal aggregate-mortar link, which keeps the aggregate particles together and provides less cracking than glass fines.

Table 9
Mechanical properties of different recycled concrete mixtures at 28 days

Batch ID	Peak stress (MPa)	Axial strain at peak stress	Transverse strain at peak stress	Ultimate strain	Poisson's ratio
NC	33.86	0.00265	0.000671	0.00311	0.253
$(GRA)_5F_{95}$	32.8	0.00391	0.00104	0.00391	0.265
$(GRA)_{10}F_{90}$	50.25	0.00201	0.000612	0.00273	0.304
$(GRA)_{15}F_{85}$	50.06	0.00227	0.000593	0.00281	0.261
$(GRA)_{20}F_{80}$	48.29	0.00243	0.000582	0.00271	0.239
$(GRA)_{25}F_{75}$	51.24	0.00245	0.000592	0.00262	0.242
$(GRA)_{30}F_{70}$	45.64	0.00239	0.000508	0.0021	0.213
$(GRA)_{35}F_{65}$	59.72	0.00205	0.000738	0.000282	0.360
$(GRA)_{40}F_{60}$	47.18	0.00253	0.000579	0.00278	0.229
$(CRA)_5F_{95}$	34.4	0.00288	0.000814	0.00276	0.283
$(CRA)_{10}F_{90}$	37.21	0.00276	0.000805	0.00271	0.292
$(CRA)_{15}F_{85}$	37.92	0.00266	0.000801	0.00279	0.301
$(CRA)_{20}F_{80}$	41.03	0.00259	0.000795	0.00275	0.301
$(CRA)_{25}F_{75}$	40.16	0.0026	0.000798	0.00277	0.307
$(CRA)_{30}F_{70}$	43.16	0.00253	0.000783	0.00267	0.309
$(CRA)_{35}F_{65}$	44.66	0.00248	0.000771	0.00279	0..311
$(CRA)_{40}F_{60}$	50	0.00227	0.000765	0.00286	0.337

F. Modulus of Elasticity

For a better understanding of the mechanical properties of recycled concrete, a clear overview of modulus of elasticity is required to discussed accordingly. From the trend derived from Figure 8, it is visible that with the increase in recycled ceramic and glass fines in concrete mixes, the modulus of elasticity increases in comparison with normal concrete.

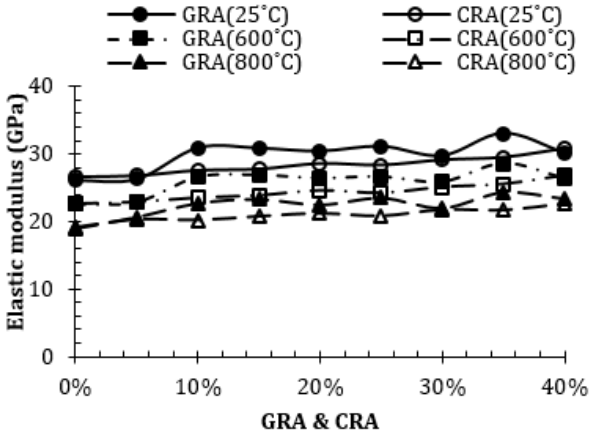

Figure 8. Modulus of elasticity of GRA and CRA concrete

At 25°C, the elastic modulus of 26.61 GPa is achieved for NC, while in CRA (20%) it is (28.59 GPa) which is 7.44% greater than NC but in the case of GRA, it is 14.32% greater than NC. At 600°C, the elastic modulus is 22.58 GPa for NC while the increment is observed 25.85% and 12.39% successively for GRA_{35} and CRA_{35}. For CRA_{40}, the elastic modulus is 18.31% greater than NC whereas it is 22.38% greater than NC for GRA. The study reveals that the quantitative alterations are simpler and slower in CRA than in GRA with increasing temperatures. Furthermore, the modulus of elasticity data specified the fact, more precisely, that CRA and GRA in concrete mixes make the concrete more stable and less fragile in tension than normal concrete.

G. Predicted Equation for Compressive and Tensile Strength

The mathematical equations for predicting the compressive strength of CRA and GRA were formulated by following the regression analysis. This operation which was performed by statistical analysis software (SPSS), resulted in a multiple linear regression model presented in Equations (2) and (3). The data for compressive strength presented in Figure 5 and Figure 6 were used during the analysis. These equations can predict for CRA/GRA substitution ratio of 0–60% accurately. Two variables, "t" temperature of the concrete and "r" CRA/GRA replacement ratio, were included as independent variables while the compressive (f'_c) strength as the dependent variable. The SPSS output results indicate that the adjusted R-square values were 86% and 97%, respectively for CRA and GRA compressive strength equations. The statistical test for the two models was proven to be significant as the p-values associated with the F-test and the t-test were less than 0.001. The validation results of equations (2) and (3) are presented in Figure 9a and 9b, and as seen, the models are predicting the strength for CRA and GRA (for all mixtures) with reasonable accuracy.

$$f_c'(CRA) = 31.72 + 131.96r - 0.021tr - 4.37e^{-8}t^3 - 224.55r^2 \quad (2)$$

$$f_c'(GRA) = 32.7 + 35.28r + 1.69e^{-13}t^5 - 1.83e^{-10}t^4 - 2.41e^{-5}t^2 \quad (3)$$

where, f'_c = compressive strength (MPa), t = temperature, and r = CRA/GRA substitution ratio (fractions).

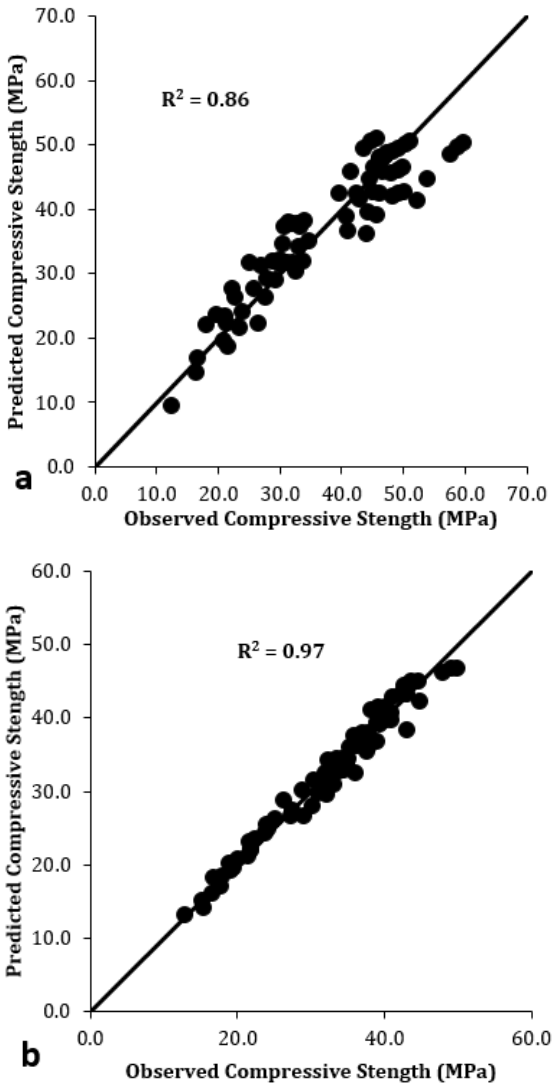

Figure 9: Comparison between the predicted and observed compressive strength values: a) CRA; b) GRA

5. CONCLUSION

The mechanical properties of recycled concrete with crushed glass and ceramic fines as partial substitutions of natural sand are extensively explored in this work. Following is a synopsis of the study's findings:

- Strength is observed to be raised with the increasing replacement of both crushed ceramic and glass particles in a comprehensive investigation of statistical values of compressive strengths. Though it is noticed that 3.13% strength reduction occurs for GRA_5 at 25°C, all other values were almost consistent. This may be due to the mechanical reading error or improper curing on that particular cylinder. The maximum strength is found for GRA_{35} (59.72 MPa), while it is 50 MPa for CRA_{40} at 25°C. From 25°C to

800°C, the strength reduction rate is somewhat more in CRA_{40} (57.02%) compared to GRA_{40} (55.77%).

- Slump value falls when the amount of fine sand substitutions (crushed ceramic and glass fines) in concrete mixes increases. Since glass and ceramic fines exhibit non-uniformity, higher angularity, and superior roughness compared to natural sand, workability reduces in recycled concretes.
- The increasing rate of involvement of recycled glass and ceramic fines create comparatively stronger bonds along the fracture plane than normal concrete, hence more durable in nature. Splitting tensile strength of NC at 25°C is 3.15 MPa, however, 0.95% and 3.49% increment is found consecutively for GRA_5 and CRA_5. With a 24.76% increase, CRA_{40} has the biggest increase, while GRA_{40} has a 20.95% gain relative to NC.
- The concrete made with recycled glass and ceramic fines exhibited a smoother nature with an intensified capacity of energy assimilation compared to normal concrete. With the increasing proportions of recycled glass and ceramic fines, Poisson's ratio has been observed to be increasing compared to normal concrete. Maximum percent increment was obtained in the Poisson's ratio of CRA_{40} (47.16%) when compared to the Poisson's ratio of GRA_{40} (0.229).
- Comprehensive analysis of the study discloses that among the concrete mixes, CRA_{35}, CRA_{40}, and GRA_{35}, GRA_{40} exhibit better performance against at elevated temperatures. The trend derived from the modulus of elasticity also reveals that it is 18.31% higher in CRA_{40} than in NC, although it is 22.38% higher in GRA_{40}. Hence, the recycled concretes with the highest inclusion of glass and ceramic fines are less fragile in tension than normal concrete.

Sustainable development along with green technology is the core essence of civil engineering construction. It can be achieved by exploiting the waste materials such as ceramic and glass in concrete, which are among the potential sources of landfills. In addition, due to the dredging activity of sand from river beds, banks of rivers erode. Furthermore, erosion will result in the loss of protection and shade from the bank vegetation. Efficient utilization of recycled materials (ceramic and glass) as substitutions for natural sand would help minimize the demand for sand to an extent, thus reducing the dredging activities of sand from the sea beds or river beds. The future investigation could incorporate the extensive replacement of sand by volume instead of the replacements used in this study to further investigate the effectiveness of fire responses along with other mechanical properties.

ACKNOWLEDGEMENTS

The authors would like to express his gratitude to the Department of Civil Engineering, Military Institute of Science and Technology, Dhaka, Bangladesh, and the Department of Civil Engineering, University of Alberta, Canada. They also would like to thank the Editors and anonymous reviewers of the article for their insightful suggestions and comments to improve the content.

REFERENCES

17a, A. C. M. (2017). Standard Test Method for Bulk Density ("Unit Weight") and Voids in Aggregate *ASTM International*. West Conshohocken, PA.

38, f. B. N. (2007). Fire Design of Concrete Structures - Materials, Structures and Modelling. Retrieved from https://www.fib-international.org/publications/fib-bulletins/fire-design-of-concrete-structures-pdf-detail.html

ACI. (2014). ACI 318-14. Building code requirements for structural concrete: ACI Farmington Hills, MI, USA.

Adaway, M., & Wang, Y. (2015). Recycled glass as a partial replacement for fine aggregate in structural concrete–Effects on compressive strength. *Electronic Journal of Structural Engineering, 14*(1), 116-122.

Al-Sibahy, A., & Edwards, R. (2012). Mechanical and thermal properties of novel lightweight concrete mixtures containing recycled glass and metakaolin. *Construction and Building Materials, 31*, 157-167.

Al Bakri, A., Norazian, M., Kamarudin, H., Salleh, M., Anuar, M. A., & Alida, A. (2013). *Strength of concrete based cement using recycle ceramic waste as aggregate.* Paper presented at the Advanced materials research.

Ali, F., Nadjai, A., Silcock, G., & Abu-Tair, A. (2004). Outcomes of a major research on fire resistance of concrete columns. *Fire Safety Journal, 39*(6), 433-445. doi:https://doi.org/10.1016/j.firesaf.2004.02.004

Arioz, O. (2007). Effects of elevated temperatures on properties of concrete. *Fire safety journal, 42*(8), 516-522.

ASTM, A. (2014). C136/C136M–14. *Standard Test Method for Sieve Analysis of Fine and Coarse Aggregates, ASTM International, West Conshohocken, PA.*

ASTM, A. (2015). Standard test method for relative density (specific gravity) and absorption of coarse aggregate. *ASTM West Conshohocken, PA.*

Aydın, S., & Baradan, B. (2007). Effect of pumice and fly ash incorporation on high temperature resistance of cement based mortars. *Cement and concrete research, 37*(6), 988-995.

Aydın, S., Yazıcı, H., & Baradan, B. (2008). High temperature resistance of normal strength and autoclaved high strength mortars incorporated polypropylene and steel fibers. *Construction and Building Materials, 22*(4), 504-512. doi:https://doi.org/10.1016/j.conbuildmat.2006.11.003

Bednář, J., Wald, F., Vodička, J., & Kohoutková, A. (2013). Experiments on membrane action of composite floors with steel fibre reinforced concrete slab exposed to fire. *Fire Safety Journal, 59*, 111-121.

Bengar, H. A., Shahmansouri, A. A., Sabet, N. A. Z., Kabirifar, K., & Tam, V. W. (2020). Impact of elevated temperatures on the structural performance of recycled rubber concrete: Experimental and mathematical modeling. *Construction and Building Materials, 255*, 119374.

Bignozzi, M., Saccani, A., Barbieri, L., & Lancellotti, I. (2015). Glass waste as supplementary cementing materials: The effects of glass chemical composition. *Cement and Concrete composites, 55*, 45-52.

Bignozzi, M. C., & Saccani, A. (2012). Ceramic waste as aggregate and supplementary cementing material: A

combined action to contrast alkali silica reaction (ASR). *Cement and Concrete composites*, *34*(10), 1141-1148.

Biolzi, L., Cattaneo, S., & Rosati, G. (2008). Evaluating residual properties of thermally damaged concrete. *Cement and Concrete Composites*, *30*(10), 907-916.

C39, A. (2018). Standard Test Method for Compressive Strength of Cylindrical Concrete Specimens. West Conshohocken, PA: ASTM International.

C131/131M, A. (2014). Standard Test Method for Resistance to Degradation of Small-Size Coarse Aggregate by Abrasion and Impact in the Los Angeles Machine. West Conshohocken, PA,: ASTM International.

C191-18a, A. (2018). Standard Test Methods for Time of Setting of Hydraulic Cement by Vicat Needle. West Conshohocken, PA: ASTM International.

Chen, S.-H., Chang, C.-S., Wang, H.-Y., & Huang, W.-L. (2011). Mixture design of high performance recycled liquid crystal glasses concrete (HPGC). *Construction and Building Materials*, *25*(10), 3886-3892.

Colombo, M., & Felicetti, R. (2007). New NDT techniques for the assessment of fire-damaged concrete structures. *Fire Safety Journal*, *42*(6-7), 461-472.

Concrete, A. I. C. C. o., & Aggregates, C. (2017). *Standard test method for splitting tensile strength of cylindrical concrete specimens1*: ASTM international.

Corinaldesi, V., Gnappi, G., Moriconi, G., & Montenero, A. (2005). Reuse of ground waste glass as aggregate for mortars. *Waste Management*, *25*(2), 197-201.

de Brito, J., Pereira, A., & Correia, J. (2005). Mechanical behaviour of non-structural concrete made with recycled ceramic aggregates. *Cement and Concrete composites*, *27*(4), 429-433.

de Castro, S., & de Brito, J. (2013). Evaluation of the durability of concrete made with crushed glass aggregates. *Journal of Cleaner Production*, *41*, 7-14.

Dilek, U. (2005). Evaluation of fire damage to a precast concrete structure nondestructive, laboratory, and load testing. *Journal of performance of constructed facilities*, *19*(1), 42-48.

Dong, H., Cao, W., Bian, J., & Zhang, J. J. M. (2014). The fire resistance performance of recycled aggregate concrete columns with different concrete compressive strengths. *7*(12), 7843-7860.

Dos Santos, J., Branco, F. A., & de Brito, J. (2002). Assessment of concrete structures subjected to fire—the FBTest. *Magazine of concrete Research*, *54*(3), 203-208.

Effting, C., Folgueras, M. V., Güths, S., & Alarcon, O. E. J. M. R. (2010). Microstructural characterization of ceramic floor tiles with the incorporation of wastes from ceramic tile industries. *13*(3), 319-323.

El-Dieb, A. S., Taha, M. R., & Abu-Eishah, S. I. (2019). The use of ceramic waste powder (CWP) in making eco-friendly concretes. *Ceramic Materials: Synthesis, Characterization, Applications and Recycling*, 1-35.

Federico, L., & Chidiac, S. (2009). Waste glass as a supplementary cementitious material in concrete–critical review of treatment methods. *Cement and Concrete composites*, *31*(8), 606-610.

Fernández-Jiménez, A., Pastor, J. Y., Martín, A., & Palomo, A. J. J. o. t. A. C. S. (2010). High-Temperature Resistance in Alkali-Activated Cement. *93*(10), 3411-3417.

Fike, R., & Kodur, V. (2011). Enhancing the fire resistance of composite floor assemblies through the use of steel fiber reinforced concrete. *Engineering Structures*, *33*(10), 2870-2878.

Georgali, B., & Tsakiridis, P. (2005). Microstructure of fire-damaged concrete. A case study. *Cement and Concrete composites*, *27*(2), 255-259.

Guo, M.-Z., Chen, Z., Ling, T.-C., & Poon, C. S. (2015). Effects of recycled glass on properties of architectural mortar before and after exposure to elevated temperatures. *Journal of cleaner production*, *101*, 158-164.

Guo, Y.-c., Zhang, J.-h., Chen, G.-m., & Xie, Z.-h. J. J. o. c. p. (2014). Compressive behaviour of concrete structures incorporating recycled concrete aggregates, rubber crumb and reinforced with steel fibre, subjected to elevated temperatures. *72*, 193-203.

Hager, I. (2013). Behaviour of cement concrete at high temperature. *Bulletin of the Polish Academy of Sciences. Technical Sciences*, *61*(1), 145-154.

Halicka, A., Ogrodnik, P., & Zegardlo, B. (2013). Using ceramic sanitary ware waste as concrete aggregate. *Construction and Building Materials*, *48*, 295-305. doi:https://doi.org/10.1016/j.conbuildmat.2013.06.063

Handoo, S., Agarwal, S., & Agarwal, S. (2002). Physicochemical, mineralogical, and morphological characteristics of concrete exposed to elevated temperatures. *Cement and concrete research*, *32*(7), 1009-1018.

Heikal, M. (2000). Effect of temperature on the physico-mechanical and mineralogical properties of Homra pozzolanic cement pastes. *Cement and Concrete Research*, *30*(11), 1835-1839.

Hernández-Olivares, F., & Barluenga, G. (2004). Fire performance of recycled rubber-filled high-strength concrete. *Cement and Concrete Research*, *34*(1), 109-117.

Higashiyama, H., Sappakittipakorn, M., Mizukoshi, M., & Takahashi, O. (2014). Efficiency of ground granulated blast-furnace slag replacement in ceramic waste aggregate mortar. *Cement and Concrete composites*, *49*, 43-49. doi:https://doi.org/10.1016/j.cemconcomp.2013.12.014

Higashiyama, H., Yamauchi, K., Sappakittipakorn, M., Sano, M., & Takahashi, O. (2013). A visual investigation on chloride ingress into ceramic waste aggregate mortars having different water to cement ratios. *Construction and Building Materials*, *40*, 1021-1028.

Holan, J., Novak, J., Müller, P., & Štefan, R. (2020). Experimental investigation of the compressive strength of normal-strength air-entrained concrete at high temperatures. *Construction and Building Materials*, *248*, 118662.

Hossain, K. M. A. (2006). High strength blended cement concrete incorporating volcanic ash: Performance at high temperatures. *Cement and Concrete Composites*, *28*(6), 535-545.

Huseien, G. F., Sam, A. R. M., Mirza, J., Tahir, M. M., Asaad, M. A., Ismail, M., . . . Materials, B. (2018). Waste ceramic powder incorporated alkali activated mortars exposed to elevated Temperatures: Performance evaluation. *187*, 307-317.

Ismail, Z. Z., & Al-Hashmi, E. A. (2008). Use of waste plastic in concrete mixture as aggregate replacement. *Waste management, 28*(11), 2041-2047.

Jin, W., Meyer, C., & Baxter, S. (2000). " Glascrete"-Concrete with Glass Aggregate. *ACI Materials Journal, 97*(2), 208-213.

Kakooei, S., Akil, H. M., Jamshidi, M., & Rouhi, J. (2012). The effects of polypropylene fibers on the properties of reinforced concrete structures. *Construction and Building Materials, 27*(1), 73-77.

Khoury, G. (1992). Compressive strength of concrete at high temperatures: a reassessment. *Magazine of concrete Research, 44*(161), 291-309.

Khoury, G. A., Grainger, B. N., & Sullivan, P. J. (1986). Strain of concrete during first cooling from 600 C under load. *Magazine of concrete Research, 38*(134), 3-12.

Khoury, G. A. J. P. i. s. e., & materials. (2000). Effect of fire on concrete and concrete structures. *2*(4), 429-447.

Kim, J., & Lee, G.-P. (2015). Evaluation of mechanical properties of steel-fibre-reinforced concrete exposed to high temperatures by double-punch test. *Construction and Building Materials, 79*, 182-191.

Kong, D. L., Sanjayan, J. G., & Sagoe-Crentsil, K. (2007). Comparative performance of geopolymers made with metakaolin and fly ash after exposure to elevated temperatures. *Cement and Concrete Research, 37*(12), 1583-1589.

Kong, D. L. Y., Sanjayan, J. G., & Sagoe-Crentsil, K. (2005). *Damage due to elevated temperatures in metakaolinite-based geopolymer pastes.* Paper presented at the International Workshop on Geopolymer Cement and Concrete.

Lankard, D. R., Birkimer, D. L., Fondriest, F. F., & Snyder, M. J. (1971). Effects of moisture content on the structural properties of portland cement concrete exposed to temperatures up to 500F. *Special Publication, 25*, 59-102.

Laperre, K., Depypere, M., van Gastel, N., Torrekens, S., Moermans, K., Bogaerts, R., . . . Carmeliet, G. (2011). Development of micro-CT protocols for in vivo follow-up of mouse bone architecture without major radiation side effects. *Bone, 49*(4), 613-622.

Lau, A., & Anson, M. (2006). Effect of high temperatures on high performance steel fibre reinforced concrete. *Cement and concrete research, 36*(9), 1698-1707.

Lee, J., Choi, K., Hong, K. J. J. o. A. A., & Engineering, B. (2009). Color and material property changes in concrete exposed to high temperatures. *8*(1), 175-782.

Li, L.-J., Xie, W.-F., Liu, F., Guo, Y.-C., & Deng, J. (2011). Fire performance of high-strength concrete reinforced with recycled rubber particles. *Magazine of concrete Research, 63*(3), 187-195.

Li, M., Qian, C., & Sun, W. (2004). Mechanical properties of high-strength concrete after fire. *Cement and Concrete Research, 34*(6), 1001-1005.

Li, W., Wang, T., & Han, L.-H. (2019). Seismic performance of concrete-filled double-skin steel tubes after exposure to fire: Experiments. *Journal of Constructional Steel Research, 154*, 209-223.

Li, X., Li, Z., Onofrei, M., Ballivy, G., & Khayat, K. H. (1999). Microstructural characteristics of HPC under different thermo-mechanical and thermo-hydraulic conditions. *Materials and structures, 32*(10), 727-733.

Li, Z., Xu, J., & Bai, E. (2012). Static and dynamic mechanical properties of concrete after high temperature exposure. *Materials Science and Engineering: A, 544*, 27-32.

Lin, W.-M., Lin, T., & Powers-Couche, L. (1996). Microstructures of fire-damaged concrete. *Materials Journal, 93*(3), 199-205.

Ling, T.-C., Poon, C.-S., & Kou, S.-C. (2012). Influence of recycled glass content and curing conditions on the properties of self-compacting concrete after exposure to elevated temperatures. *Cement and Concrete composites, 34*(2), 265-272. doi:https://doi.org/10.1016/j.cemconcomp.2011.08.010

Liu, M. (2011). Incorporating ground glass in self-compacting concrete. *Construction and Building Materials, 25*(2), 919-925.

López-Buendía, A. M., Romero-Sánchez, M. D., Climent, V., & Guillem, C. (2013). Surface treated polypropylene (PP) fibres for reinforced concrete. *Cement and Concrete Research, 54*, 29-35.

Lopez, V., Llamas, B., Juan, A., Moran, J., & Guerra, I. (2007). Eco-efficient concretes: impact of the use of white ceramic powder on the mechanical properties of concrete. *Biosystems engineering, 96*(4), 559-564.

Matesová, D., Bonen, D., & Shah, S. P. (2006). Factors affecting the resistance of cementitious materials at high temperatures and medium [0] heating rates. *Materials and structures, 39*(4), 455-469.

Medina, C., de Rojas, M. I. S., & Frías, M. (2013). Freeze-thaw durability of recycled concrete containing ceramic aggregate. *Journal of Cleaner Production, 40*, 151-160.

Medina, C., Sánchez de Rojas, M. I., & Frías, M. (2012). Reuse of sanitary ceramic wastes as coarse aggregate in eco-efficient concretes. *Cement and Concrete composites, 34*(1), 48-54. oi:https://doi.org/10.1016/j.cemconcomp.2011.08.015

Mujib, S., Md, J., Pal, A., Ibrahim, I., & Mustafy, T. (2022). Numerical Modelling of Concrete-Filled Steel Tube Columns Under Eccentric Loading. Paper presented at the Proceedings of the 5th International Conference on Sustainable Civil Engineering Structures and Construction Materials (pp. 221-240).

Mujib, J. M. S., Shuvo, N. A., Ishmam, A. B. S., & Mustafy, T. (2022). High Temperature Performance of Concrete Incorporating Recycled Glass Powders. Paper presented at the Proceedings of the 5th International Conference on Sustainable Civil Engineering Structures and Construction Materials (pp. 391-403).

Mujib, J. M., Hasan, M., Rasel Molla, M., Zahid, T. M., & Mustafy, T. (2022). Investigation on Fire Resistance of Concrete Incorporating Recycled Ceramic Fine Aggregate. Paper presented at the Proceedings of the 5th International Conference on Sustainable Civil Engineering Structures and Construction Materials (pp. 417-434).

Mustafy, T., & Ahsan, R. (2010, August). FE modeling and experimental verification of a CFRP strengthened steel section subjected to transverse end bearing force. Paper presented at the IABSE-JSCE Joint Conference on Advances

in Bridge Engineering-II, August (pp. 8-10).

Mustafy, T., Pal, A., Islam, M., & Ahsan, R. Development of plastic hinge length expression for fiber reinforced polymer strengthened concrete bridge pier. Paper presented at the IABSE-JSCE Joint Conference on Advances in Bridge Engineering-IV, August 26-27, 2020, Dhaka, Bangladesh.

Oliveira, R., de Brito, J., & Veiga, R. (2015). Reduction of the cement content in rendering mortars with fine glass aggregates. *Journal of Cleaner Production, 95*, 75-88.

Özkan, Ö., & Yüksel, İ. (2008). Studies on mortars containing waste bottle glass and industrial by-products. *Construction and Building Materials, 22*(6), 1288-1298.

Pacheco-Torgal, F., & Jalali, S. (2010). Reusing ceramic wastes in concrete. *Construction and Building Materials, 24*(5), 832-838.

Park, S. B., Lee, B. C., & Kim, J. H. (2004). Studies on mechanical properties of concrete containing waste glass aggregate. *Cement and Concrete Research, 34*(12), 2181-2189.

Peng, G., Chan, S. Y. N., Yan, J., Liu, Y., & Yi, Q. (2005). Characteristics of crack growth in high performance concrete subjected to fire. *Journal of Materials Science and Technology, 21*(1), 118-122.

Phan, L. T., & Carino, N. J. (2000). Fire performance of high strength concrete: research needs *Advanced Technology in Structural Engineering* (pp. 1-8).

Poon, C.-S., Azhar, S., Anson, M., & Wong, Y.-L. (2003). Performance of metakaolin concrete at elevated temperatures. *Cement and Concrete composites, 25*(1), 83-89.

Ramezanianpour, A., Esmaeili, M., Ghahari, S.-A., & Najafi, M. (2013). Laboratory study on the effect of polypropylene fiber on durability, and physical and mechanical characteristic of concrete for application in sleepers. *Construction and Building Materials, 44*, 411-418.

Rashid, K., Hameed, R., Ahmad, H. A., Razzaq, A., Ahmad, M., & Mahmood, A. (2018). Analytical framework for value added utilization of glass waste in concrete: Mechanical and environmental performance. *Waste Management, 79*, 312-323.

Raval, A. D., Patel, D., & Pitroda, P. (2013). Ceramic waste: Effective replacement of cement for establishing sustainable concrete. *International Journal of Engineering Trends and Technology (IJETT), 4*(6), 2324-2329.

Salem, Z. T. A., Khedawi, T. S., Baker, M. B., & Abendeh, R. (2017). Effect of waste glass on properties of asphalt concrete mixtures. *Jordan Journal of Civil Engineering, 11*(1).

Sarker, P. K., Kelly, S., & Yao, Z. (2014). Effect of fire exposure on cracking, spalling and residual strength of fly ash geopolymer concrete. *Materials & Design, 63*, 584-592.

Schwarz, N., Cam, H., & Neithalath, N. (2008). Influence of a fine glass powder on the durability characteristics of concrete and its comparison to fly ash. *Cement and Concrete composites, 30*(6),486-496.

Senthamarai, R., Manoharan, P. D., & Gobinath, D. (2011). Concrete made from ceramic industry waste: Durability properties. *Construction and Building Materials, 25*(5), 2413-2419.

Serrano, R., Cobo, A., Prieto, M. I., & de las Nieves González, M. (2016). Analysis of fire resistance of concrete with polypropylene or steel fibers. *Construction and Building Materials, 122*, 302-309.

Shao, Y., Lefort, T., Moras, S., & Rodriguez, D. (2000). Studies on concrete containing ground waste glass. *Cement and Concrete Research, 30*(1), 91-100.

Shi, C., Wu, Y., Riefler, C., & Wang, H. (2005). Characteristics and pozzolanic reactivity of glass powders. *Cement and Concrete Research, 35*(5), 987-993. doi:https://doi.org/10.1016/j.cemconres.2004.05.015

Short, N., Purkiss, J., & Guise, S. (2001). Assessment of fire damaged concrete using colour image analysis. *Construction and Building Materials, 15*(1), 9-15.

Son, K. S., Hajirasouliha, I., & Pilakoutas, K. (2011). Strength and deformability of waste tyre rubber-filled reinforced concrete columns. *Construction and Building Materials, 25*(1), 218-226.

Standard, A. (2015). C143, ASTM International, West Conshohocken, PA. *Standard Test Method for Slump of Hydraulic-Cement Concrete*.

Standard, A. (2016). C187, Standard Test Method for Amount of Water Required for Normal Consistency of Hydraulic Cement Paste. *ASTM International, West Conshohocken, PA*.

Sukontasukkul, P., & Wiwatpattanapong, S. (2009). Moderate lightweight concrete mixed with recycled crumb rubber. *Thammasat Int. J. Sc. Tech, 14*(1), 1-9.

Terro, M. J. (2006). Properties of concrete made with recycled crushed glass at elevated temperatures. *Building and Environment, 41*(5), 633-639. doi:https://doi.org/10.1016/j.buildenv.2005.02.018

Topcu, I. B., & Canbaz, M. (2004). Properties of concrete containing waste glass. *Cement and Concrete Research, 34*(2), 267-274.

Topçu, İ. B., & Canbaz, M. (2004). Properties of concrete containing waste glass. *Cement and Concrete Research, 34*(2), 267-274. doi:https://doi.org/10.1016/j.cemconres.2003.07.003

Torkittikul, P., & Chaipanich, A. (2010). Utilization of ceramic waste as fine aggregate within Portland cement and fly ash concretes. *Cement and Concrete composites, 32*(6), 440-449. doi:https://doi.org/10.1016/j.cemconcomp.2010.02.004

Wang, X.-S., Wu, B.-S., & Wang, Q.-Y. (2005). Online SEM investigation of microcrack characteristics of concretes at various temperatures. *Cement and concrete research, 35*(7), 1385-1390.

Westerholm, M., Lagerblad, B., Silfwerbrand, J., & Forssberg, E. (2008). Influence of fine aggregate characteristics on the rheological properties of mortars. *Cement and Concrete Composites, 30*(4), 274-282.

Zega, C. J., & Di Maio, A. A. (2009). Recycled concrete made with different natural coarse aggregates exposed to high temperature. *Construction and Building Materials, 23*(5), 2047-2052.

MIJST
MIST International Journal of Science and Technology

Assortment of Dispatch Strategies with the Optimization of an Islanded Hybrid Microgrid

Sk. A. Shezan[1]*, Md. Fatin Ishraque[2], Liton Chandra Paul[3], Md Rasel Sarkar[4], Md Masud Rana[5], Moslem Uddin[6], Mohammad Belayet Hossain[7], Md Asaduzzaman Shobug[8], and Md. Imran Hossain[9]

[1]Department of Electrical Engineering and Industrial Automation, Engineering Institute of Technology, Melbourne, Australia
[2,3,9]Department of Electrical Electronic and Communication Engineering, Pabna University of Science and Technology, Pabna-6600, Bangladesh
[4,6]School of Engineering & Information Technology, The University of New South Wales, Canberra, ACT 2610, Australia
[5]Centre for Smart Grid Energy Research (CSMER), Electrical and Electronic Engineering Department, Universiti Teknologi PETRONAS, 32610, Seri Iskandar, Tronoh, Perak, Malaysia
[7]School of Information Technology, Deakin University Faculty of Science Engineering and Built Environment, Geelong, Victoria, Australia
[8]Department of Electrical and Electronic Engineering, Pabna University of Science and Technology, Pabna-6600, Bangladesh

emails: [1]*shezan.ict@gmail.com;* [2]*fatineeeruet@gmail.com;* [3]*litonpaulete@gmail.com;* [4]*raselbdeee@gmail.com;* [5]*emdmasudrana@gmail.com;* [6]*moslem.uddin.bd@gmail.com;* [7]*m.hossain@deakin.edu.au; and* [8]*imranete.pust@gmail.com*

ARTICLE INFO

Article History:

Received: 04th November 2021
Revised: 16th January 2022
Accepted: 06th March 2022
Published online: 26th June 2022

Keywords:

Microgrid
System stability
Dispatch strategies
Optimization
Renewable energy

ABSTRACT

In this work, the optimization of an off-grid micro-hybrid system is evaluated. This is conducted with the estimation of the proper sizing of each element and the steady-state voltage, frequency, and power responses of the microgrid. Kangaroo Island in South Australia is considered to be the test case location and the grid incorporates solar PV (photo-voltaic), diesel generator, battery storage, and wind turbine. Optimal sizing of the studied microgrid is carried out for four various power dispatch techniques: (i) cycle charging (CC), (ii) generator order (GO), (iii) load following (LF), and (iv) combined dispatch (CD). The proposed off-grid micro-hybrid is optimized for three performance indices; minimal Levelized Cost of Energy (LCOE), CO_2 emission, and Net Present Cost (NPC). Using iHOGA (improved hybrid optimization by genetic algorithm), microgrid optimization software, all the above-mentioned dispatch strategies have been implemented and following this, MATLAB/Simulink platform has been used for the steady-state studies. The results show that the LF strategy is the utmost optimum dispatch technique in terms of the studied performance indices i.e. considering the optimal size and voltage and frequency responses. The results obtained from these studies provide a pathway for the estimation of the resource-generation-load combination for the islanded off-grid microgrid for its optimal operation with the various dispatch strategies.

1. INTRODUCTION

Power is the main strength behind urbanization and industrialization. The conventional electrical power plants mostly depend on fuels like coal or HFO (heavy fuel oil), which emits a large amount of polluting greenhouse gasses (GHG) like CO_2, creating a threat to the environment and mankind and is one of the reasons behind global warming (Ishraque et al., 2021). Moreover, day by day, the production cost of electrical power is getting higher and higher as the amount of fossil fuel reserve is decreasing. As an obvious result, research interest in renewable and non-conventional types of sources of energy like wind, solar, biomass, wave energy, hydro and geothermal energy is increasing day by day. Among the many other renewables and non-conventional energy resources, because of the ease of availability and accessibility of wind and sunlight, wind and solar energy systems are considered the most significant renewable energy resources (Ishraque, Shezan, et al., 2021). Over the last decades, the fields of both wind and solar power have availed their advancements independently of each other (Sinha & Chandel, 2015).

Solar and wind have intermittent nature and that's why they have some limitations (Ishraque & Ali, 2021; Shezan

& Ishraque, 2019). The variable nature of wind speed and solar radiation may cause some uncertainty issues in the off-grid microgrid. The quality of power in a hybrid microgrid is always a vital issue because of the fluctuation between the amount of generated power and load demand (Sarangi et al., 2020). Moreover, a sudden change in the load demand can lead to a sudden voltage and frequency fluctuation in the system (Al-Hinai et al., 2021; Ishraque et al., 2021). Besides all these facts, the integration of more than one renewable energy source can make the system unstable and infeasible (Ishraque et al., 2021; Shezan et al., 2022).

The world is looking for longer-lasting power sources emphasizing solar radiation and wind power-based renewable systems. Al Busaidi et al. in (Al Busaidi et al., 2016) suggested a probable solution to the uncertainty issues with solar and wind resources and load-related issues as well. Voltage deviation in an off-grid microgrid affects the stability of the system. STATCOM (Static Synchronous Compensator) can be a solution to this problem with the implementation of the genetic algorithm (GA) proposed by Hale Bakir (Bakir & Kulaksiz, 2020). The main concept of various optimization techniques and control strategies to minimize different parameters like frequency and voltage stabilization, Net Present Cost, and pollutions are shown by Tao ma et al. (2014). PI (proportional integral) based on a modified controller along with genetic algorithm (GA) integration-based control technique is studied by Obara et al. (2018) for the output voltage control.

In (Wang et al., 2016), Wang et al. assessed an optimal dispatch technique for an islanded micro-hybrid grid system by keeping in mind vehicle-to-grid (V2G) technology under TOU (time of use) tariffs. The use of optimal and coordinated dispatch strategy methodologies can ensure power production minimization as well as maximum renewable resource usage. A voltage-frequency stabilization methodology has been demonstrated by Zhao et al. (2015). They designed a second-storied optimized dispersed dispatch regulator technique applicable for an off-grid microgrid system for voltage-frequency stabilization.

Chowdhury et al. demonstrated the advancement in the field of economic dispatch for unorthodox power sources. The correlation between the optimal power flow and the economic dispatch has been reported and pointed out in (Chowdhury & Rahman, 1990). Many researchers have already expressed their views regarding the dispatch strategies with the techno-economic analysis and optimization of islanded microgrid (Liu et al., 2018). Liu et al. evaluated and proposed a method based on distributed economic alternative dispatch strategies for designing an islanded microgrid (Liu et al., 2019). An optimal dispatch technique for the islanded hybrid microgrid is assessed by Abdullah et al. by incorporating V2G operation under time-of-use tariffs (Abdullah et al., 2014). MAS (multi-agent system) based energy management system for the decentralized optimization approach facilitating power dispatch control techniques for an islanded microgrid that working at high elevation is proposed by B. Zhao et al. in (Zhao et al., 2015). Qadrdan et al. introduced an operative power dispatch strategy to enhance the generation schedulability of a wind-BESS (battery energy storage system) hybrid microgrid system (Qadrdan et al., 2013). An energy management platform based on a MAS considering real-time power dispatch strategies is proposed by Zhang et al. (Zhang et al., 2013). Researchers introduced a modified operating dispatch strategy for a compact electricity and gas network system considering the stochastic behavior of wind power predictions (Ye et al., 2019).

Many research scholars have already implemented their ideas regarding the system stability and mitigation of voltage and frequency fluctuations for the islanded hybrid microgrid (Ishraque et al., 2021). Another decentralized optimization control methodology is suggested to keep the system frequency within the specified operating range and minimum operating cost (Chowdhury, 1992). In (Nasr et al., 2020), a first-level decentralized hang pay control method has been applied for load sharing and other force dispersion results keeping up as per the foreordained inventory request succession. Voltage fluctuation issues are very common for an off-grid microgrid. To solve this issue, a solution is suggested by Mahmud et al. by utilizing Static Synchronous Compensator (STATCOM) alongside the usage of the hereditary calculation improvement technique in (Kumar et al., 2019). In (Vergara et al., 2018), Vergara et al. introduced different optimization and control strategies to minimize NPC, COE, environmental pollution, frequency, voltage, and power fluctuations. A novel control technique is implemented by Chowdhury et al. to improve the power system performance of an islanded microgrid by considering the bidirectional interlinking converter (BIC) (Chowdhury & Taylor, 2000). Hale et al. demonstrated a multi-agent-based distributed control technique suitable for the islanded hybrid microgrid to mitigate the voltage and frequency stability (Bakir & Kulaksiz, 2020).

The main lacking in the existing literature is the lack of correlation between the techno-economic analysis and optimal sizing along with the system stability such as frequency and voltage stability according to the dispatch strategies. The proper operation of an off-grid microgrid can be ensured by fulfilling three criteria which are technical, system stability and economic feasibility. The possible solution might be ensured by a proper co-relation and combination of these criteria for an off-grid microgrid. The proposed Kangaroo Island is situated in the southwest of Adelaide, South Australia. Moreover, the proposed Kangaroo Island has enough renewable resources such as wind speed and solar irradiation to produce enough renewable power to fulfill the need. The main target of the conducted research is to build a strategy of an off-grid PV-wind-diesel generator-battery storage-based hybrid microgrid network that will be connected along with the already established power distribution system for the proposed Island. The wind turbine, solar PV, battery storage and diesel generator are the power sources for the proposed micro-hybrid grid. The principal contribution of this work is two-fold: the first contribution includes the

optimal design of an off-grid microgrid based on minimum NPC, CO_2 emissions and COE according to various dispatch strategies and the second contribution incorporates the voltage, power, and frequency stabilization for the whole system according to the optimized size. The rest of this article has been systematized as tracks: The architecture of an off-grid Microgrid along with the system components and energy transformation method has been summarized in Section 2; System methodology and working principles of this research work are represented briefly in section 3; Section 4 compassions the research and simulation outcomes and a brief discussion with indispensable diagrams and tables to illustrate the proportional studies among the premeditated microgrid and the non-renewable power system networks; Then the later segments converse the conclusion along with the acknowledgment and references.

2. ARCHITECTURE OF AN ISLANDED MICROGRID

The power that comes from the solar cell and Battery both are Direct Currents (DC) and thus using DC/AC converters are converted to Alternating Current (AC) before going to the AC bus bar. The Diesel Generator and Wind Turbine both generate AC power and thus are directly connected to AC bus-bar after a simple voltage conversion. The loads are then fed from the AC bar. VSC (Voltage Source Controller) is introduced for the converter unit.

In Figure 1, a block representation of the proposed off-grid Microgrid along with the system components is depicted. The Microgrid consists of a wind turbine, solar PV, diesel generator, various loads, system converter module, and battery storage unit.

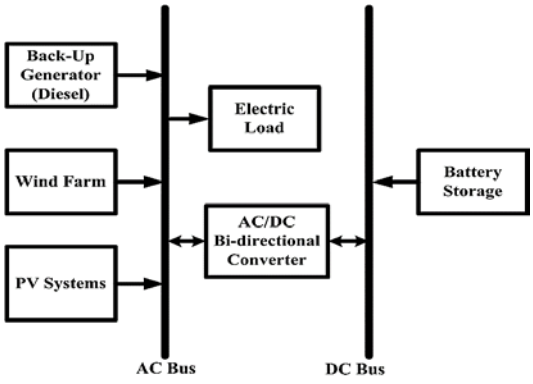

Figure 1: A Schematic diagram of the optimization strategy for the proposed hybrid Microgrid

3. METHODOLOGY

By considering the load profile, power sources, and meteorological conditions of Kangaroo Island, various optimization strategies adopt various dispatch techniques.

Load following (LF) strategy makes a generator deliver just enough power to fulfill the demand whenever it is required. This technique is ideal especially in systems having a large amount of renewable power that exceed the demand occasionally (Shezan, 2019).

In Cycle Charging (CC) strategy, the generator works at its full rating whenever it is required. The excess power produced by the generator charges the battery units. In general, the CC technique is an ideal choice for the frameworks having practically no renewable sources of power (Ishraque et al., 2021; Shezan, 2019).

In, Generator Order (GO) dispatch strategy, the operating capacity is fulfilled by the first combinations in the rundown process. GO strategy supports frameworks that have generators, wind turbines, converters, solar PVs, and extra battery units (Bukar & Tan, 2019).

In Combined Dispatch (CD) strategy, future net loading assumption is avoided by the utilization of the current net load for deciding on the battery if the battery module is to be charged using the generator unit or not. The CD strategy abstains from using the generator unit when the amount of load is low. The CD chooses the cheapest option to make CC or LF in each time step (Shezan et al., 2019).

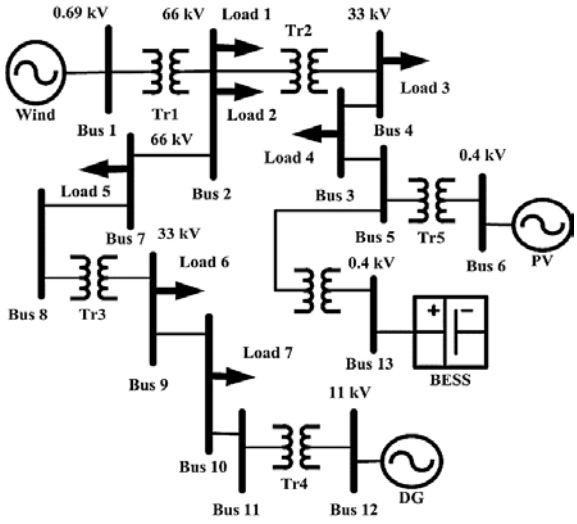

Figure 2: A single line diagram of proposed Kangaroo Island Microgrid with the power distribution network

Figure 2 depicts a simplified single line diagram for the distribution system for the proposed off-grid Kangaroo Island microgrid system is shown. The distribution network consists of a total of twelve busses, five transformers, a Solar PV module, a wind turbine module, a diesel generator, and seven loads. The 7 loads are connected at various nodes of the distribution network having voltages of 11 kV, 33 kV, and 66 kV. The sun-based PV, Wind Turbine unit, and Diesel Generator modules in the dissemination network are associated with three unique focuses having a voltage level of 11 kV. Utilizing venture up transformers this 11 kV is then ventured up to 33 kV. An underlying voltage of 575 V is set for the Wind Turbine, Solar PV and Diesel generator. A recurrence of 50 Hz is considered for the entire framework (Shezan et al., 2019).

Figure 3 shows the flowchart for the proposed work showing the research methodology at a glance. Firstly, the required inputs are needed to be put in the simulation software. According to the load profile, meteorological condition, and dispatch algorithm the simulation should suggest some optimum solutions. Upon the satisfaction of the load demand the optimum solution is chosen and simulated in Simulink microgrid model in order to assess the proposed microgrid on the basis of power system

responses. Upon the satisfaction of the requirements, the optimum solution is finalized.

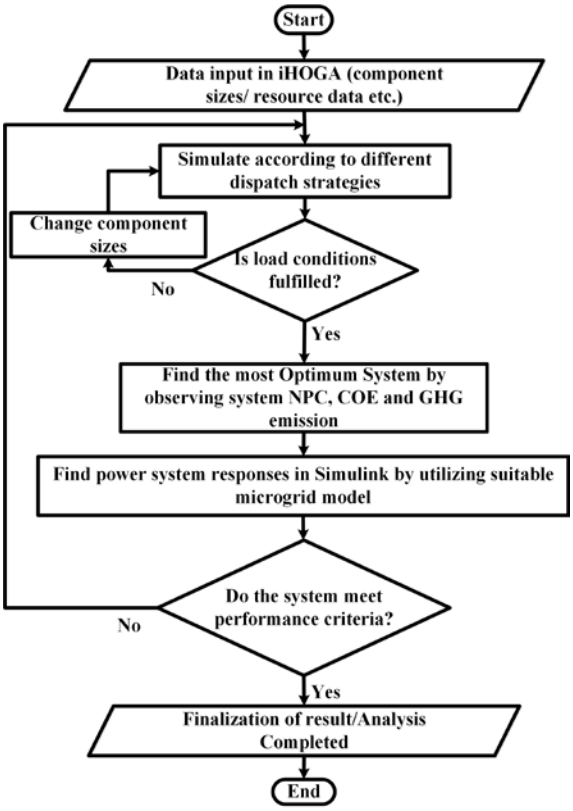

Figure 3: Flow chart for the proposed research work

Figure 4 shows the cost curve for solar PV used in the proposed Kangaroo Island Microgrid system is shown. From the cost curve, the optimal sizes of the solar PV setup and the replacement and capital costs have a proportional relationship. The maintenance and operation cost ratios are approximately the same because of the fixed cost for maintenance and operation. In this work, the PV module has a size of a maximum of 15 MW that is considered in this cost curve.

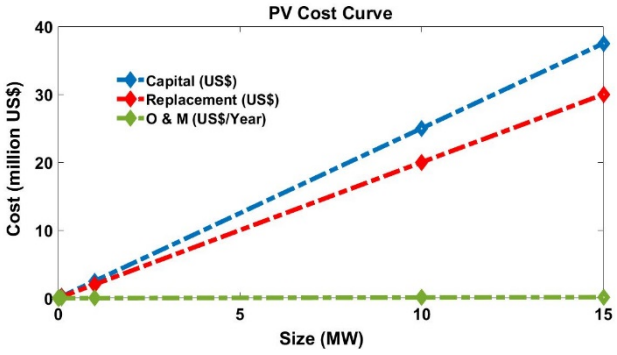

Figure 4: Cost curve for Solar PV

Figure 5 depicts the Wind Turbine cost curve used in the proposed Kangaroo Island Microgrid system is shown. From the cost curve, along with the optimal size of the turbine setup, the replacement and capital costs also increase. The maintenance and operation cost ratios are approximately the same because of the fixed cost for maintenance and operation. In this work, the Turbine module has a size of a maximum of 1.5 MW that is considered in this cost curve. In this analysis, a total of 10 turbines are considered having a 1.5 MW size each.

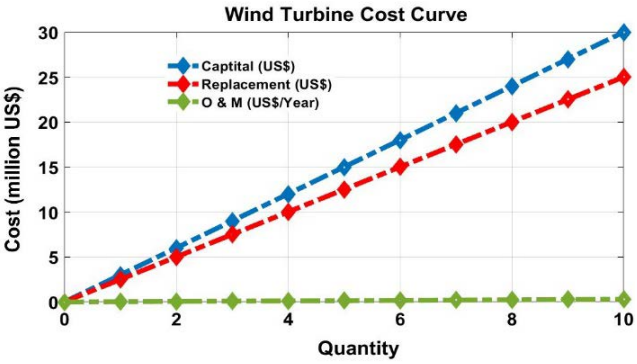

Figure 5: System cost curve for Wind Turbine system

In Figure 6, the diesel generator cost curve used in the proposed Microgrid system is shown. From the cost curve, along with the optimal size of the generator setup, the replacement and capital costs also increase. The maintenance and operation cost ratios are approximately the same because of the fixed cost for maintenance and operation. In this work, the generator module has a size of a maximum of 8 MW that is considered in this work.

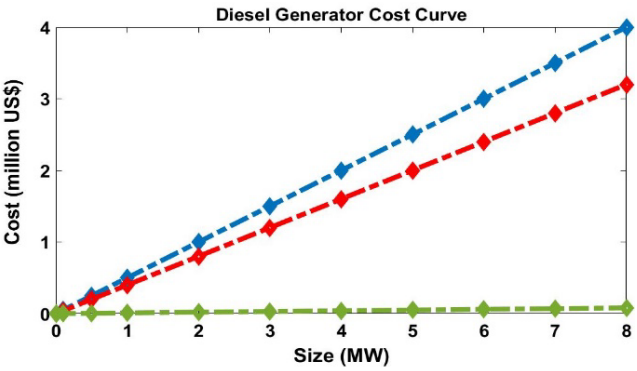

Figure 6: Cost curve for Diesel Generator unit used in the system

Figure 7 shows the battery storage cost curve used in the proposed Microgrid system is shown. From the cost curve, along with the optimal size of the battery module, the replacement and capital costs also increase. The maintenance and operation cost ratios are approximately the same because of the fixed cost for maintenance and operation. In this work, the battery storage module has a total size of a maximum of 10 MW that is considered in this cost curve for both analyses.

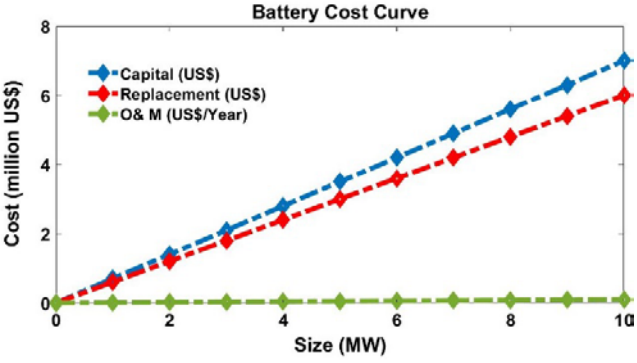

Figure 7: System cost curve for Battery

4. RESULTS AND DISCUSSION

A. Optimal Sizing of the Network

Table 1 shows, a brief comparison between the required sizes of various components for the proposed Microgrid under different dispatch strategies have been highlighted. From the comparison of the results, a clear difference can be observed in the sizes of different components for different dispatch techniques with the same load profile. Various dispatch strategy causes different optimal sizes of the Wind turbine module, battery storage unit, Solar PV, and converter. The table further illustrates that a wind turbine needs the highest size among the others under the LF technique. On the other hand, Solar PV has the highest size among others under the CD technique. The Diesel Generator (DG) occupies the same 1 MW size for CC and LF as well as for GO strategies. For CD strategy, the size of DG increases to 5 MW. This is because of the combination variation offered by the CD Strategy. The highest 10 MW battery size is required for LF strategy because the total power generation from the Wind turbine module and PV solar cell is higher than the load size. Thus, surplus power is needed to be stored for future usage. From Table 1, it is further observable that for GO dispatch technique, the optimum sizes of the Solar PV, converter, and the battery module are lowest than any other dispatch techniques. This is attributable to the Generator Order technique in which the segment sizes are picked by absolute burden and force generator succession. Along these lines, as the interest is fulfilled by the most minimal sizes of the various parts as indicated by the meteoroidal condition, the cycle of ideal estimating of finding further least sizes will be ended.

Table 1
Comparison of sizes of every component for Proposed Microgrid for Various dispatch strategies

Dispatch Strategies	PV (kW)	Wind (kW)	Diesel Generator kW)	Battery (kWh)	Converter Size (kW)	Load Profile
Load Following (LF)	2,700	8,000	1,000	5,000	1,200	82,656.32 kWh/d 7345.00 kW
Cycle Charging (CC)	2,900	8,500	1,200	2,000	1,400	
Generator Order (GO)	600	7,000	1,400	500	600	
Combined Dispatch (CD)	3,200	6,500	4,500	4,000	2700	

For various dispatch techniques, the differences in COE, NPC, operating costs, and CO_2 emissions are shown in Table 2 applicable for Kangaroo Island. The table shows that a significant difference lies between the four dispatch strategies on behalf of the CO_2 emissions, COE and NPC. The CO_2 emissions, COE and NPC are highest in the Combined Distance strategy and lowest in the Load Following strategy. In Figure 8, the total amount of electrical power production a year is depicted according to various dispatch strategies and meteorological conditions. The NPC can be varied by equipment cost, fuel cost, maintenance and operation cost, and lifetime. The analysis shows that NPC for the designed off-grid microgrid has been successfully lessened than the conventional power plant.

Table 2
Comparison of NPC, COE, CO_2 emissions and operating cost of proposed design for various controller

IHOGA Controller	NPC (million US$)	COE (US$/kWh)	CO_2 Emissions (kt/yr.)	Operating Cost (million US$)
Load Following (LF)	28.03	0.08	2.7	0.97
Cycle Charging (CC)	37.24	0.10	3.7	2.17
Generator Order (GO)	39.98	0.12	4.7	3.01
Combined Dispatch (CD)	69.97	0.18	6.9	4.11

Table 3
Comparison between the proposed hybrid microgrid and the non-renewable power stations

Criteria	Dispatch Strategies				Non-Renewable Power Station
	(LF)	(CC)	(GO)	(CD)	
CO_2 Emission/ Year (Kt)	2.7	3.7	4.7	6.9	12.45
NPC/Year (million US$)	28.03	37.24	39.98	69.97	245
COE (US$/kWh)	0.08	0.10	0.12	0.18	1.48
Operating Cost/Year (million US$)	0.97	2.17	3.01	4.11	11.13

The results obtained from the analysis and simulation, the COE, NPC, CO_2 emissions/year, and operating cost have been reported and compared with the conventional power station. The comparison in Table 3 highlights the noteworthy differences in between the designed off-grid Microgrid and a similar conventional generation plant on the reference of COE, NPC, operating cost, and total CO_2 emission.

B. Steady-state Frequency and Voltage Response

Analyzing the optimal output results from iHOGA, the optimal sizing of each component in the proposed microgrid has been evaluated. In MATLAB/Simulink platform, the optimal sizes of the components have been set. The power responses for diesel generator, PV, wind, load profile, and battery module are captured and the simulation results have been plotted.

In Figures 9-12, the frequency responses for the time of 3 - 4 seconds as a steady-state response for all the generation strategies are depicted. From the result in Figures 9-10, it can be observed that the frequency is slightly higher than the nominal value for CD and GO strategies.

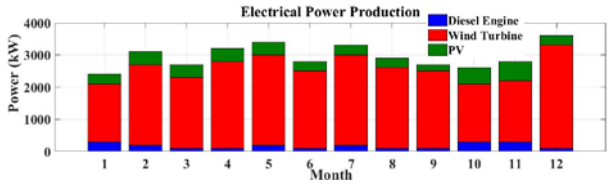

(a) LF

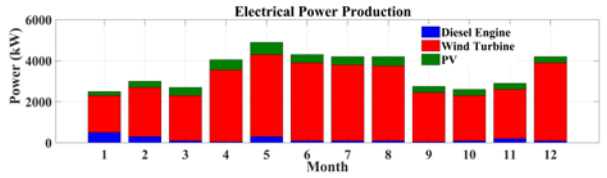

(b) CC

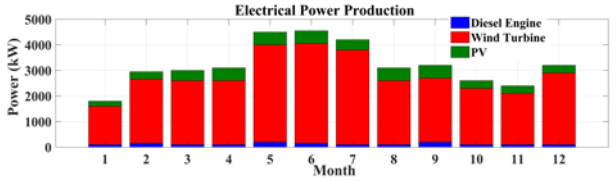

(c) GO

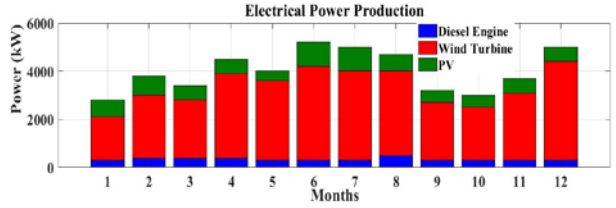

(d) CD

Figure 8: Electrical Power Production according to the four dispatch strategies for Kangaroo Island

Figure 11 shows that the frequency lies within the acceptable range of 50+/-2% Hz for the power distribution system of Australia. However, the LF strategy shows the best response in consideration of the minimum and the maximum frequency values. This range of frequency can clearly depict the efficacy of the optimized size of the network which maintains the steady-state operation limit. The Islanded microgrid system may suffer from an unexpected fluctuation in frequency due to a huge deviation between the load demand and the supplied power which on the other hand results in due to an unexpected deviation in the wind and solar power output.

In Figures 13-17, the voltage response of the off-grid microgrid under the base case and with the proposed four dispatch strategies are shown. The figures depict that a stable voltage response can be obtained for all four dispatch strategies. The comparative results of voltage illustrate that the LF strategy results in the best response among all other dispatch strategies. For all the dispatch strategies, wind turbine voltage is similar. The voltage output from the PV unit also stays within the considerable limit and within the rated capacity. The voltage of the battery module fluctuates in between 300V to 350V. The voltage across load seems more stable for LF and CC strategies. For CD and GO, the voltage is distorted. The voltage across the DG output is better in LF than observed in CC. The outputs discussed are so obtained because of the different operating principles of the dispatch control algorithms. The outputs obtained are satisfactory as they are stable within the considerable limit and hence, the proposed microgrid can be determined feasible with respect to voltage outputs performances.

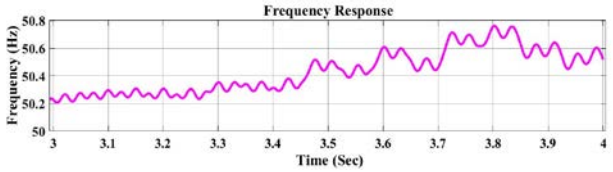

Figure 9: Frequency response of Islanded wind-PV Microgrid for CD dispatch Strategy

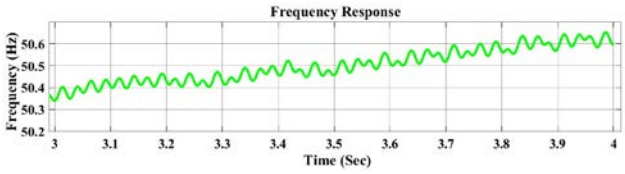

Figure 10: Frequency responses of off-grid PV-wind Microgrid for GO dispatch Strategy

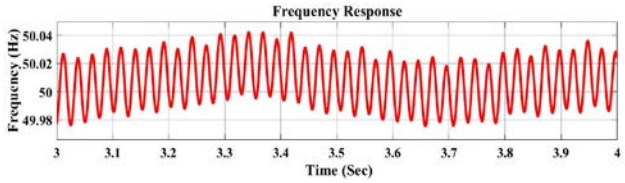

Figure 11: Frequency response of off-grid wind-PV Microgrid for LF dispatch Strategy

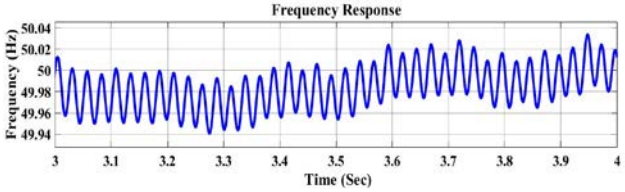

Figure 12: Frequency response of off grid PV-wind Microgrid for CC dispatch strategy

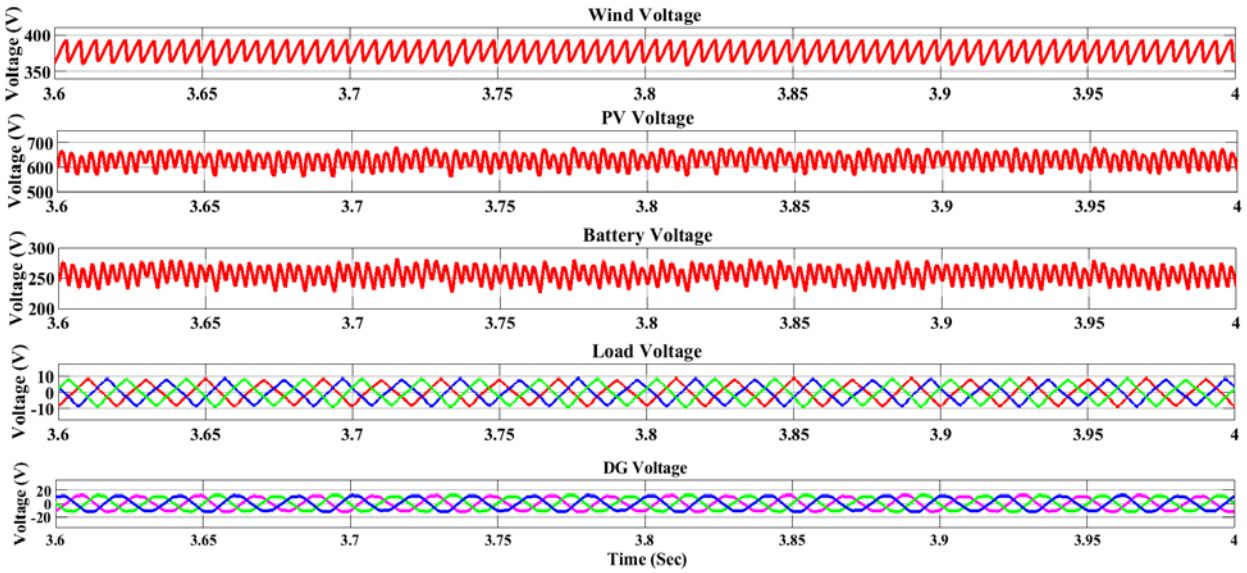

Figure 13: Voltage responses from wind, PV, Battery, Load, and DG module of IHMS for LF dispatch Strategy

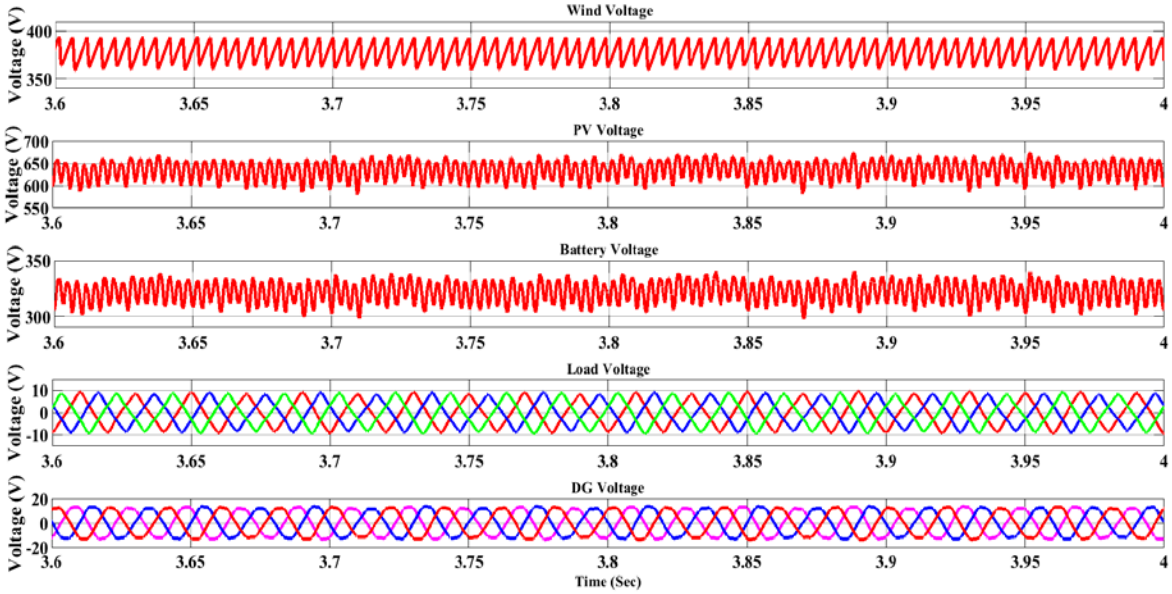

Figure 14: Voltage responses from wind, PV, Battery, Load, and DG module of IHMS for CC dispatch Strategy

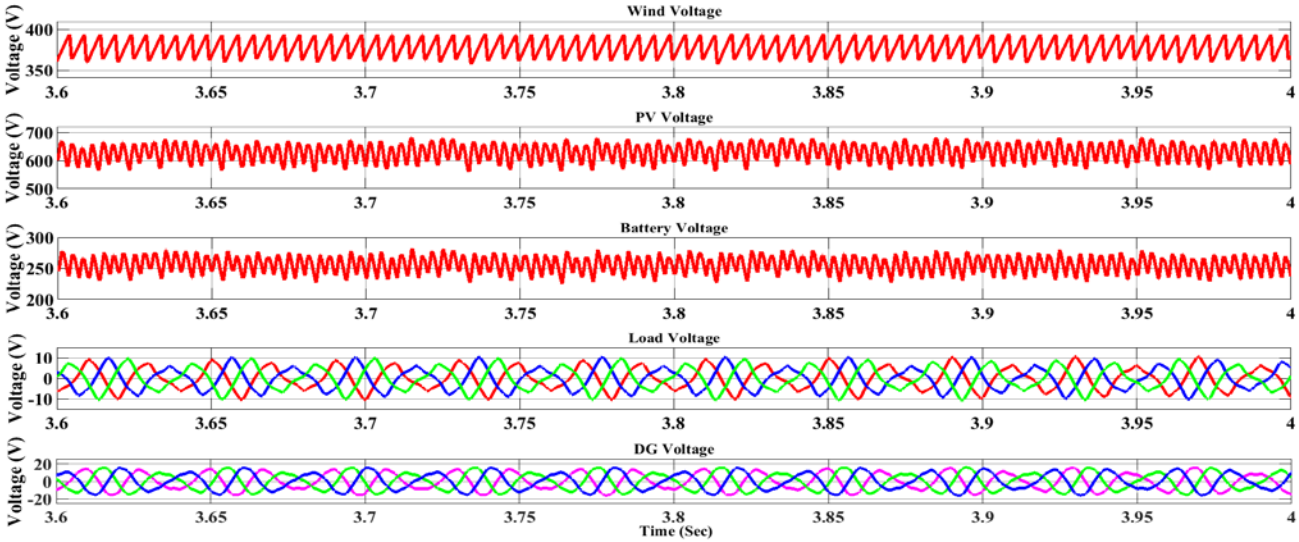

Figure 15: Voltage responses from wind, PV, Battery, Load, and DG module of IHMS for CD dispatch Strategy

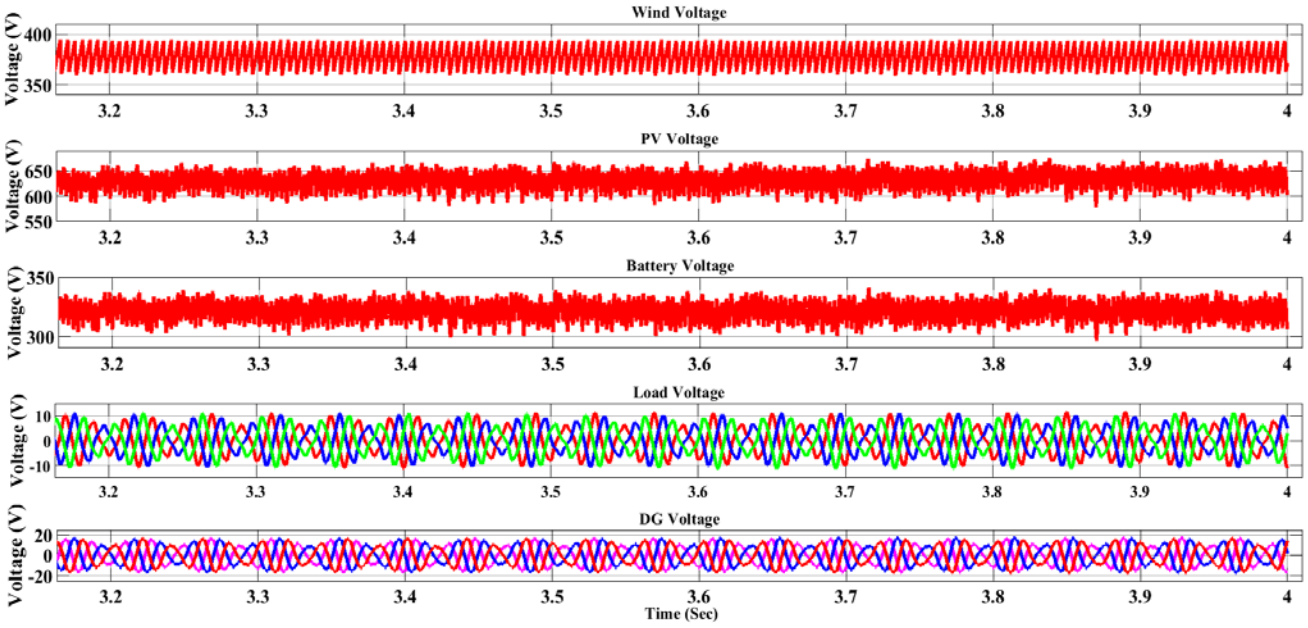

Figure 16: Voltage responses from wind, PV, Battery, Load, and DG module of IHMS for GO dispatch Strategy

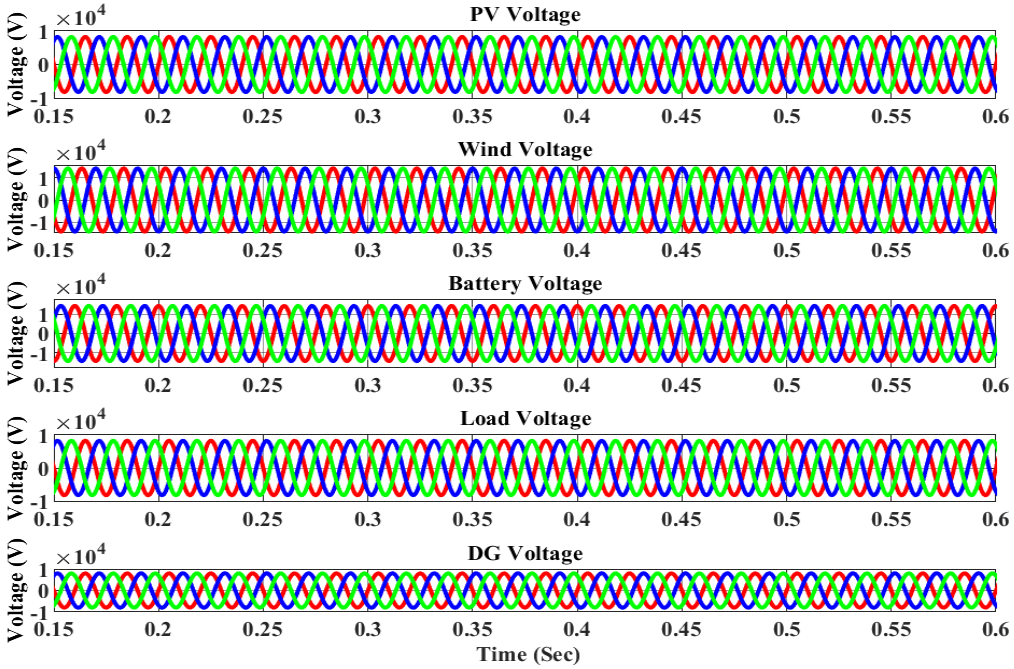

Figure 17: Voltage response from all modules with programmable three-phase voltage as a base case

5. CONCLUSIONS

To cope up with the increasing demand for electrical power, a renewable energy-based solar PV-wind turbine-diesel-battery islanded system has been designed. Analyzing the simulation results obtained under various dispatch strategies, the LF strategy can be stated as the most optimum dispatch technique based on the minimum CO_2 emission, NPC and LCOE. Because of having the maximum CO_2 emission, NPC and LCOE, the CD strategy can be concluded as the worst one. For dedicated loading, each component has been checked for frequency and voltage stability. The most optimal combinations of the components have been simulated and the combination having the highest efficiency has been selected. Matlab/Simulink analysis, according to the most optimal sizes, the frequency, and voltage responses, it can be said that the LF dispatch strategy performed as the best among others for the designed islanded hybrid microgrid. So, finally, it can be concluded that according to the brief studies of dispatch strategies in terms of optimal sizing, techno-economic analysis, and system stability of the designed IHMS, LF dispatch strategy has been proved as the most efficient dispatch technique in terms of economic, environmental and technical aspects. The proposed hybrid renewable off-grid energy model is especially applicable to

isolated and islanded areas. The optimal sizing of the generation sources while maximizing the renewables and their transient behaviour would be taken into consideration in future work.

ACKNOWLEDGEMENTS

The authors would like to express their gratitude to the Engineering Institute of Technology, Melbourne, Australia; Pabna University of Science and Technology, Pabna, Bangladesh; The University of New South Wales, Canberra, Australia; Universiti Teknologi PETRONAS, Perak, Malaysia; and Deakin University Faculty of Science Engineering and Built Environment, Geelong, Victoria, Australia. They also would like to thank the Editors and anonymous reviewers of the article for their insightful suggestions and comments to improve the content.

REFERENCES

Abdullah, M. A., Muttaqi, K. M., Sutanto, D., & Agalgaonkar, A. P. (2014). An effective power dispatch control strategy to improve generation schedulability and supply reliability of a wind farm using a battery energy storage system. *IEEE Transactions on Sustainable Energy*, *6*(3), 1093-1102.

Al-Hinai, A., Alyammahi, H., & Alhelou, H. H. (2021). Coordinated intelligent frequency control incorporating battery energy storage system, minimum variable contribution of demand response, and variable load damping coefficient in isolated power systems. *Energy Reports*, *7*, 8030-8041.

Al Busaidi, A. S., Kazem, H. A., Al-Badi, A. H., & Khan, M. F. (2016). A review of optimum sizing of hybrid PV–Wind renewable energy systems in oman. *Renewable and sustainable energy reviews*, *53*, 185-193.

Bakir, H., & Kulaksiz, A. A. (2020). Modelling and voltage control of the solar-wind hybrid micro-grid with optimized STATCOM using GA and BFA. *Engineering Science and Technology, an International Journal*, *23*(3), 576-584.

Bukar, A. L., & Tan, C. W. (2019). A review on stand-alone photovoltaic-wind energy system with fuel cell: System optimization and energy management strategy. *Journal of Cleaner Production*, *221*, 73-88.

Chowdhury, B. H. (1992). Optimizing the integration of photovoltaic systems with electric utilities. *IEEE Transactions on Energy Conversion*, *7*(1), 72-78.

Chowdhury, B. H., & Rahman, S. (1990). A review of recent advances in economic dispatch. *IEEE Transactions on power systems*, *5*(4), 1248-1259.

Chowdhury, B. H., & Taylor, C. W. (2000). Voltage stability analysis: VQ power flow simulation versus dynamic simulation. *IEEE Transactions on power systems*, *15*(4), 1354-1359.

Fatin Ishraque, M., Shezan, S. A., Ali, M. M., & Rashid, M. M. (2021). Optimization of load dispatch strategies for an islanded microgrid connected with renewable energy sources. *Applied Energy*, *292*, 116879. https://doi.org/https://doi.org/10.1016/j.apenergy.2021.116879

Ishraque, M. F., & Ali, M. M. (2021, 8-9 July 2021). Optimized Design of a Hybrid Microgrid using Renewable Resources Considering Different Dispatch Strategies. 2021 International Conference on Automation, Control and Mechatronics for Industry 4.0 (ACMI),

Ishraque, M. F., Ali, M. M., Arefin, S., Islam, M. R., Masrur, H., & Rahman, M. M. (2021, 26-30 Sept. 2021). Dispatch Strategy Based Optimized Design of an Offgrid Hybrid Microgrid Using Renewable Sources. 2021 31st Australasian Universities Power Engineering Conference (AUPEC),

Ishraque, M. F., Shezan, S. A., Nur, J. N., & Islam, M. S. (2021). Optimal Sizing and Assessment of an Islanded Photovoltaic-Battery-Diesel Generator Microgrid Applicable to a Remote School of Bangladesh. *Engineering Reports*, *3*(1), e12281.

Ishraque, M. F., Shezan, S. A., Rana, M. S., Muyeen, S. M., Rahman, A., Paul, L. C., & Islam, M. S. (2021). Optimal Sizing and Assessment of a Renewable Rich Standalone Hybrid Microgrid Considering Conventional Dispatch Methodologies. *Sustainability*, *13*(22), 12734. https://www.mdpi.com/2071-1050/13/22/12734

Ishraque, M. F., Shezan, S. A., Rashid, M. M., Bhadra, A. B., Hossain, M. A., Chakrabortty, R. K., . . . Das, S. K. (2021). Techno-Economic and Power System Optimization of a Renewable Rich Islanded Microgrid Considering Different Dispatch Strategies. *IEEE Access*, *9*, 77325-77340. https://doi.org/10.1109/ACCESS.2021.3082538

Kumar, J., Kumpulainen, L., & Kauhaniemi, K. (2019). Technical design aspects of harbour area grid for shore to ship power: State of the art and future solutions. *International Journal of Electrical Power & Energy Systems*, *104*, 840-852.

Liu, G., Jiang, T., Ollis, T. B., Zhang, X., & Tomsovic, K. (2019). Distributed energy management for community microgrids considering network operational constraints and building thermal dynamics. *Applied Energy*, *239*, 83-95.

Liu, W., Zhuang, P., Liang, H., Peng, J., & Huang, Z. (2018). Distributed economic dispatch in microgrids based on cooperative reinforcement learning. *IEEE transactions on neural networks and learning systems*, *29*(6), 2192-2203.

Ma, T., Yang, H., & Lu, L. (2014). A feasibility study of a stand-alone hybrid solar–wind–battery system for a remote island. *Applied Energy*, *121*, 149-158.

Nasr, M.-A., Rabiee, A., & Kamwa, I. (2020). MPC and robustness optimisation-based EMS for microgrids with high penetration of intermittent renewable energy. *IET Generation, Transmission & Distribution*, *14*(22), 5239-5248.

Obara, S. y., Sato, K., & Utsugi, Y. (2018). Study on the operation optimization of an isolated island microgrid with renewable energy layout planning. *Energy*, *161*, 1211-1225.

Qadrdan, M., Wu, J., Jenkins, N., & Ekanayake, J. (2013). Operating strategies for a GB integrated gas and electricity network considering the uncertainty in wind power forecasts. *IEEE Transactions on Sustainable Energy*, *5*(1), 128-138.

Sarangi, S., Sahu, B. K., & Rout, P. K. (2020). Distributed generation hybrid AC/DC microgrid protection: A critical review on issues, strategies, and future directions. *International Journal of Energy Research*, *44*(5), 3347-3364.

Shezan, S. A. (2019). Optimization and assessment of an off-grid photovoltaic–diesel–battery hybrid sustainable energy system for remote residential applications. *Environmental Progress & Sustainable Energy*, *38*(6), e13340.

Shezan, S. A., Hasan, K. N., & Datta, M. (2019). Optimal sizing of an islanded hybrid microgrid considering alternative dispatch strategies. 2019 29th Australasian Universities Power Engineering Conference (AUPEC),

Shezan, S. A., & Ishraque, M. F. (2019, 26-28 Sept. 2019). Assessment of a Micro-grid Hybrid Wind-Diesel-Battery Alternative Energy System Applicable for Offshore Islands. 2019 5th International Conference on Advances in Electrical Engineering (ICAEE),

Shezan, S. A., Ishraque, M. F., Muyeen, S. M., Arifuzzaman, S. M., Paul, L. C., Das, S. K., & Sarker, S. K. (2022). Effective dispatch strategies assortment according to the effect of the operation for an islanded hybrid microgrid. *Energy Conversion and Management: X*, *14*, 100192. https://doi.org/https://doi.org/10.1016/j.ecmx.2022.100192

Sinha, S., & Chandel, S. (2015). Review of recent trends in optimization techniques for solar photovoltaic–wind based hybrid energy systems. *Renewable and sustainable energy reviews*, *50*, 755-769.

Vergara, P. P., Rey, J. M., Shaker, H. R., Guerrero, J. M., Jørgensen, B. N., & Da Silva, L. C. (2018). Distributed strategy for optimal dispatch of unbalanced three-phase islanded microgrids. *IEEE transactions on smart grid*, *10*(3), 3210-3225.

Wang, G., Konstantinou, G., Townsend, C. D., Pou, J., Vazquez, S., Demetriades, G. D., & Agelidis, V. G. (2016). A review of power electronics for grid connection of utility-scale battery energy storage systems. *IEEE Transactions on Sustainable Energy*, *7*(4), 1778-1790.

Ye, L., Zhang, C., Tang, Y., Zhong, W., Zhao, Y., Lu, P., . . . Li, Z. (2019). Hierarchical model predictive control strategy based on dynamic active power dispatch for wind power cluster integration. *IEEE Transactions on power systems*, *34*(6), 4617-4629.

Zhang, Y., Gatsis, N., & Giannakis, G. B. (2013). Robust energy management for microgrids with high-penetration renewables. *IEEE Transactions on Sustainable Energy*, *4*(4), 944-953.

Zhao, B., Xue, M., Zhang, X., Wang, C., & Zhao, J. (2015). An MAS based energy management system for a stand-alone microgrid at high altitude. *Applied Energy*, *143*, 251-261.

Zhao, Z., Yang, P., Guerrero, J. M., Xu, Z., & Green, T. C. (2015). Multiple-time-scales hierarchical frequency stability control strategy of medium-voltage isolated microgrid. *IEEE transactions on power electronics*, *31*(8), 5974-5991.

MIJST
MIST International Journal of Science and Technology

Logical analysis of built-in DBSCAN Functions in Popular Data Science Programming Languages

Md Amiruzzaman[1*], Rashik Rahman[2], Md. Rajibul Islam[3], and Rizal Mohd Nor[4]

[1]West Chester University, West Chester, PA, USA
[2,3]University of Asia Pacific, Dhaka, Bangladesh
[4]International Islamic University Malaysia, Kuala Lumpur, Malaysia

emails: [1]*m.amiruzzaman@gmail.com;* [2]*17201012@uap-bd.edu;* [3]*md.rajibul.islam@uap-bd.edu; and* [4]*rizalmohdnor@iium.edu.my*

ARTICLE INFO

Article History:

Received: 21st March 2022
Revised: 21st May 2022
Accepted: 23rd May 2022
Published online: 26th June 2022

Keywords:

Clustering
DBSCAN
Geo-coordinates
Machine learning
Spatial

ABSTRACT

DBSCAN algorithm is a location-based clustering approach; it is used to find relationships and patterns in geographical data. Because of its widespread application, several data science-based programming languages include the DBSCAN method as a built-in function. Researchers and data scientists have been clustering and analyzing their study data using the built-in DBSCAN functions. All implementations of the DBSCAN functions require user input for radius distance (i.e., eps) and a minimum number of samples for a cluster (i.e., min_sample). As a result, the result of all built-in DBSCAN functions is believed to be the same. However, the DBSCAN Python built-in function yields different results than the other programming languages those are analyzed in this study. We propose a scientific way to assess the results of DBSCAN built-in function, as well as output inconsistencies. This study reveals various differences and advises caution when working with built-in functionality.

1. INTRODUCTION

Identifying and classifying classes in the spatial domain is a common practice in many investigations. For example, research such as Rizvee et al., (2021) for locating accident-prone locations and Islam et al., (2021) for locating densely populated areas. The Density-Based Spatial Clustering of Applications with Noise (i.e., DBSCAN) is a clustering approach for location-based data. The DBSCAN clustering method locates the neighboring points of a given spatial point and groups the neighbors if they meet multiple clustering requirements within the given adjacent distance (Amiruzzaman, et al., 2021).

Clustering in the spatial realm can be useful in a variety of applications. DBSCAN is commonly used for clustering in planar space. It can produce reasonable results when used to map the impact of natural catastrophes or to plot the position of weather stations in a city. It can also be utilized when the data is made up of non-discrete points and has outliers. DBSCAN is used by many systems nowadays that provide recommendation services, such as a Recommender engine, to propose goods or things to its clients. It is also utilized to identify typical events, such as finding areas where frequent road accidents occurred, in other applications (Rizvee et al., 2021; Amiruzzaman et al., 2018).

Clustering techniques is one of the most renowned, powerful, and widely used unsupervised learning approaches in data mining (Berry et al., 2019). This is a way of classifying comparable or similar data members into a set or group based on some preset resemblance (Fischer et al., 2003). Some real-world uses of clustering include book sorting in a library, consumer segmentation in marketing, and fraud detection in insurance (Mahmoudi et al., 2020). Larger challenges, such as seismic analysis or perhaps urbanization analysis, may benefit from clustering as well. According to (Limwattanapibool et al., 2017), clustering algorithms are classified into seven types: (i) hierarchical clustering algorithms, (ii) graph-based algorithms, (iii) density-based clustering algorithms, (iv) partitioning clustering algorithms, (v) model-based clustering algorithms, (vi) combinational clustering algorithms, and (vii) grid-based algorithms. Among them, the DBSCAN method is widely used as an unsupervised machine learning techniques, that is taken into account for this study (i.e., in the spatial domain).

Although, the most clustering approaches in the literature, for example, k-means (Macqueen et al., 1967; Islam et al., 2021), Single-Linkage clustering (SLINK) (Sibson et al., 1973), and other centroid-based clustering approaches, share computational similarities, they are not powerful or

adaptable enough to be considered in a wide range of clustering use. These are recognized for their capacity to recognize clusters of any form (Wu et al. 2014). They are, however, susceptible to noise and have the major limitation of recognizing groups based on only density and data points spherical-shaped clusters (Jain et al., 2010).

In this case, DBSCAN appears to be a promising solution to several clustering issues. It contrasts in a number of ways (Amiruzzaman, et al., 2021). It classifies clusters based on the density of data members in their feature space as a substitute of the position of the computed centroids like k-means does (Dudik et al., 2015). These provide more exact evidence of identification and segregation of clusters of varying sizes and forms, particularly when they form a shape of a convex clusters of data. DBSCAN's ability to extract noisy data members or outliers make them stand out from other algorithms (Luchi et al., 2019). Importantly, rather than arbitrarily selecting the first positions of the cluster centroids, the DBSCAN method employs a deterministic approach (Handra et al., 2011). This paper's contributions are as follows:

- Present a methodology as to how a built-in function can be compared among different programming languages.
- Provide comparable results obtained from the experiment.
- Provide visual output as evidence for easier exploration.
- Provide implications and detailed discussion on the evidence.

A. Motivation

The DBSCAN method is a well-known technique for grouping geographical data. Nevertheless, there are several programming languages, and virtually almost all of the languages provide built-in functions that can help with user data clustering. Often, programmers utilize these built-in functions in good faith in order to avoid inventing difficult procedures or algorithms on their own (Cranor et al., 1994; Ramalho et al., 2015).

Commonly Java implementation of DBSCAN can be found in Apache Common Math and Environment for DeveLoping KDD-Applications Supported by Index-Structures (ELKI). C++ implementation can be found in mlpack and pyclustering. In python, DBSCAN is included in the scikit-learn or sklearn library and R contains a package for DBSCAN. There are applications like Weka and SPMF that provide their implementation of DBSCAN.

There are few studies that demonstrate a systematic review of such built-in functions to offer a technique to identify similarities and variations in the outcomes produced by the accessible libraries (Amiruzzaman, et al., 2021). This study aims to address a necessity in evaluation-based studies by demonstrating a methodical approach of evaluating built-in functionalities.

B. Objective

The goal of this study was to explore how the built-in DBSCAN algorithm provides output, and if the obtained outputs from different programming languages are comparable. We wanted to see where similarities and differences lies in the output obtained from different implementations of DBSCAN. We focused on following research questions for this study:

- Are there any differences in clustering results produced by DBSCAN built-in clustering among data science based programming languages, when the same parameter values are used?
- If there are any differences in results and similarities, then which ones are providing pairing results?

2. RELATED WORK AND USE OF DBSCAN IN EXISTING STUDIES

In computer science, there are different cluster methods for class identification (Amiruzzaman, et al., 2021). Since we have more than one algorithm, hence we must select the one that fits the dataset and offers most optimal result. Performance analysis allows us to select the best algorithm from a set of algorithms to solve a problem. There is indeed a large number of study in the literature on the comparative investigation of DBSCAN. In one study, authors examined the performance of DBSCAN and concluded that the DBSCAN clustering technique does not scale well for big datasets (Gan & Tao, 2015). While studying deep learning clustering approaches for bioinformatics, Karim et al. (2020) utilized DBSCAN to compare several clustering methods in a different study. Particularly, Karim compared machine learning approaches in clustering algorithms such as K-means, DBSCAN, OPTICS which is an extension of DBSCAN, GMM, AC and the Partial Mix Model (PMM). For each algorithm, Karim describes the parameters being used, scalability of sample sizes, geometry used for calculating distances, its use cases in bioinformatics and its limitations. Among its notable limitations for DBSCAN is the difficulty of separating nearby clusters and the quadratic computational complexity. However, he also noted that it is a good algorithm for uneven cluster size with non-flat geometry and hence used in many bioinformatics analysis.

Many essential criteria, for example, the accuracy of the result, precision, recall values, the complexity of the algorithm, and others, can be found in the existing works that have been used to appraise the DBSCAN clustering algorithm's performance (Zhou et al., 2000). Schubert et al. (2017) presented a strong argument about why we should still use DBSCAN as a rebuttal to a previous paper misrepresenting DBSCAN of having poor performance. In Schuberts argument, he explains that choosing the right parameters is important to achieve both meaningful results and good performance. Schubert conducted experiments to show that other suggested methods do not appear to offer practical benefits if the DBSCAN parameters are well chosen and thus they are primarily of theoretical interest. Schubert concluded that the original DBSCAN algorithm with effective indexes and reasonably chosen parameter values performs competitively compared to the method proposed by others claiming to achieve better results. Clearly, DBSCAN remains relevant in many scientific

research work and requires constant revision on how we use DBSCAN to achieve meaningful results.

There are several software libraries or tools available, and most of those provide built-in functions that aid with consumer data clustering. Authors of an existing study described several clustering techniques as well as the software packages/tools associated with such approaches (Oyelade et al., 2016).

Often, data technologists, programmers, and academics rely on these built-in clustering functions and avoid constructing difficult algorithms (Amiruzzaman, et al., 2021). Nevertheless, there is a scarcity of research that compares the built-in functionalities offered by various software packages/tools' libraries. This research sought to address a gap in evaluation-based studies by demonstrating a systematic approach to evaluating built-in functionalities. Figure 1 depicts how many articles in the last 7 years employed the DBSCAN technique in their study. The data shown in Figure 1 was collected in May of 2022.

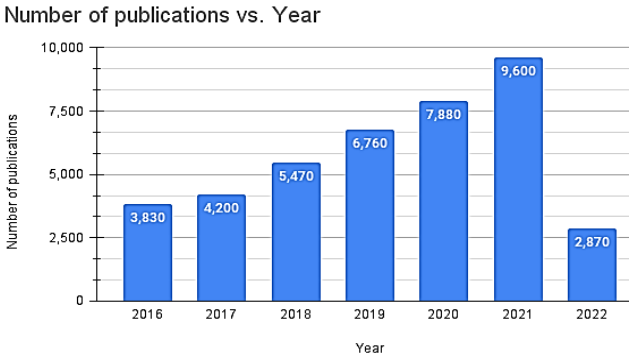

Figure 1. The DBSCAN algorithm used in studies over the last 7 years

For example, 3830 papers published in 2016 used DBSCAN as an analysis or as a clustering tool. Subsequently, in 2017, 4,200 papers were published that somehow used DBSCAN in their work. Furthermore, there were 5,470 papers in 2018, 6,760 papers in 2019, 7,880 papers in 2020, and 9,600 papers in 2021. Most interestingly, in 2022 (up to mid-May 2022), 2,870 papers used the DBSCAN algorithm. These results are based on a search in Google scholar using the keywords "BDSCAN as an analysis tool". Perhaps, in reality, these numbers may change slightly, however, these numbers give us an idea about how popular the DBSCAN algorithm is in data-science-related studies or clustering in general. From Figure 1, it is evident that the popularity of the DBSCAN algorithm is experiencing an upward trend. As shown in Figure 1, by the end of the year 2022, the search quantity may exceed that of the previous year. Research related to DBSCAN is showing an increasing trend, so it is very important to justify various approaches to the DBSCAN algorithm.

3. METHOD

A. Opening discussion

DBSCAN clustering algorithm helps in computing distances in between points of data given and outputs high density cluster areas. The focus for DBSCAN clustering is highly dependent on neighborhood computation. Generally, the computations as follows: a point p_1 is said to be the neighbor of another point p_2, *iff* p_1 and p_2 are located less than or equal to the radius distance of *eps* distance. This computational process continues discovering other points, p_1 and p_2 which are neighbors and these points form a cluster if they meet the goal of min_sample or minPts (see Figure 2).

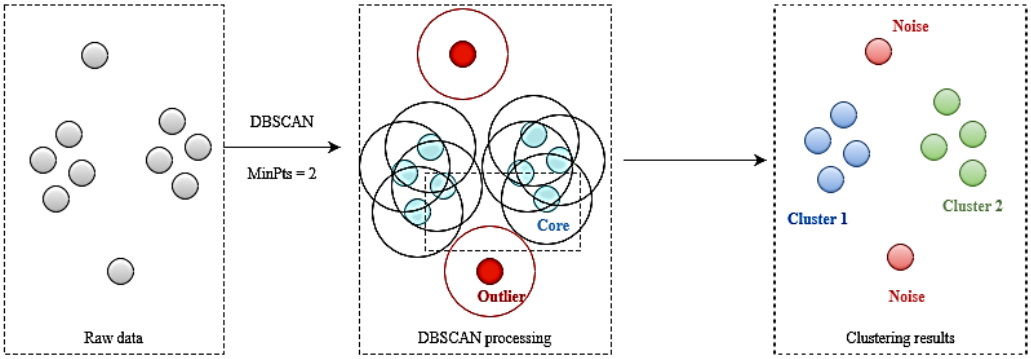

Figure 2. Working procedure of DBSCAN algorithm

Based on the above discussion the DBSCAN algorithm depends on two basic parameters:

- **minPts (min_sample):** The minimum number of points to form a cluster.
- **eps (ε):** The minimum distance to form a neighboring relationship among points.

Throughout this study of DBSCAN clustering algorithms, numerous programming languages were utilized to compare the accuracy, consistency and reliability of the DBSCAN clustering algorithm implemented. Particularly, we were interested in producing the same results despite the programming language given, hence a similar approach to Ester et al, 1996 was taken to discover clusters in large spatial databases with noise. In doing so, we also took the approach of Davies-Bouldin (Davies et al., 1979) and Silhouette Coefficient (Rousseeuw et al., 1987) by first calculating the appropriate number of clusters. Consequently, we employed seven distinct geo-coordinate location coordinates from Lexington, North Carolina, United States (refer to Table 1) with the use of four different computer languages, which includes the Python programming language. Also, we considered other languages, such as the, R programming language, Javascript, and Postgres with the postgis library.

As for the selection of geo-coordinates, points were selected using a pseudo-random generator as suggested by most researchers in literature to enhance the validity of the research (Niemierko *et al.*, 1990). As a recall to what was mentioned, the DBSCAN clustering algorithm attempts to group data points together provided that they are neighbors and within a certain distance (ε). It can best be described mathematically in the equation below (see Equation (1)) that determines if two data points are within the same neighborhood.

$$N_\epsilon(p1): \{p2 | d(p1, p2) \leq \epsilon\} \quad (1)$$

Using the spatial distance denoted as *d*, and the provided distance *ε*, the function $N_\varepsilon(.)$ attempts to identify whether coordinate point p_1 and coordinate point p_2 are considered to be neighbors. If coordinate point p_1 and coordinate point p_2 is less than ε, then p_1 and p_2 are considered as neighbors. It is common that the DBSCAN method requires at least 2 parameters, such as *epsilon* and *MinPts*. To be consistent with our study, we employed identical parameters for all of the above-mentioned programming languages for our experiments. Therefore, for brevity, it is enough to say that all epsilon and MinPts, for all programming languages studied, are identical.

To determine the 2D space distance, it is pretty common practice to use Euclidean distance as a method for measurement. The Euclidean distance between two points can be calculated as such, consider point (x_1, y_1) denoted as p_1 and point (x_2, y_2) denoted as p_2, then the Euclidean distance may be calculated as follows:

$$d = \sqrt{((x2 - x1)^2 + (y2 - y1)^2)} \quad (2)$$

where *d* denotes the distance between two points, which is p_1 and p_2.

In some other occasions, Haversine distance is largely preferred. This is usually the case when it is necessary to take into consideration the distance between two geo-coordinates that are intersecting with the circumference line of the circle or the circumference of the sphere. While Haversine is particularly more accurate for distances between two points on earth, it is not always used since planar distances may not have any curvatures, or it is too small of a distance to provide significant differences. It is for this reason that the Haversine formula is frequently utilized in spatial distance calculations as opposed to Euclidean distances. The Haversine distance may be calculated as follows:

$$d = r\, sin^{-1}\left(\sqrt{\sin^2\left(\frac{y2-y1}{2}\right) + \cos(y1)\cos(y2)\sin^2\left(\frac{x2-x1}{2}\right)}\right) \quad (3)$$

where, the notation *d* represents the distance between two geo-locations, such as point p_1 and point p_2, here note that *r* represents the radius of the earth, which is approximately 6371 km, x_1, x_2 are longitude, and y_1, y_2 are latitude values in spatial coordinates. It is important to note that the Haversine distance calculation approach is inconsequential when geo-locations are not spacious enough with each other (Prasetya *et al.*, 2020). This means that when distances between the data points in terms of their geo-coordinates are not spacious enough from each other, then the consequence of the great-circle effect can be forgiven.

Table 1
Data used in experiment, detail of the data presented in section 4(A)

Position	latitude	longitude
0	44.9438	-76.1083
1	44.9414	-76.1073
2	44.9427	-76.0940
3	44.9396	-76.0897
4	44.9383	-76.0850
5	44.9384	-76.0817
6	44.9549	-76.0814

In this study, we conducted our first experimental observation with grouped data from Table 1. The programming languages Python, Postgis, R, and JavaScript were used as tools for our experiment. Firstly, we calculated the matrix of distances between all seven coordinates (see Table 1) and revealed that the geolocations were in the middle for index 4 and index 5, which was exactly 284 meters or 0.284 kilometers as in Table 2. As a result, we selected eps = 0.00548 and min sample = 2 as configuration 1 and eps = 0.00548, min samples = 5 is selected as configuration 2. Figure 3(A) and Figure 3(B) shows a map visualization of clusters with configuration 1 and 2 respectively. The mapview visualization was used to cross-check the obtained results. The corresponding mapview was then transformed to the eps value to match the eps with meter space as the circle's radius. The circles indicate which surrounding points are within its eps range and should be treated as a cluster neighbor (see Equation (1)). It should be noted that eps is the ε as specified in Equation (1).

Table 2
Obtained distance matrix based on the data presented in Table 1

Index	0	1	2	3	4	5	6
0	0.000000	0.282715	1.128214	1.537755	1.935583	2.180580	2.450144
1	0.282715	0.000000	1.053958	1.399959	1.790722	2.044759	2.534211
2	1.128214	1.053958	0.000000	0.488360	0.866289	1.085500	1.682116
3	1.537755	1.399959	0.488360	0.000000	0.398247	0.645561	1.825003
4	1.935583	1.790722	0.866289	0.398247	0.000000	0.260446	1.866630
5	2.180580	2.044759	1.085500	0.645561	0.260446	0.000000	1.833376
6	2.450144	2.534211	1.682116	1.825003	1.866630	1.833376	0.000000

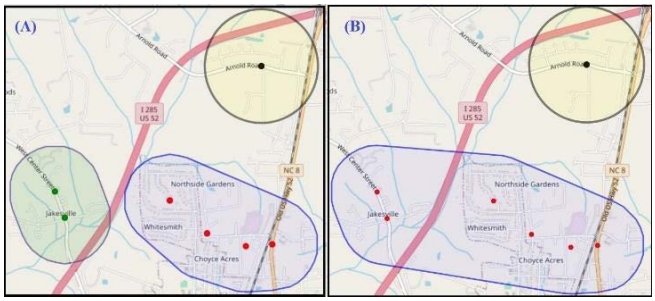

Figure 3. Two different results: (a) results obtained by configuration 1 with other languages, (b) results obtained by configuration 1 and 2 with python's DBSCAN.

4. RESULTS

A. *Investigation 1*

i. *Analysis using Python*

The "sklearn" package of the Python programming language has a built-in DBSCAN function. In general, there are several parameters used in this function. However, often the majority of the settings are not set by the users, which means those are set to the default system values and so no user input is required. However, the parameters eps (the distance between two points), minimum number of samples (i.e., number of samples required to be classified as a cluster), and the standard metric scale (the metric scale used for distance calculation) were changed for this study. Data used in this experiment is presented in Table 1. We noticed one cluster and an outlier using both configurations. However, according to the other programming languages, they consider all the data points as outliers for configuration 2 and only make two clusters and an outlier for configuration 1 as shown in Figures 5(a) and 5(b). Only the built-in function of Python demonstrates the same outcome for both configurations.

ii. *Analysis using Postgis*

The experimental data used in this study is presented in Table 1, where we used eps = .00548, and then the min_sample = 2. The clustering results we discovered were two clusters and an irregular that is an outlier data point.

iii. *Analysis using JavaScript*

Data used in this experiment presented in Table 1, we used eps = 0.00548, and as for min_sample = 2.0. The obtained result indicated that there are two clusters and an outlier (see Figure 4).

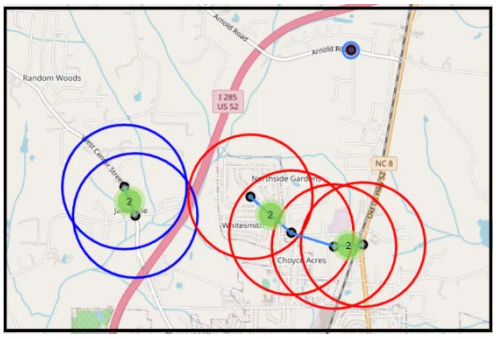

Figure 4. Clustering results obtained from JavaScript's DBSCAN function

iv. *Analysis using R*

Using the given data from Table 1, with the same configuration of eps = 0.00548, and parameter min_sample = 2.0, we discovered two clusters and an irregular outlier. Later on, we repeated our configuration with eps = 0.00548 and the parameter min sample = 5 and discovered that if the cluster needs at least 5 minimum points to form, then it decides to label all the data points as outliers.

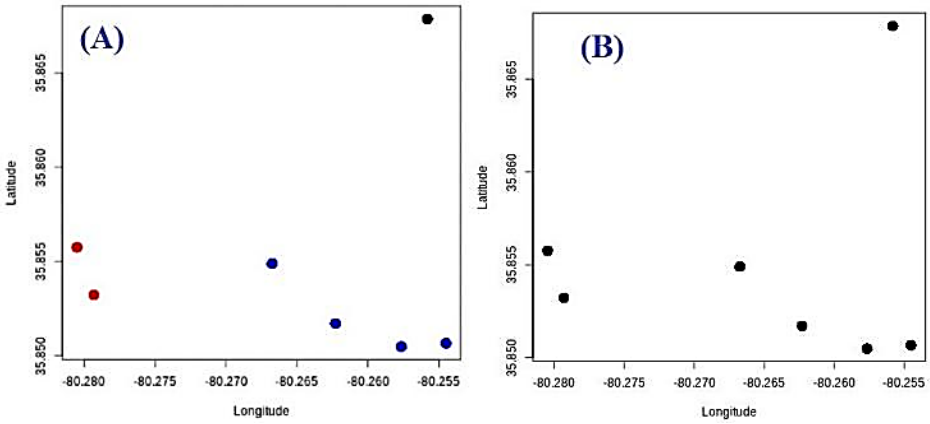

Figure 5. Results were obtained from all the other programming languages except python considering (a) configuration 1 and (b) configuration 2

B. *Investigation 2*

We conducted a second experimental observation to acquire further evidence. In contrast to previous experiments, in the second experiment, we used all four programming languages to evaluate the results of the DBSCAN clustering function. In the second trial, the settings were eps = 0.00548 and min sample = 2.0. Table 3 displays the obtained results. Table 3 shows the cluster findings based on the experimental data shown in Table 1.

C. *Investigation 3*

In the third experimental observation, the built-in function of sklearn was reevaluated, and the intention was to find the reason why the function was not providing the same results as other languages. For spatial data, often degree and radian concepts are used, so, for the sake of analysis, the longitude and latitude values were converted to radians and then passed in the built-in function of sklearn.

Table 3
Experimental results from different programming languages (data used in this experiment is presented in Table 1)

Language name	Results with configuration 1	Results with configuration 2
Python	Two clusters with an outlier	Two clusters with an outlier
Postgis	Two clusters with an outlier	All data points are outliers.
Javascript	Two clusters with an outlier	All data points are outliers.
R	Two clusters with an outlier	All data points are outliers

This time, the built-in function provided the same result as other languages. So, the evidence from this study suggests that sklearn's DBSCAN function requires radians as input, unlike other languages. So, despite the similar parameter settings, sklearn's built-in function requires different types of input than the rest of the languages (see Figure 6).

Figure 6. Clustering results from Sklearn's DBSCAN function. (a) Shows results before converting to radians, and (b) shows the results after converting to radians

5. EVALUATION

Further, publicly accessible data was utilized to evaluate the built-in functions. The locations of all countries' names, as well as the associated latitude and longitude numbers, were contained in the publicly available data. The data was obtained from Google data (Google: Dataset publishing language). The specifications utilized in the assessment study were eps = 0.9000009 and min_sample = 4 which is considered configuration 3. Figure 7 depicts the obtained results. According to the evidence, JavaScript, R, and Postgis produced identical outcomes. The programming language Python, on the other hand, produced a different outcome (see Figure 8). In Python, the findings shown in Figure 4 exhibited just a cluster but no outliers. However, the aesthetic map in Figure 3 demonstrates that there seemed to be just four geospatial information in a cluster, with the remainder being outliers. To validate the countries' records, we created a distance matrix among all geospatial data, and the findings showed that only four geospatial data might as well have produced a cluster, as seen in Figure 7.

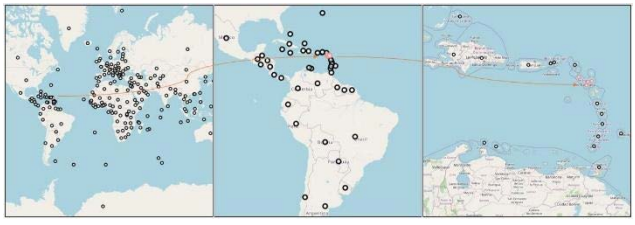

Figure 7. Clustering result: A single cluster formed using four geo-locations (i.e., red markings) and the rest geolocations did not form any cluster (i.e., those are considered as outliers)

Figure 8. Clustering results on the world map, center of each countries and territories are used in the experiment to cluster them

Figure 7 and Figure 8 uses configuration 3 to form clusters where the clusters illustrated in Figure 7 is the output of PostGis, R, and JavaScript implementations of DBSCAN, and Figure 8 is the output of Python's implementation of DBSCAN. This variation may be caused due to Python's built-in function requiring a different type of input, namely radian input as the eps than the rest of the languages (see Figure 6).

6. DISCUSSION

Numerous software engineers and specialists have faith in using the functions of the integrated library and regularly use them to acquire research results and take care of issues (Hao *et al*., 2019). Applications of such built-in library functions (e.g. DBSCAN algorithm) can be found in several exploration studies. DBSCAN is one of the well-known spatial data algorithms (Hahsler *et al*., 2019). However, as far as we know, no such research exists that compares and evaluates DBSCAN's implementation across all platforms. Usually, researchers rely solely on the built-in DBSCAN function (Hao *et al*., 2019). Hence, research to assess DBSCAN algorithms integrated into numerous programming languages or platforms was long overdue. This analysis looks at how the DBSCAN algorithm performed in several languages, for example, R, Python, R, JavaScript, and PostGis. And the identical hyper-parameters, for example, eps, and min_points were used to accomplish this.

Built-in DBSCAN functions in three computer languages, including R, Postgis, JavaScript, and R, appear to provide the same findings. Conversely, the Python language's built-in function appears to produce results that differ from those of other languages. As a result, the study advises researchers to exercise caution while using the built-in DBSCAN tool. Perhaps researchers should experiment with different languages for spatial clustering. The implementation of Python's built-in DBSCAN function was not covered by this study. DBSCAN implementations in other programming languages should be compared in a future study.

The Python programming language's dissimilarity might be attributed to the unit of the eps value (Starczewski et al., 2019). Evidence reveals that the eps value is used in degree distance by three programming languages: JavaScript,

Postgis, and R. As a result, in Python, the eps value is not in degrees. One possible cause is that Python's eps unit is measured in radians (Boeing et al., 2018). According to the authors of research (Boeing et al., 2018), the Python language library use the eps value in radian distance. This, on the other hand, should not have happened. As a result, the Python implementation will be distinct from other implementations.

7. CONCLUSIONS

In this paper, we assessed the built-in DBSCAN function in a variety of computer languages, including R, Python, Javascript, and PostGIS. The input numbers and parameters used to perform these comparisons were identical in each case. Our results reveal that the Python scikit-learn DBSCAN implementation generates conflicting outcomes than the other implementations. As demonstrated in the benchmark section, DBSCAN of scikit-learn prefers to group all of the geospatial data from publicly accessible countries csv into one cluster, whereas built-in DBSCAN of PostGis only groups four geospatial data from all data points into one cluster.

This inexplicable response of DBSCAN's Python implementation verifies our assumption that "we should not simply entrust the results of built-in functions undoubtedly," and this investigation backs this up. According to our study, scikit-learn's DBSCAN implementation has a high level of abnormality, whereas all other platforms produce similar results when the same parameters are used. DBSCAN is used to cluster geospatial data, so the clustering should be the same across all platforms. Despite the fact that all of the other platforms clusters identically and properly, scikit-learn's DBSCAN performs completely differently as well as turns as an outlier when equated to the other programming languages. The next step will be to identify the elements that influence Python's Scikit-learn outcomes.

According to the findings from this investigation, the eps (i.e., ε) value in DBSCAN functions across many programming languages is in degree; particularly the ones investigated in this study. Apparently, it appears to be ineffective for Python's installed DBSCAN algorithm. Furthermore, there is no clear information on the Python official website regarding the unit of eps [32]. In the integrated DBSCAN function, a deeper analysis may look at how many past researches utilized degree as an eps unit against how many utilized radian as an eps unit.

ACKNOWLEDGEMENTS

The part of this research was supported by the Institute of Energy, Environment, Research, and Development (IEERD, UAP), the University of Asia Pacific. Md Amiruzzaman was supported by West Chester University tenure-track faculty start-up grand.

REFERENCES

Amiruzzaman, M. (2018, November). Prediction of traffic-violation using data mining techniques. In *Proceedings of the Future Technologies Conference* (pp. 283-297). Springer, Cham.

Amiruzzaman, M., Rahman, R., Islam, M. R., & Nor, R. M. (2021, November). Evaluation of DBSCAN algorithm on different programming languages: An exploratory study. In *2021 5th International Conference on Electrical Engineering and Information & Communication Technology (ICEEICT)* (pp. 1-6). IEEE.

Berry, M. W., Mohamed, A., & Yap, B. W. (Eds.). (2019). *Supervised and unsupervised learning for data science*. Springer Nature.

Boeing, G. (2018). Clustering to reduce spatial data set size. *arXiv preprint arXiv:1803.08101*.

Cranor, L. F. (1994). Programming perl: an interview with larry wall. *XRDS: Crossroads, The ACM Magazine for Students*, *1*(2), 10-11.

Clustering algorithms: their application to gene expression data. *Bioinformatics and Biology insights*, *10*, BBI-S38316.

Dudik, J. M., Kurosu, A., Coyle, J. L., & Sejdić, E. (2015). A comparative analysis of DBSCAN, K-means, and quadratic variation algorithms for automatic identification of swallows from swallowing accelerometry signals. *Computers in biology and medicine*, *59*, 10-18.

Davies, D., & Bouldin, D. (1979). A cluster separation measure, IEEE transactions on patter analysis and machine intelligence. vol.

Ester, M., Kriegel, H. P., Sander, J., & Xu, X. (1996, August). A density-based algorithm for discovering clusters in large spatial databases with noise. In *kdd* (Vol. 96, No. 34, pp. 226-231).

Fischer, B., & Buhmann, J. M. (2003). Path-based clustering for grouping of smooth curves and texture segmentation. *IEEE Transactions on Pattern Analysis and Machine Intelligence*, *25*(4), 513-518.

Gan, J., & Tao, Y. (2015, May). DBSCAN revisited: Mis-claim, un-fixability, and approximation. In *Proceedings of the 2015 ACM SIGMOD international conference on management of data* (pp. 519-530).

Google: Dataset publishing language. https://developers.google.com/public-data/docs/canonical/countriescsv, accessed: 2021-01-12.

Handra, S. I., & Ciocârlie, H. (2011, May). Anomaly detection in data mining. Hybrid approach between filtering-and-refinement and DBSCAN. In *2011 6th IEEE International Symposium on Applied Computational Intelligence and Informatics (SACI)* (pp. 75-83). IEEE.

Hao, J., & Ho, T. K. (2019). Machine learning made easy: a review of scikit-learn package in python programming language. *Journal of Educational and Behavioral Statistics*, *44*(3), 348-361.

Hahsler, M., Piekenbrock, M., & Doran, D. (2019). dbscan: Fast density-based clustering with R. *Journal of Statistical Software*, *91*(1), 1-30.

Islam, M. R., Jenny, I. J., Nayon, M., Islam, M. R., Amiruzzaman, M., & Abdullah-Al-Wadud, M. (2021, August). Clustering Algorithms to Analyze the Road Traffic Crashes. In *2021 International Conference on Science & Contemporary Technologies (ICSCT)* (pp. 1-6). IEEE.

Jain, A. K. (2010). Data clustering: 50 years beyond K-means. *Pattern recognition letters*, *31*(8), 651-666.

Karim, M. R., Beyan, O., Zappa, A., Costa, I. G., Rebholz-Schuhmann, D., Cochez, M., & Decker, S. (2021). Deep learning-based clustering approaches for bioinformatics. *Briefings in Bioinformatics*, *22*(1), 393-415.

Limwattanapibool, O., & Arch-int, S. (2017). Determination of the appropriate parameters for K-means clustering using selection of region clusters based on density DBSCAN (SRCD-DBSCAN). *Expert Systems*, *34*(3), e12204.

Luchi, D., Rodrigues, A. L., & Varejão, F. M. (2019). Sampling approaches for applying DBSCAN to large datasets. *Pattern Recognition Letters*, *117*, 90-96.

Mahmoudi, M. R., Baleanu, D., Mansor, Z., Tuan, B. A., & Pho, K. H. (2020). Fuzzy clustering method to compare the spread rate of Covid-19 in the high risks countries. *Chaos, Solitons & Fractals*, *140*, 110230.

MacQueen, J. (1967, June). Some methods for classification and analysis of multivariate observations. In *Proceedings of the fifth Berkeley symposium on mathematical statistics and probability* (Vol. 1, No. 14, pp. 281-297).

Niemierko, A., & Goitein, M. (1990). Random sampling for evaluating treatment plans. *Medical physics*, *17*(5), 753-762.

Oyelade, J., Isewon, I., Oladipupo, F., Aromolaran, O., Uwoghiren, E., Ameh, F., ... & Adebiyi, E. (2016).

Prasetya, D. A., Nguyen, P. T., Faizullin, R., Iswanto, I., & Armay, E. F. (2020). Resolving the shortest path problem using the haversine algorithm. *J. Crit. Rev*, *7*(1), 62-64.

Rizvee, M. M., Amiruzzaman, M., & Islam, M. R. (2021). Data Mining and Visualization to Understand Accident-Prone Areas. In *Proceedings of International Joint Conference on Advances in Computational Intelligence* (pp. 143-154). Springer, Singapore.

Rousseeuw, P. J. (1987). Silhouettes: a graphical aid to the interpretation and validation of cluster analysis. *Journal of computational and applied mathematics*, *20*, 53-65.

Ramalho, L. (2015). *Fluent Python: Clear, concise, and effective programming*. " O'Reilly Media, Inc.".

Sibson, R. (1973). SLINK: an optimally efficient algorithm for the single-link cluster method. *The computer journal*, *16*(1), 30-34.

Schubert, E., Sander, J., Ester, M., Kriegel, H. P., & Xu, X. (2017). DBSCAN revisited, revisited: why and how you should (still) use DBSCAN. *ACM Transactions on Database Systems (TODS)*, *42*(3), 1-21.

Starczewski, A., & Cader, A. (2019, June). Determining the EPS parameter of the DBSCAN algorithm. In *International Conference on Artificial Intelligence and Soft Computing* (pp. 420-430). Springer, Cham.

sklearn.cluster.dbscan,"https://scikit-learn.org/stable/modules/generated/sklearn.cluster.DBSCAN.html, accessed: 2021-01-22.

Wu, C. H., Ouyang, C. S., Chen, L. W., & Lu, L. W. (2014). A new fuzzy clustering validity index with a median factor for centroid-based clustering. *IEEE Transactions on Fuzzy Systems*, *23*(3), 701-718.

Zhou, A., Zhou, S., Cao, J., Fan, Y., & Hu, Y. (2000). Approaches for scaling DBSCAN algorithm to large spatial databases. *Journal of computer science and technology*, *15*(6), 509-526.

MIJST
MIST International Journal of Science and Technology

Cascaded Fuzzy Logic for Adaptive Cruise Control

Milan Simic

School of Engineering, RMIT University, Australia

emails: *milan.simic@rmit.edu.au*

ARTICLE INFO

Article History:

Received: 16th November 2021
Revised: 18th May 2022
Accepted: 23rd May 2022
Published online: 26th June 2022

Keywords:

Fuzzy logic control
Adaptive cruise control
Cascade controller
Road vehicles
Driver assistance

ABSTRACT

Application of fuzzy logic is a powerful approach that could be applied in a large number of disciplines, starting with engineering control systems, as shown here, but also in other business areas. After a short introduction to fuzzy logic, its application for adaptive cruise control (ACC) is presented. ACC is a driver assistance feature that deals with the problem of speed control, while keeping the safe distance from the vehicle ahead. In the hierarchy of autonomous vehicles autonomy levels, as defined by Society of Automotive Engineers (SAE) International, adaptive cruise control appears in the vehicles at the level 1 and above. We developed a fuzzy logic controller where controlled variables are speed and distance. Input variables include weather conditions, style or mode of driving, vehicle speed and steering angle. A large number of input variables improve control but lead to a large fuzzy rules table. Because of that, in the design presented here, a tree of connected fuzzy inference systems (FIS) is applied. Fuzzy inference systems with a smaller number of variables are developed, algorithms explained, rule base defined, and obtained control surfaces presented. This approach requires less processing time enabling real time applications. Since the rules are defined based on drivers' experiences, fuzzy logic control systems make decisions in the same way as humans do, i.e., as experience drivers. This paper gives a comprehensive presentation of a novel cascaded fuzzy system development. This novel design also involves algebraic subtraction performed through a FIS subsystem.

1. INTRODUCTION

Fuzzy logic is a relatively new way of thinking and application development compared to well-known Boolean logic. It is established in the last century, by Lotfi A. Zadeh (Zadeh, 1965). That is 118 years after George Boole published, for the first time, his book *The Mathematical Analyses of Logic*, reprinted later (Boole, 2009). Boolean algebra is used to express and analyse operations of logic gates. Claude Shannon first applied Boolean algebra to analyse and design logic circuits (Shannon, 1938).

While in Boolean algebra, the values of variables could be just *true*, or *false*, expressed as integer values of 1 or 0, in fuzzy logic, values of variables are real numbers ranging between 0 and 1, including them. This enables fuzzy logic to be applied in control system design when input information is unreliable, or there is lack of certainty.

We could say that Boolean algebra deals with symbol manipulations and exact reasoning, leading to probability. We can quantify probability, i.e., assign a value. Further to that, Shannon has defined information as negative log of probability as given by Equation (1).

$$Information = -\log(p) \quad (1)$$

There is a difference between probability and possibility. Probability of an event, p, means that something may happen, and we believe that it is more likely than not. It can be quantified like p=0, 0.2, 0.5, …, 1. If we look at the system that can generate just 2 events, then in Equation (1) base of the log is 2. If events have the same probability of appearance, i.e., p=0.5, then the information carried by a single event is equal to 1bit.

On the other side, possibility means that something may happen, but we do not know how likely. Fuzzy logic applies symbol manipulations and numerical computations to come to approximate reasoning. It essentially deals with possibilities. Everything is a matter of degree. Fuzzy logic variables are represented by sets of values. That can be represented by mathematical formulations which give a degree of membership within the set. We can have unions and intersections of fuzzy sets. As humans, we make fuzzy

logic decisions. Artificial Intelligence (AI) is effectively an application of fuzzy logic. Fuzzy logic is applied in many control engineering systems, when other strategies are not powerful enough to deal with uncertainties and unreliable data (Carter, Chiclana, Khuman, & Chen, 2021; Matía, Marichal, & Jiménez, 2014). It is also applied in business decision making, as shown in numerous references, like here (Bezděk, 2014) and here (M. Todorovic & M. Simic, 2019) in the process of *Transition to Electrical Vehicles Based on Multi-Attribute Decision Making. Managing Transition to Autonomous Vehicles Using Bayesian Fuzzy Logic* is also investigated and reported (Todorovic & Simic, 2019b).

At RMIT University, School of Engineering, research in autonomous vehicles (Elbanhawai, Simic, & Jazar, 2015; Elbanhawi & Simic, 2014; Elbanhawi, Simic, & Jazar, 2015a, 2015b; Elbanhawi, Simic, & Jazar, 2015; Elbanhawi, Simic, & Jazar, 2016; Elbanhawi, Simic, & Jazar, 2018), as well as, research in the process of new technology introduction (Aldakkhelallah, Todorovic, & Simic, 2021; Todorovic & Simic, 2019a, 2019b; Todorovic & Simic, 2019; Todorovic, Simic, & Kumar, 2017), are conducted concurrently.

Driving a car is a good example of fuzzy logic decisions that we make as drivers. We must take care of the speed, acceleration, path conditions and curvatures, visibility, our vehicle performances, especially available power in critical situations and many other. When we design a fully autonomous vehicle (AV), knowledge and skills of the best drivers should be embedded into the vehicle control system. On the road, AV decisions must be made in the real time. All of this was the motivation for the research conducted and presented here. The main contribution of this paper is a comprehensive report of an original cascaded fuzzy system development. Other publications available (Emmanuel, 2017), (Panse, Singh, & Satsangi, 2015), (Basjaruddin, Kuspriyanto, Saefudin, & Nugraha, 2014), although very valuable, do not give details and algorithms on defining safe distance and speed or speed error. This original design also involves algebraic subtraction performed through a FIS subsystem.

2. RELATED WORKS

Adaptive cruise control is one of the driver assistance features introduced on level 1 and 2 of SAE AV ranking. This can be achieved by various methods of control such as using Proportional-Integral-Derivative (PID) controller, state-space controller, fuzzy logic, (Osman, Rahmat, & Ahmad, 2009), Internal Model Control (IMC), neural networks or other, like coordinated throttle and brake control for ACC (Bala, Sadiq, Aibinu, & Folorunso, 2021). PID and IMC are not suitable for nonlinear operations on the road, such as aerodynamic drag and friction (Bala et al., 2021), or slippery road. All of those are effected by weather conditions. Further to that, it is shown that the fuzzy logic controller has faster response than neural network solutions and is less complex to implement (Panse et al., 2015).

Another recent publication, (Nchena, 2020) considers type of the road, i.e., downhill, and uphill driving. In this report on fuzzy logic controller (FLC) application in AV control, two types of controllers were investigated. It is shown that FLC outperforms a Proportional Integral (PI) controller. Since fuzzy logic can easily handle nonlinear conditions and shows superiority compared to other controller approaches, our investigation has proceeded in that direction. Large number of input variables are included in our novel design to enable better control. All stages and algorithms of the controller design are presented, what cannot be found so comprehensively given in existing works. The presented controller covers all road types and weather conditions.

Example of a generic fuzzy logic controller is shown in Figure 1.

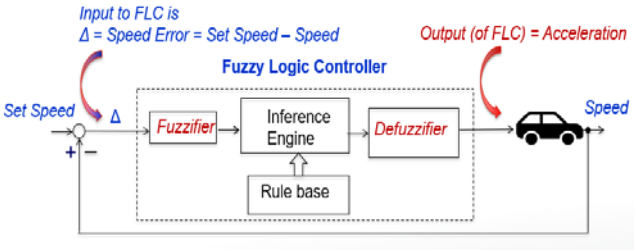

Figure 1: Generic fuzzy logic controller for cruise control

Basic components of this control approach, i.e., of fuzzy inference system, are presented. Fuzzifier block is converting an input variable into fuzzy sets through membership functions as shown later by Equations (5) and (6). Transfer of input variable values to outputs is performed using rules. Rule base, or database of rules, is defined based on human operator expertise, or drivers experience. It has numerous *if then* statements, as following

$$\boldsymbol{If}\ speed\ is\ below\ the\ set\ speed, \boldsymbol{then}\ speed\ up$$

Inference engine is applying fuzzy rules to the input variables, to generate fuzzy output. In the next step, defuzzification, output fuzzy set is converted to a crisp set. Center of gravity method is often used defuzzification method. When plain cruise control is implemented, the driver is responsible for maintaining the safe distance behind the car ahead. In our case, that function is performed by the fuzzy controller, which is now becoming more comprehensive.

3. ADAPTIVE CRUISE CONTROL SYSTEM

An adaptive cruise control, as a driver assistance feature, is monitoring and controlling the speed of our Cruise Car (CC) while simultaneously keeping the safe distance from the Car Ahead (CA). The speed of the CC is labeled as S_{CC} and the Speed of CA is S_{CA}. Safe distance is defined by the traffic authorities. In addition to that, it also depends on the vehicle speed, traffic, weather conditions and the driver, or driving mode. An additional variable, *Distance Error (DE)*, is introduced as the difference between *Measured Distance* and *Safe Distance*, as given by Equation (2).

$$DE = Distance - Safe\ Distance \quad (2)$$

Different scenarios on the road are given in Figure 2.

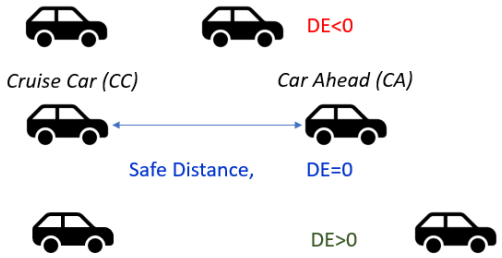

Figure 2: Defining distance error (DE) cases

We also need to define speed error, which is calculated as given by Equation (3).

$$SE = Speed_{Set} - Speed_{CC} \quad (3)$$

Considering distance error and speed error we can define a new rule such as the following:

***If** distance error is positive **and** speed error is positive, **then** accelerate*

The rule base consists of all possible rules, i.e., has responses for all scenarios that could appear on the road.

4. FUZZY LOGIC VARIABLES

According to SAE defined levels of driving automation, if adaptive cruise control, or lane centering, appears as driver support feature, the vehicle is level 1 automated. If both features are included, that vehicle is categorized as level 2. Manufacturers have different names for ACC and different control strategies are applied. For any control system we need to define input variables, control strategy, controller, and output variables. In this project, a cascaded fuzzy logic approach is applied in controller design.

In 1965 Zadeh has introduced *fuzzy set* as a class of objects with a continuum of membership grades (Zadeh, 1965). They are foundation of any logic regardless of truth levels assumed. For fuzzy variables we have continuum of logic levels between 0, associated to *false*, to 1 for completely *true*. We can label a space of points as *X*. Equation (4) defines an *x* as a generic element of space *X*.

$$x \in X \quad (4)$$

A *fuzzy set A* in the universe *X* is defined by a membership function $\mu_A(x)$, which associates point *x* to a real number in the interval [0, 1]. Value $\mu_A(x)$ represents *grade of membership* of *x* in *A*. As an illustration, membership functions' plots for the measured *Speed* input variable are shown in Figure 3.

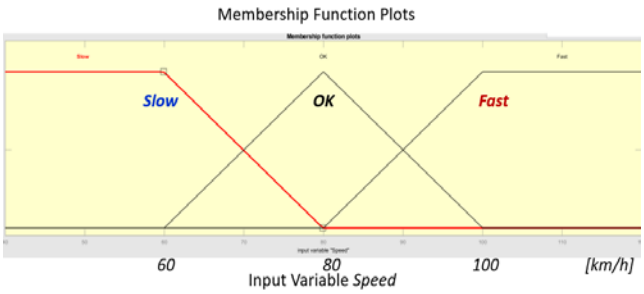

Figure 3: Membership functions' plots for the *Measured Speed* input variable

The most popular membership functions are Triangular, Trapezoidal, Piecewise linear, Gaussian and Singleton. Triangular membership function labeled as μ_{Tri} is given by Equation (5).

$$\mu_{Tri}[a,b,c](x) = \begin{cases} 0 & x < a \\ \frac{x-a}{b-a} & a \le x \le b \\ \frac{c-x}{c-b} & b < x \le c \\ 0 & x > c \end{cases} \quad (5)$$

As shown in Figure 3, our membership function *OK* is a triangular type, where braking points are $a = 60km/h$, $b = 80km/h$ and $c = 100km/h$.

Functions *Slow* and *Fast* are trapezoidal type μ_{Trap} and they are defined as given by Equation (6). In our case, both are particular cases of a generic trapezoidal function. For membership function *Slow*, we have $a = b = 0$, $c = 60km/h$ and $d = 80km/h$. For membership function *Fast*, $a = 80km/h$, $b = 100km/h$, and $c = d \to \infty$.

$$\mu_{Trap}[a,b,c,d](x) = \begin{cases} 0 & x < a \\ \frac{x-a}{b-a} & a \le x < b \\ 1 & b \le x \le c \\ \frac{d-x}{d-c} & c < x \le d \\ 0 & x > d \end{cases} \quad (6)$$

Our control system has six input variables and two outputs. Inputs, with associated membership functions in brackets, are given here:

- *Driving mode* (*Eco*, *Comfort*, *Sport*),
- *Weather* conditions (*Good*, *Bad*),
- Measured *speed* (*Slow*, *OK*, *High*),
- *Distance* from the vehicle ahead (*Big*, *OK*, *Too close*)
- *Speed error* (ranges from very negative to very positive, i.e., *NN*, *N*, *Z*, *P*, *PP*)
- *Steering angle* (ranging from very high, to moderate and zero, *PP*, *P*, *Z*).

Outputs of our control system, with associated membership functions in brackets, are as following:

- *Corrected acceleration* (from negative to zero and positive *NN*, *N*, *Z*, *P*, *PP*)
- *Braking* (from hard braking, *BB*, braking, *B*, to no braking, *Z*).

When the number of inputs to a fuzzy system is large than that requires large number of rules. In our case it is $3 * 2 * 3 * 3 * 5 * 3 = 810$ per output, i.e., 1620 in total for two outputs. Because of that complexity, controller is designed as a cascaded fuzzy inference system (FIS), i.e., it has four interconnected FIS subsystems inside.

5. FUZZY CONTROL SYSTEM STRUCTURE

In order to overcome the need for a large number of rules, fuzzy inference system is implemented as a hierarchical tree of smaller interconnected subsystems. Following that, block diagram of the fuzzy logic based adaptive cruise control is shown in Figure 4. It is an incremental structure.

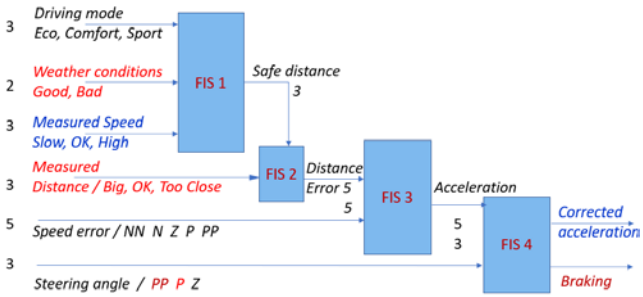

Figure 4: Incremental structure of the fuzzy control system. Number of membership functions for each input is given and all input / output variables are labelled

Each FIS has its own inputs and outputs, where outputs of the lower-level fuzzy systems are used as inputs to the higher-level fuzzy systems.

As shown, there are four interconnected levels. Fuzzy tree structure approach is more computationally efficient and easier to follow than a single FIS with the same number of inputs.

Level 1 in the tree has 3 inputs with $3 + 2 + 3 = 8$ membership functions in total. This gives number of rules $3 * 2 * 3 = 18$.

In level 2 we have 2 inputs, both with 3 membership functions. It creates 9 fuzzy rules.

On level 3 we have 2 inputs with 5 membership functions each, which leads to 25 rules.

Finally, on the level 4 we have 2 inputs, with 5 and 3 functions, creating 15 rules, for each output, i.e., 30 rules for the final, output level FIS.

The total number of rules is now $(18 + 9 + 25 + 2 * 15) = 82$, compared with 1620 which we would have if we did not use hierarchical tree structure.

6. FIS SYBSYSTEMS DESIGN

The following section presents design steps for each of the FIS subsystems included in the cascaded controller.

A. Level One FIS Design

Inputs at the first level in the tree, with associated membership functions in brackets, are given here:

- *Driving Mode* (*Eco, Comfort, Sport*)
- *Weather* conditions (*Good, Bad*)
- Measured *Speed* (*Slow, OK, High*)

Membership functions for variable *Speed* are already shown in Figure 3. Membership functions for *Weather* variable are given in Figure 5. It is a dimensionless variable displayed in the range 0 to 10, on *x* axes. Value 0 corresponds to bad weather, while 10 corresponds to good weather. In this initial stage we have defined just two membership functions, but later, if needed, we could include more to better cover the real weather conditions on the road.

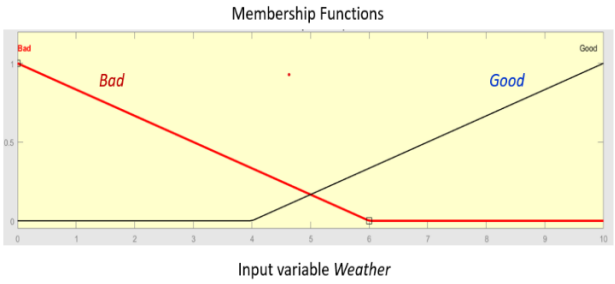

Figure 5: Membership functions for input variable *Weather*

Our *Weather*, as an input variable here, could be an output variable from another fuzzy inference system that should consider onboard sensors' readings of temperature and detections of snow, rain, fog, and strong winds. This could also be a task for onboard Artificial Intelligence (AI).

Inference engine is using the rule base to define output, i.e., *Safe Distance* in this case. Rule base is shown in Figure 6 – which is a screen capture from the MATLAB Rule Editor. There are 18 rules because there are 3 membership functions for *Driving Mode*, 2 for *Weather* and 3 for the measured *Speed*.

FIS responses can be seen through the control surface. Since we have 3 input variables and one output, it makes 4 dimensions. That could not be presented on a single 3D graph. Following that, MATLAB can visualize three control surfaces

- S_1 = *Safe Distance (Speed, Weather)*
- S_2 = *Safe Distance (Driving mode, Speed)*
- S_3 = *Safe Distance (Weather, Driving mode)*

We are presenting here just one, but all of them are available for investigation. The first one is selected because drivers are usually selecting driving mode and do not change it that often. At the same time *Speed* and *Weather* are extremely important inputs, i.e., variables for real time processing and autonomous driving.

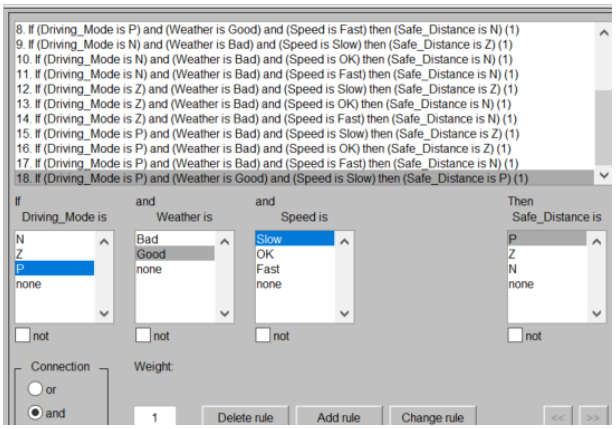

Figure 6: Fuzzy rules for variable Safe Distance as seen in MATLAB Rule Editor

Figure 7 shows S_1 control surface. We can see that the *Safe distance* is larger when the *Speed* is greater, and the *Weather* is Bad.

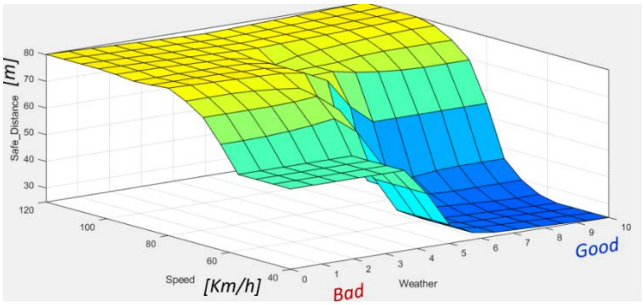

Figure 7: S_1 control surface for *Safe Distance*

B. Level Two FIS Design

Inputs for the second FIS level in the tree, with associated membership functions in brackets, are given here:

- *Safe Distance* (*P(Low), Z(OK), N(Higher)*),
- Measured *Distance* (*Big, OK, Too Close*)

Safe Distance comes out of the FIS at the level 1, as just shown. *Measured Distance* comes from the distance sensor readings (Radar or LIDAR). Control surface is shown in Figure 8. Output variable is *Distance Error (DE)*, which has 5 membership functions. Visual presentation of the DE meaning is already given in the Figure 2. *Distance error* and *Speed error*, with five membership functions as well, are two key control variables in the feedback control loop. This, the most important logic, is realized on the next FIS level.

As an illustration of the functionality for this stage, let us analyze a scenario when the safe distance if 70m and our measurement shows 70m as well. Distance error is 0 as it can be seen from the location of the red point P on the surface.

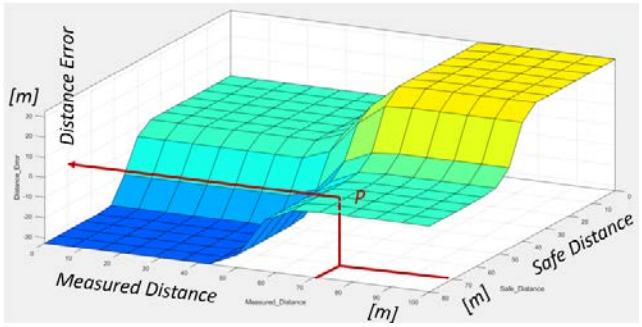

Figure 8: Control surface for FIS 2 i.e., *Distance Error*

Because FIS 2 output variable *Distance Error* is input variable for next level FIS 3, in order to follow the logic, this variable is shown in Figure 9 with its 5 membership functions.

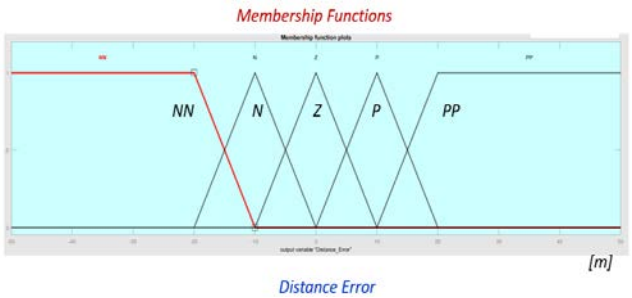

Figure 9: *Distance Error* variable membership functions

C. Level Three FIS Design

Inputs at the third level in the tree have five membership functions each. They are given here with associated membership functions in brackets:

- *Distance Error* (ranges from very negative to very positive, i.e., *NN, N, Z, P, PP*), as shown in Figure 9
- *Speed error* (ranges from very negative to very positive, i.e., *NN, N, Z, P, PP*)

Speed Error is calculated by Equation (3), as a difference between set speed and instant cruising speed, outside of this controller structure, and then fuzzified. These variable membership functions are shown in the Figure 10.

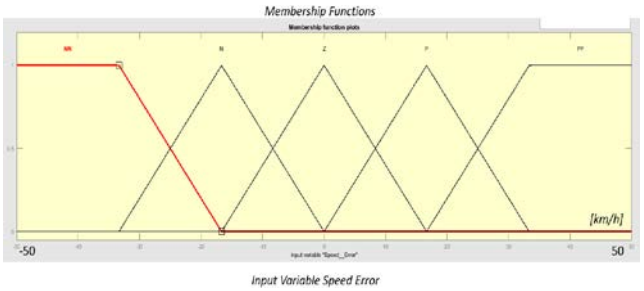

Figure 10: Input variable *Speed Error* membership functions

Since we have 5 functions for each variable, the total number of rules is 25. For easier tracking of rule base design, it is initially created in Excel and then transferred to MATLAB by Rule Editor. Excel rule base is given in Figure 11.

DE Distance Error = Measured Distance - Safe Distance

Speed Error SE	NN	N	Z	P	PP
NN	NN	NN	N	N	N
N	NN	NN	N	N	N
Z	NN	N	Z	Z	Z
P	NN	N	Z	P	P
PP	NN	N	Z	P	PP

Figure 11: Whole rule base for FIS 3 *Acceleration*

For example, from the rule base shown in Figure 11 we crate rules as following.

If *SE is NN, and DE is NN* ***then*** *Acceleration is NN, …,*
If *SE is P, and DE is Z* ***then*** *Acceleration is Z,*

When the rules are in the system, using MATLAB Rule Viewer, we could see and verify all of them. Rule View for FIS 3 is shown in the Figure 12.

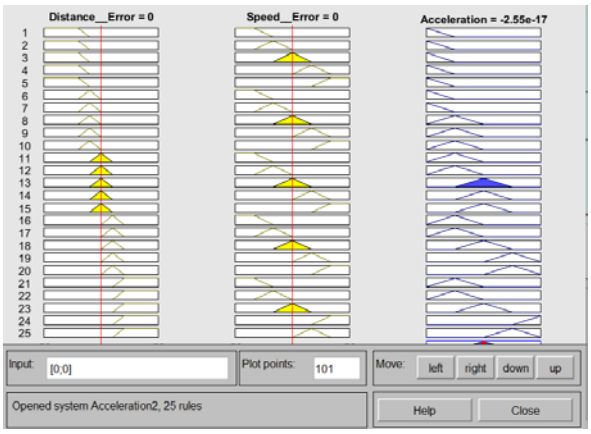

Figure 12: Rule View for all FIS 3 i.e., for output variable *Acceleration*

When this is all set up properly, we can see the control surface for *Acceleration* as shown in Figure 13.

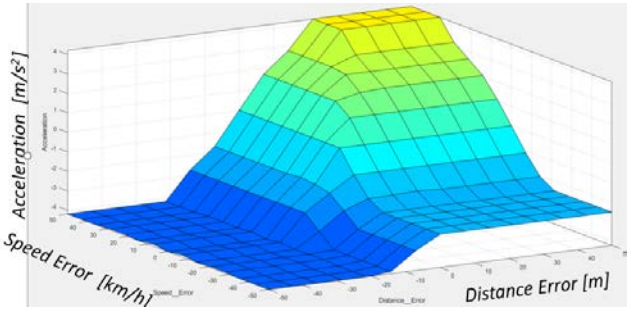

Figure 13: Control surface for *Acceleration*

Both input variables for FIS3, could be positive, zero or negative. As we can see from the Figure 13, *Acceleration*, as output, also could be positive, to speed up, and negative, when needed to slow down. For higher distance error or higher speed error we have higher acceleration. There should be a limit to acceleration and that is defined by the steering angle. The correction of the acceleration, as well as braking, is introduced by the last FIS4 in the tree structure.

D. Level Four FIS Design

Inputs to the fourth level FIS in the tree, are given here with associated membership functions in brackets:

- *Acceleration* (ranges from very negative to very positive, i.e., *NN, N, Z, P, PP*)
- *Steering Angle* (ranges from zero, positive, to very positive, i.e., *Z, P, PP*)

From this FIS we have two output functions:

- *Corrected Acceleration* (ranges from very negative to very positive, i.e., *NN, N, Z, P, PP*)
- *Braking* (ranges from zero to very positive, i.e., *Z, P, PP*)

Acceleration is output variable from FIS 3 and input for FIS 4. Its values, as FIS output, can be seen in the Figure 13. Membership functions are shown in the Figure 14.

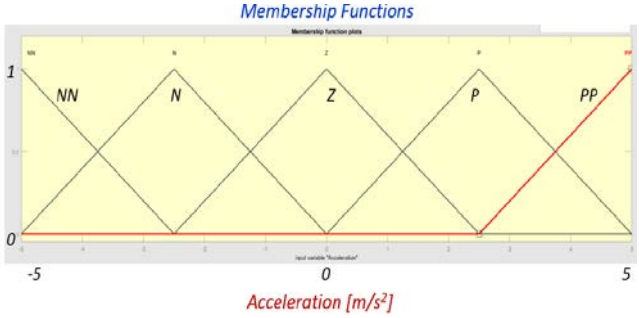

Figure 14: FIS 4 Input variable *Acceleration* membership functions

When defining the range for this variable we have taken values that could be found for a relatively powerful vehicles available to the market, like up to 5m/sec^2. For the *Steering Angle* vales are also relatively widely used, in the range of -30^0 to +30^0, expressed in degrees. In defining the rule base, we have considered absolute values because from the point of vehicle dynamics constraints, it does not matter if we have to turn left, or right.

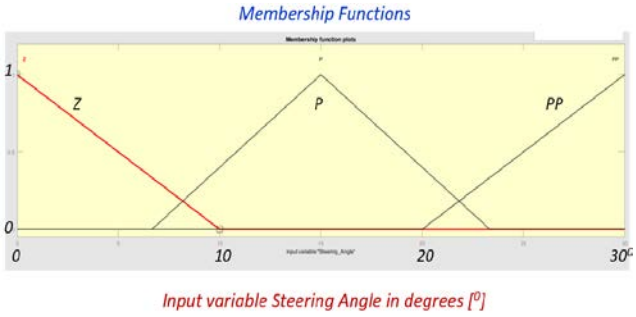

Figure 15: FIS 4 Input variable *Steering Angle* membership functions, shown as absolute value of real angle

Total number of rules is $2 * (3 * 5) = 30$, or 15 integrated rules, for two outputs, as in MATLAB Rule Editor. All rules, i.e., whole rule base, are shown in Figure 16. Based on that, we have control surfaces as shown in Figure 17 and Figure 18. Comparing Figure 13 and Figure 17 we can see the difference, i.e., acceleration corrections. If the path curvature is too large, we, as drivers, must adjust acceleration, or deceleration, accordingly.

1. If (Acceleration is NN) and (Steering_Angle is Z) then (CorrectedAcceleration is NN)(Braking is PP) (1)
2. If (Acceleration is NN) and (Steering_Angle is P) then (CorrectedAcceleration is NN)(Braking is PP) (1)
3. If (Acceleration is NN) and (Steering_Angle is PP) then (CorrectedAcceleration is N)(Braking is P) (1)
4. If (Acceleration is N) and (Steering_Angle is Z) then (CorrectedAcceleration is N)(Braking is P) (1)
5. If (Acceleration is N) and (Steering_Angle is P) then (CorrectedAcceleration is N)(Braking is P) (1)
6. If (Acceleration is N) and (Steering_Angle is PP) then (CorrectedAcceleration is N)(Braking is P) (1)
7. If (Acceleration is Z) and (Steering_Angle is Z) then (CorrectedAcceleration is Z)(Braking is Z) (1)
8. If (Acceleration is Z) and (Steering_Angle is P) then (CorrectedAcceleration is Z)(Braking is Z) (1)
9. If (Acceleration is Z) and (Steering_Angle is PP) then (CorrectedAcceleration is Z)(Braking is Z) (1)
10. If (Acceleration is P) and (Steering_Angle is Z) then (CorrectedAcceleration is P)(Braking is Z) (1)
11. If (Acceleration is P) and (Steering_Angle is P) then (CorrectedAcceleration is P)(Braking is Z) (1)
12. If (Acceleration is P) and (Steering_Angle is PP) then (CorrectedAcceleration is Z)(Braking is Z) (1)
13. If (Acceleration is PP) and (Steering_Angle is Z) then (CorrectedAcceleration is PP)(Braking is Z) (1)
14. If (Acceleration is PP) and (Steering_Angle is P) then (CorrectedAcceleration is P)(Braking is Z) (1)
15. If (Acceleration is PP) and (Steering_Angle is PP) then (CorrectedAcceleration is Z)(Braking is Z) (1)

Figure 16: FIS 4 rule base for output variables *Corrected Acceleration* and *Braking*

For example, if the angle is extreme, such as 30^0, *Corrected Acceleration* is 0. If *Steering Angle* is 0 then there is no correction as shown clearly in Figure 17.

From Figure 18 we can see that there is no braking while *Acceleration* is positive, and that it increases as deceleration increases.

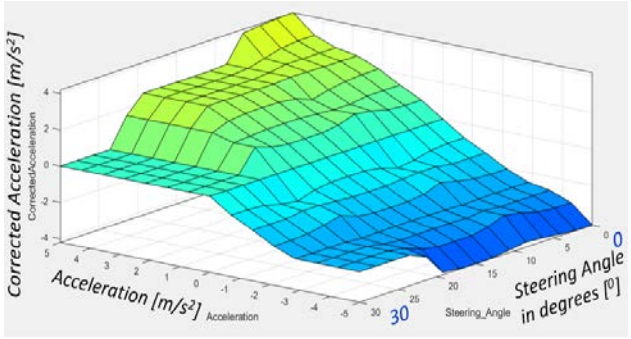

Figure 17: FIS 4 control surface for output variable *Corrected Acceleration*

Intensity of braking is defined in the range from 0 to 10, but for the particular car it will be converted to the braking force intensity in the range of 0 to *xx* N.

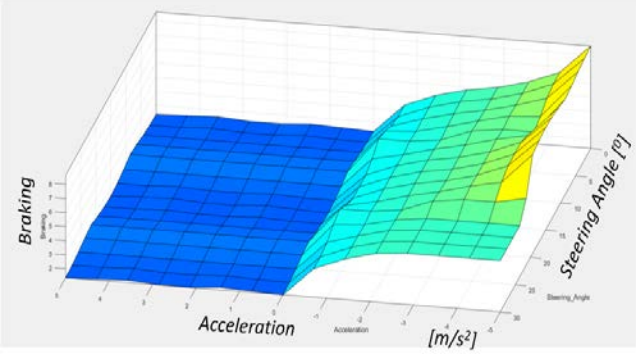

Figure 18: FIS 4 control surface for output variable *Braking*

In summary, membership functions, fuzzy rules and control surfaces for all control levels are presented. The system has 6 inputs, with 19 membership functions and two outputs with a total of 8 functions. When the number of inputs, and membership functions increase the number of rules increase as a product of the number of functions per input.

Compared to single fuzzy inference system, not cascaded, which must have 1620 rules, the presented design has just 82 rules. With 6 input variables, through 3 cascaded levels, the presented design enables better control, more akin to human operator's actions. Other publications do not give as much detail in the FIS subsystem design. Additionally, instead of calculating *Distance Error* with Boolean logic, as shown in other research reports (Basjaruddin et al., 2014), (Chen, Zhang, & Liu, 2016), in our controller, the output variable from FIS 2, derived through fuzzy logic, is further appearing as input variable on level 3 FIS. The same could be conducted for the *Speed Error* but was not presented here for the simplicity of design and presentation.

7. CONCLUSIONS

Design of a cascaded, incremental fuzzy control system is presented. At the beginning, the basics of two logic systems are explained: Boolean and Zadeh's Fuzzy logic. They both have their application areas and deal with uncertainties through handling probability, or possibility in the systems' design and control. Fuzzy logic and Artificial Intelligence are now widely used in all types of engineering systems, in business, medicine and other areas.

Adaptive cruise control is one of the driver assistance features. Car manufacturers have different controller solutions and names for this active safety system. The presented cascaded, incremental fuzzy logic controller uses data collected from all available vehicle onboard sensors. Membership functions, fuzzy rules and control surfaces for all control levels are presented. When the number of inputs, and membership functions increase, the number of rules increases as a product of functions per input. A large number of rules increase computation time and is not suitable for real time processing. The presented approach using a fuzzy tree is simplified and uses an order of magnitude less fuzzy rules.

In the further research, both distance and speed errors will be derived through fuzzy logic, and then the complete vehicle dynamic system modeling will be conducted. Through the model testing, fine tuning of the fuzzy logic controller will be conducted, the same as we improve our driving through experience.

The final step is to go from MATLAB code, to hardware description language (HDL) code, and then to field-programmable gate array (FPGA) that could be used for field testing.

ACKNOWLEDGEMENTS

The author would like to express his gratitude to the RMIT University, Australia. He also would like to thank the Editors and anonymous reviewers of the article for their insightful suggestions and comments to improve the content of the manuscript.

REFERENCES

Aldakkhelallah, A., Todorovic, M., & Simic, M. (2021). *Investigation in Introduction of Autonomous Vehicles.* Paper presented at the IASTEM - 1082nd International Conference on Control, Automation, Robotics and Vision Engineering(ICCARVE), Riyadh, Saudi Arabia.

Bala, J. A., Sadiq, T., Aibinu, A. M., & Folorunso, T. A. (2021, 15-16 July 2021). *A Fuzzy Super Twisting Sliding Mode Control Scheme for Velocity Regulation in Autonomous Vehicles.* Paper presented at the 2021 1st International Conference on Multidisciplinary Engineering and Applied Science (ICMEAS).

Basjaruddin, N. C., Kuspriyanto, K., Saefudin, D., & Nugraha, I. K. (2014). Developing Adaptive Cruise Control Based on Fuzzy Logic Using Hardware Simulation. *International journal of electrical and computer engineering (Malacca, Malacca), 4*(6), 944. doi:10.11591/ijece.v4i6.6734

Bezděk, V. (2014). Using Fuzzy Logic in Business. *Procedia - Social and Behavioral Sciences, 124*, 371-380. doi:https://doi.org/10.1016/j.sbspro.2014.02.498

Boole, G. (2009). *The Mathematical Analysis of Logic: Being an Essay Towards a Calculus of Deductive Reasoning*. Cambridge: Cambridge University Press.

Carter, J., Chiclana, F., Khuman, A. S., & Chen, T. (2021). *Fuzzy Logic: Recent Applications and Developments*. Cham: Springer International Publishing AG.

Chen, X.-w., Zhang, J.-g., & Liu, Y.-j. (2016). Research on the Intelligent Control and Simulation of Automobile Cruise System Based on Fuzzy System. *Mathematical problems in engineering, 2016*, 1-12. doi:10.1155/2016/9760653

Elbanhawai, M., Simic, M., & Jazar, R. N. (2015). Improved Manoeuvring of Autonomous Passenger Vehicles: Simulations and Field Results. *Journal of Vibration and Control*, 35. doi:10.1177/1077546315605666

Elbanhawi, M., & Simic, M. (2014). Sampling-Based Robot Motion Planning: A Review. *IEEE Access, 2*, 56-77. doi:10.1109/ACCESS.2014.2302442

Elbanhawi, M., Simic, M., & Jazar, R. (2015a). In the Passenger Seat: Investigating Ride Comfort Measures in Autonomous Cars. *IEEE Intelligent Transportation Systems Magazine, 7*(3), 4-17. doi:10.1109/MITS.2015.2405571

Elbanhawi, M., Simic, M., & Jazar, R. (2015b). Randomized Bidirectional B-Spline Parameterization Motion Planning.

Intelligent Transportation Systems, IEEE Transactions on, *PP*(99), 1-1. doi:10.1109/TITS.2015.2477355

Elbanhawi, M., Simic, M., & Jazar, R. (2015). The Role of Path Continuity in Lateral Vehicle Control. *Procedia Computer Science, 60*, 1289-1298. doi:http://dx.doi.org/10.1016/j.procs.2015.08.194

Elbanhawi, M., Simic, M., & Jazar, R. (2016). Solutions for Path Planning Using Spline Parameterization. In N. R. Jazar & L. Dai (Eds.), *Nonlinear Approaches in Engineering Applications: Advanced Analysis of Vehicle Related Technologies* (pp. 369-399). Cham: Springer International Publishing.

Elbanhawi, M., Simic, M., & Jazar, R. (2018). Receding horizon lateral vehicle control for pure pursuit path tracking. *Journal of Vibration and Control, 24*(3), 619-642. doi:10.1177/1077546316646906

Emmanuel, I. (2017). Fuzzy Logic-Based Control for Autonomous Vehicle: A Survey. *International Journal of Education and Management Engineering, 7*(2), 41-49. doi:10.5815/ijeme.2017.02.05

Matía, F., Marichal, G. N. s., & Jiménez, E. (2014). *Fuzzy modeling and control : theory and applications* (1st ed. 2014. ed.). Paris, France]: Atlantis Press.

Nchena, L. (2020, 16-18 Sept. 2020). *Fuzzy Logic Application in Automation Control.* Paper presented at the 2020 10th International Conference on Advanced Computer Information Technologies (ACIT).

Osman, K., Rahmat, M. F., & Ahmad, M. A. (2009, 6-8 March 2009). *Modelling and controller design for a cruise control system.* Paper presented at the 2009 5th International Colloquium on Signal Processing & Its Applications.

Panse, P., Singh, A., & Satsangi, C. (2015). Adaptive Cruise Control using Fuzzy Logic. *International Journal of Digital Application & Contemporary research, 3*, 7.

Shannon, C. (1938). *Symbolic Analysis of Relay and Switching Circuits.* (Masters). MIT, Boston USA. Retrieved from https://dspace.mit.edu/handle/1721.1/11173

Todorovic, M., & Simic, M. (2019a, 2019//). *Current State of the Transition to Electrical Vehicles.* Paper presented at the Intelligent Interactive Multimedia Systems and Services, Cham.

Todorovic, M., & Simic, M. (2019b, 2019//). *Managing Transition to Autonomous Vehicles Using Bayesian Fuzzy Logic.* Paper presented at the Innovation in Medicine and Healthcare Systems, and Multimedia, Singapore.

Todorovic, M., & Simic, M. (2019, 13-15 Feb. 2019). *Transition to Electrical Vehicles Based on Multi-Attribute Decision Making.* Paper presented at the 2019 IEEE International Conference on Industrial Technology (ICIT).

Todorovic, M., Simic, M., & Kumar, A. (2017). Managing Transition to Electrical and Autonomous Vehicles. *Procedia Computer Science, 112*, 2335-2344. doi:https://doi.org/10.1016/j.procs.2017.08.201

Zadeh, L. A. (1965). Fuzzy sets. *Information and Control, 8*(3), 338-353. doi:https://doi.org/10.1016/S0019-9958(65)90241-X

MIJST
MIST International Journal of Science and Technology

An Optimized Energy Harvesting Circuit for Low-Power IoT Applications

Arnob Barua[1], and Salauddin Rasel[2*]

[1]Department of Electrical and Electronic Engineering, University of Science and Technology Chittagong (USTC), Bangladesh
[2]Department of Electrical and Electronic Engineering, East Delta University, East Nasirabad, Khulshi, Chattogram, Bangladesh

emails: *[1]arnob303@gmail.com; and [2]salauddin.rasel@gmail.com*

ARTICLE INFO

Article History:

Received: 15th March 2022
Revised: 22nd May 2022
Accepted: 25th May 2022
Published online: 26th June 2022

Keywords:

energy harvesting
power management circuit
self-regulating
stable output power
internet of things

ABSTRACT

The concept and development of an independent energy harvesting mechanism functioning intermittently are described in this paper. A power management circuit (PMC) that is self-regulating, an energy scavenging module, a circuit for charging batteries, as well as an electronic load are all a component of the system that has been proposed. This proposed circuit is designed to attain a fixed output power with a diverse input range. In the unavailability of an additional voltage supply, the PMC can react, maintain, and smartly control the electronic load's power supply. The self-powered energy accumulating technique is expected to be used in situations when supplied power is inadequate to drive the load properly, such as Internet of Things (IoT) applications. IoT is a dispersed architecture of reduced-power, limited-storage, lightweight, and nodes that are adaptive. The majority of embedded IoT devices and low-power IoT sensors are driven by short-life batteries that must be replaced every few years. This procedure is expensive and efficient energy regulation could be critical in enabling energy savings for connecting IoT devices. Experiments with the proposed PMC show that the voltage stored in the capacitor remained mostly fixed at 3.3V at widely diverse inputs that vary from 850mV to 4V. At 3.5V input voltage, a peak efficiency of 88.67% is achieved while the load resistance considered is 230Ω.

1. INTRODUCTION

Nowadays, many applications of wireless sensors and wearable devices have exploded. Wireless Sensor Networks (WSN) which operate at relatively low power is an important part of the Internet of Things' growth (IoT). That kind of sophisticated sensors is projected to be exploited in a variety of circumstances, including environment observation (Sim & Choi, 2020; Tan, 2017), traffic supervising (Jayakumar et al., 2021), remote observation (Shyni et al., 2020), biomedical monitoring, etc. (Mayer et al., 2021). All of these applications have potential uses in a variety of fields, including bioengineering, materials engineering, communications, medicine, etc. (Gomez-Casseres et al., 2016). The Internet of Things (IoT) includes regular objects like laptops, medical equipment, cell phones, and other electronic devices, and it may one day include items as common as furniture or clothing (Udoh & Kotonya, 2018). It is an innovation that enables devices to connect by sensing, processing, and transmitting data. The sensing terminal is a vital part of the IoT that converts a variety of physical parameters, such as humidity, temperature, pressure, light intensity, and other environmental factors are converted into digital signals (Qin et al., 2018; Raad, 2020). Sensors in the IoT consume very little energy, but they are large and widely dispersed, with the capability of being movable (Krishnamurthi et al., 2020). Current advancements in wireless communications, sensors and integrated processing platforms have paved the way to design affordable, low-power compact electronics that can access the internet. These are the core features of the emerging Internet of Things concept (Bkheet & Agbinya, 2021; Marinakis & Doukas, 2018; Samie et al., 2016; Villamil et al., 2020). The rapid spread of the Internet of Things as a prospect for the electronics sector necessitates highly proficient sensor node development (Ahmad et al., 2017; Kaur & Sood, 2017). Each functional equipment in the IoT system needs a specific volume of energy to execute its functions properly (Zeadally et al., 2020). However, securing long-term power sources for such sophisticated sensors, and IoT devices, in particular, is a huge concern. Although batteries have been the most common strategy for powering wireless devices, they must be checked

regularly to ensure continued functionality. Any such requirement is undesirable because the major limitations for battery-powered devices are inadequate life cycle, lower energy density, current dissipation (even when it's not being used), labor cost, and toxic disposal (Adu-Manu et al., 2018; Siddique et al., 2015), while cabled energy connections have drawbacks including the expense of wire materials, connectivity challenges for multiple devices, and electricity resistance. Conversely, wireless energy connections, have none of these issues (Vanhecke et al., 2015; L. Wang et al., 2019). Furthermore, it may be tough or even impossible to change the battery in applications with a vast quantity of IoT devices (thousands or more) (Statista, 2015). Therefore, finding a feasible way to continuously distribute such a large quantity of components is a hotly discussed research objective (Newell & Duffy, 2019).

Energy Harvesting, a way of generating energy from environmental resources is a promising option to produce constantly operated IoT modules that do not have to be recharged throughout their total operation since it provides a consistent and reliable energy supply with lower installation and maintenance expenses (Mishra et al., 2019). Ambient energy sources are increasingly playing a supporting role in meeting the constantly growing demand for wireless and portable electronic gadgets (Z. Zhao et al., 2017). Harvested energy from ambient energy sources like solar (Cabello et al., 2020), wind (Shi et al., 2021), ocean (T. Zhao et al., 2021), etc. have been employed as a power source to operate wearable devices or wireless sensors nodes (Hu et al., 2018). It is the most promising approach to extracting energy from natural resources and developing WSN devices that do not require recharging for the duration of their operation (Ababneh et al., 2019; Miglani et al., 2020). Energy harvesting is a reliable technique that may be applied either in industrial or residential applications. [29]. Several well-established energy harvesting methods including the electromagnetic effect (Yan et al., 2020), the piezoelectric effect (Z. Wang et al., 2021), and the triboelectric effect (C. Zhao et al., 2021), etc. have been established in recent years to acquire energy from the surroundings that are required to run low-power, portable smart electronics. The energy harvesting technology harvests and captures relatively small quantities of readily available energy from the surroundings. However, many energy resources are incapable to deliver the vast amounts of energy needed to power IoT gadgets (Fu et al., 2020). Moreover, using an energy harvester as an input imposes supplementary circuitry and energy regulation technologies when contrasted to both main-powered and battery-powered systems.

Energy harvesting circuits provide the advantage of extending battery life, allowing gadgets to function for longer periods perhaps forever (Procel et al., 2019). Given the features of low voltage and power of micro energy harvesting resources, and also the imbalance among the load and the source's output power level, this additional circuit is necessary. As a response, driving a wireless instrument demands a PMC, a DC/DC converter, and an energy preserver. The power management circuit's main objective is to provide highly efficient energy transfer and accumulation between both the energy harvester and the load since an energy harvester's average output power is in the μW range (Lin et al., 2020). To achieve stable output from energy harvesters for convenient applications, power management circuits are typically used. When working with low energy, circuit design should prioritize low power consumption and quick startup times (Kalaivaani & Krishnamoorthi, 2020; Priya et al., 2019; Tamrin & Ahmad, 2020). The application of the PMC in IoT equipment has stimulated attention to harvesting micropower (Muhtaroğlu, 2017; Woias, 2015). Likewise, due to their inability to respond to fluctuations in input power, most typical PMC that execute a set of criteria are inadequate for low-power energy harvesters. To ensure a constant output power, a ubiquitous adaptive power regulation circuit to extract the maximum power from it and a higher power altering capability is drawing consideration to be implemented in the wireless sensor node built on IoT (Prasad & Chawda, 2018).

To maximize energy harvesting proficiency and to produce a stable output voltage with little variation, an enhanced and effective power regulation system for ultra-low powered IoT sensors is suggested in this study. The suggested design employs a converter IC that works on the buck-boost principle which is capable of handling different input voltages varying from 850mV to 4V. Because of the PMC's unique architecture, it's been successful in retaining the output voltage steady at 3.3V and it has a conversion efficiency of 88.67% for the stated input voltage levels which makes it appropriate for the operation of IoT devices. This proposed design additionally includes a battery charging IC to preserve the optimal energy and to assist IoT equipment to operate constantly.

2. DESIGN OF THE PROPOSED SYSTEM

Figure 1 represents a schematic representation of an independent and universal energy harvesting method, which includes an ultra-low-power managing circuit, several energy harvesters, some loads, and a battery charging circuit. Due to the enormous number of nodes in an IoT infrastructure, it is necessary to stimulate the accessibility of alternative resources. Batteries are often used to power IoT nodes. As a result, the energy consumption of specific devices and the complete system (i.e., actuators, sensors, and microcontrollers) must be controlled throughout the design of an IoT setup.

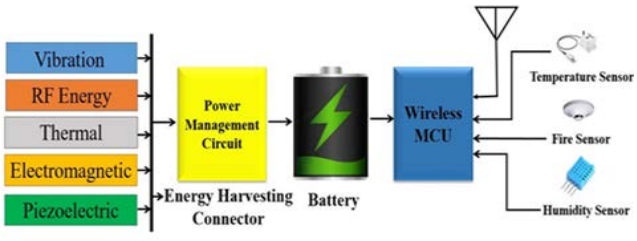

Figure 1: Schematic representation of a ubiquitous energy scavenging system

The main concern of this work while designing the circuit is to provide a regulated output voltage (3.3V in this work)

from any energy harvester available in the environment. Figure 2 depicts the entire power management system, which includes an energy source, a DC/DC converter, a full-wave bridge rectifier, and a battery charging circuit. The complete circuit was designed and simulated using the LTspice XVII software.

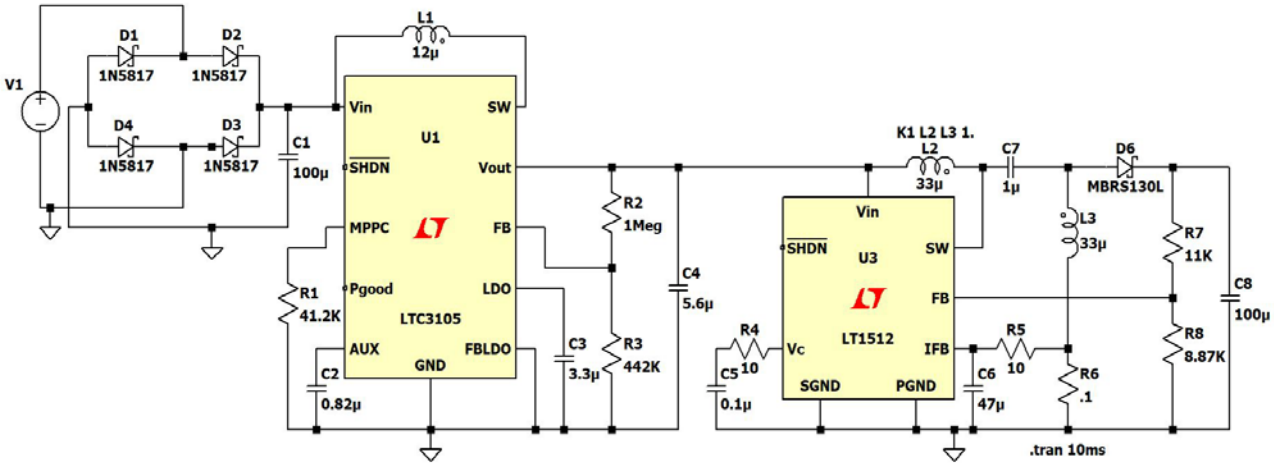

Figure 2: Circuit diagram for the ubiquitous ultra-low power management system

A. Modeling of the proposed Rectifier Circuit

Although energy harvesters generate ac voltage, whereas a power storage unit typically functions at dc to drive the sensor node load, therefore it demands an ac-dc rectifier circuit linked at both ends of the generator in the first stage. The electrical power can be harvested directly if the output voltage from the rectifier is larger than the energy storage device. The rectifying bridge circuit of the proposed system is made up of four compact Schottky diodes. The rectified input and output voltages are shown in Figure 3.

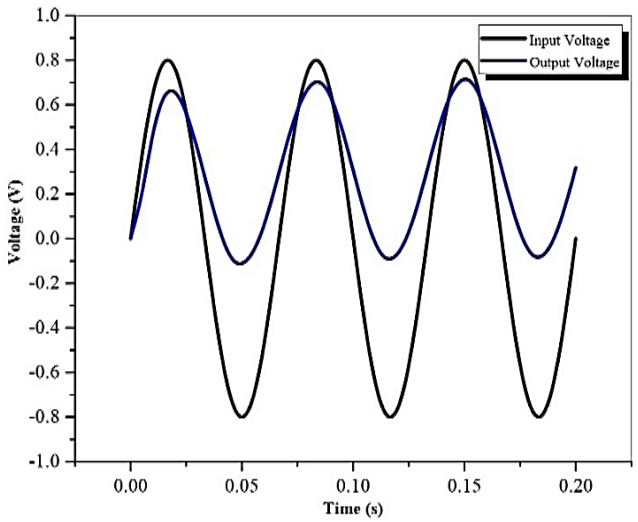

Figure 3: Input and output voltage waveforms of the rectifier

Origin 2016 software was utilized to visualize the output voltage graph. Here, the considered input voltage is 850mV, and the rectified output voltage is 772.49mV (Vpk). Conventional rectifiers based on silicon diode bridges are ineffective as an AC-to-DC conversion since energy harvesters' output voltage peaks are frequently less than 1 V_{pk}. A Schottky diode, on the contrary, can consume a lesser voltage than a regular silicon diode since its terminals only consume 0.3~0.4V. The satisfactory forward voltage loss of a Schottky diode over a conventional diode is one of its core advantages. Schottky diodes also have a quicker recovery rate than other types of diodes which makes them suitable for fast switching operations. It also works well in low-voltage scenarios since it demands lower power. Such diodes have been selected specifically for rectification since they have a modest forward voltage loss and leakage current.

B. Modeling of the proposed DC-DC Converter

The energy harvesting module produces a variable order of voltages, whereas the load circuit requires a consistent DC voltage. In some situations, however, the output voltage of the rectifier is smaller than that of the storage elements. Therefore, the generated voltage must be regulated and boosted. Moreover, since the electronic load may necessitate higher power, the harvesting module may struggle to produce suitable power consistently. The primary goal of a DC/DC converter in a compact device is to link up a battery to the different components of a system if the battery voltage does not align with the required voltage. The voltage of the battery may be either too low or too high. In that scenario, DC/DC upconversion is necessary. Consequently, if the battery voltage is relatively larger than the highest allowable feed voltage, DC/DC down conversion is necessary. However, from the perspective of efficiency, converting the battery voltage to the minimum supply voltage V_{min} required by the load is always a smart idea because of the reasons mentioned. To begin with, once a DC/DC converter is utilized, the load can be designed for the lowest supply voltage rather than the entire voltage span of the battery. In most circumstances, this will result in a better load performance. Second, driving a system component with a greater voltage supply than required is a misuse of energy. A PMC is used to recharge a storage capacitor. The suggested PMC has the feature of not requiring an external power source because it is self-powered owing to the front-end harvesting device. The PMC has an autonomous regulatory circuit that can deliver constant functional power to the

load even if the accumulated power is insufficient. We utilized an LTC3105 step-up DC to DC converter in our suggested circuit design, which was capable to retain the output voltage constant at 3.3V for input voltage varies from 450mV to 4V.

C. Modeling of the proposed Battery Charging Circuit

A wireless sensor module consumes a lot more optimum power than an energy extractor can provide. The energy storage device should be used to store any excess generated energy for a prolonged period to efficiently operate the load. In the proposed methodology, we have used LT1512 Constant Current/Voltage Battery Charger to charge a capacitor. The LT1512 is a 500 kHz current mode switch regulator that has been particularly designed to generate a constant-current/voltage battery charger. It has a current sensor feedback circuit in addition to the conventional voltage feedback node for precisely managing the output current of a flyback topology charger. The LT1512 has a peak switch current of 1.5A. For a single lithium-ion cell, this permits charging currents of up to 1A. As a storage element, a capacitor C8 with a capacitance of 100F is considered, which stores energy for proper use of quick power output bursts. To inhibit energy dissipation from the load, the load's capacitor should be disconnected during the energy storage phase, and it can only be reconnected if the energy generated is adequate to run it.

3. SIMULATION AND RESULTS

Figure 4 demonstrates the output voltage of the PMC. The input of the energy harvester is a sinusoidal voltage with a magnitude of 850mV, a frequency of 15Hz, and a DC offset voltage of 0V. Three different capacitors (5.6F, 10F, and 15F) are considered at the PMC's output to produce the best possible regulated voltage. The utmost output voltage is 3.3V when a 5.6F capacitor is adapted, as presented in the picture. If the 10F and 15F capacitors are employed, still, the output voltage falls below 3.3V. Because the 5.6F capacitor can generate a stable output voltage of 3.3V, it's been chosen particularly.

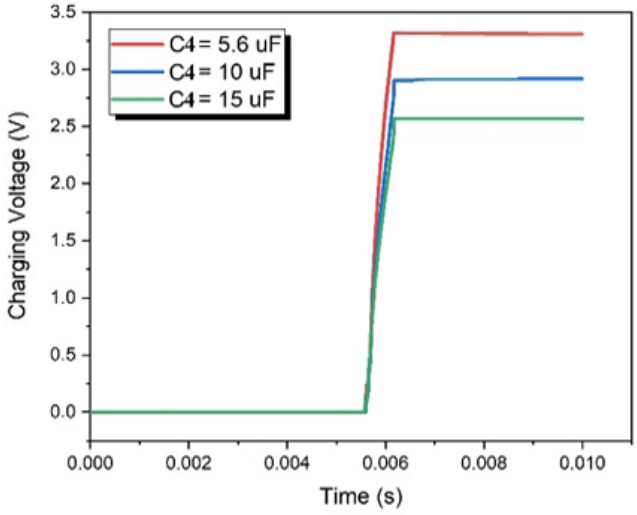

Figure 4: Regulated output voltage graphs for different charging capacitors

The output voltage from three different charging capacitors (47F, 100F, and 150F) is shown in Figigure 5. The proposed battery charging IC delivers higher than 3.5V, 3.3V, and lower than 3.3V, correspondingly, at 47F, 100F, and 150F capacitance. Furthermore, reaching saturation at 150F capacitance takes some time. We chose this capacitor since the IC can generate a stable voltage of 3.3V with a capacitance of 100F.

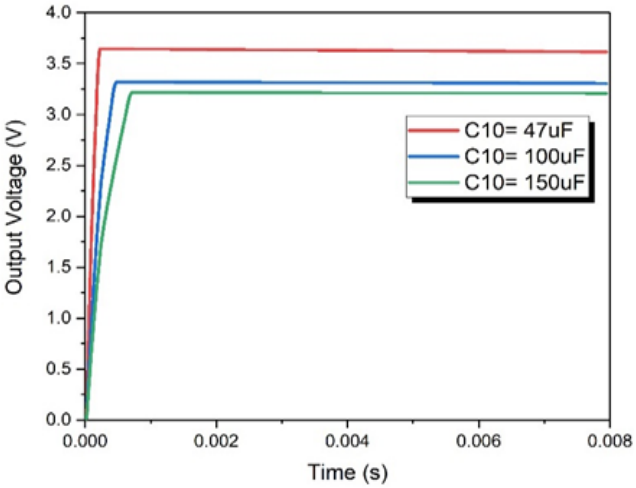

Figure 5: Output voltage graphs for different capacitors considered as batteries

The energy harvester's characteristics are used to determine output power, output voltage, optimum load, and resonant frequency. The energy harvester's output voltage is shown in Figure 6 when the frequency varies from 5Hz to 50Hz. The least possible voltage is below 1V for frequencies ranging from 0Hz to 14Hz, while the highest voltage goes between 3.30V to 3.35V for frequencies varying from 15Hz to 50Hz, as shown in the figure.

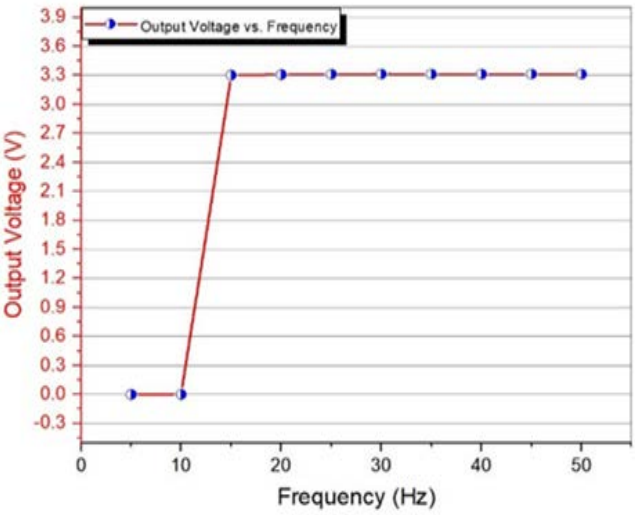

Figure 6: Output voltage at the different input frequencies

Figure 7 shows the load voltage and output power vs. load resistance curves. It is clear to visualize that the voltage level steadily rises with increasing load, reaching 3.3 V at 230 Ω. at that stage, the highest power was delivered to the load. At a load resistance of 220k Ω, the peak output power

is 68.5W. The $P=V^2/R_L$ equation can be utilized to approximate the imminent power output of an energy harvester.

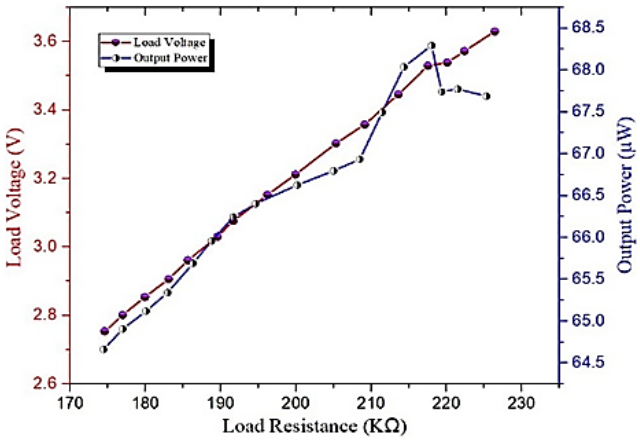

Figure 7: Load voltage and output power waveform vs. load resistance

The output power waveform as a parameter of the duty cycle is illustrated in Figure 8. The highest power can be generated by the energy harvesting system to a battery throughout a variety of duty cycles, as presented in this diagram. Moreover, the voltage that passes across the voltage multiplier from the energy harvesting system is consistently at the ideal duty cycles.

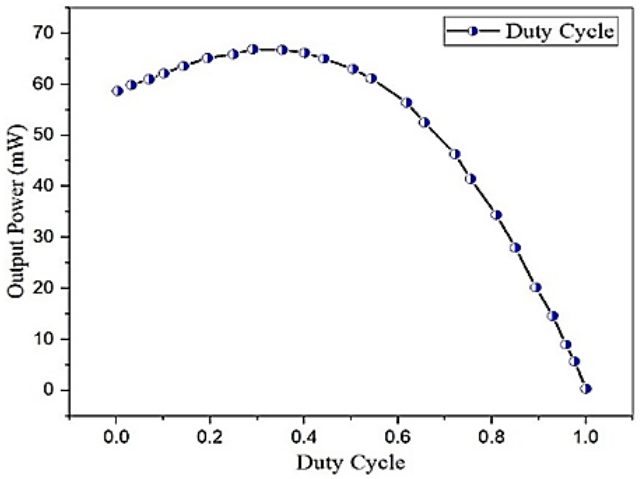

Figure 8: Output power as a factor of the duty cycle

Switching regulators transform one voltage to other by momentarily accumulating energy and then delivering it at various voltages to the output. To convert one voltage to another, the switch pauses the transfer of current to energy-storing equipment, such as a capacitor or an inductor. A switching regulator is equivalent to a transformer. As a result, energy wastage is reduced. To deliver energy from the source to the output, an inductor is used. Figure 9 shows the input voltage vs. power conversion efficiency graph of the suggested PMC. Efficiency can be obtained by dividing the output power by the input power. When the output power equals the input power, the power conversion efficiency is 100 percent, and the regulator loses no energy. This is the ideal state, but it is unreachable. From the figure, it can be seen that from 0.85V to 2.5V, the power conversion efficiency is low because in that case, both the output and input power is low hence lower efficiency is obtained. When the input voltage increases from 2.5V to 3.5V, the ratio of output and input power becomes higher, and therefore significantly higher power conversion efficiency is achieved which is 88.67%. In (Safwat & Ibrahim, 2021) and (Leeuw & Srivastava, 2021), the peak efficiencies reported are 91.6% and 74.21%, respectively which are slightly higher and considerably lower, respectively than our proposed circuit. After 3.5V, since the input power is increasing but the output power remains fixed, the efficiency is getting lower as seen in the figure.

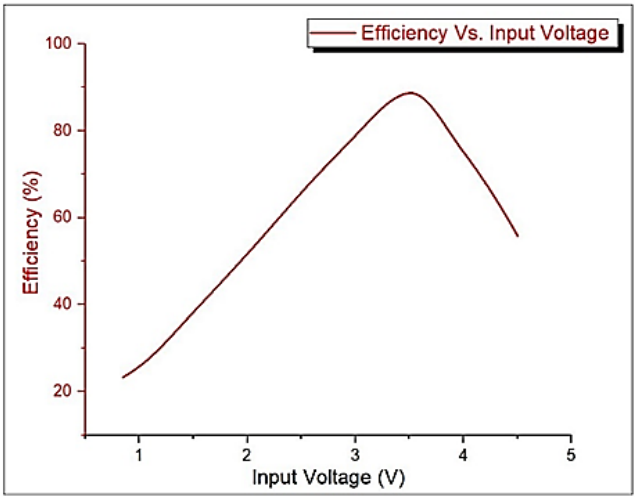

Figure 9: Input voltage vs. circuit efficiency graph

To the best of the author's understanding, among the other circuit works that have been reported, this suggested power regulation circuit delivers one of the best outcomes. Table 1 shows an analysis of the suggested power management circuit and multiple harvesting circuits.

Table 1
Analysis of the performance of several energy harvesting technologies

Reference	Mechanism	Output Voltage	Power Density
Zhang et al., 2019	Triboelectric	3.5V	16.780mW/m3
Li & Jing, 2021	Electromagnetic	2.8V	0.240mW/m3
Uchino, 2018	Piezoelectric	2.33V	0.0013mW/m3
Fang et al., 2021	Hybrid	1.06V	1.580mW/m3
This work	Universal	3.3V	23.60mW/m3

The prices of different parts of the system obtained from different electronic device manufacturers are shown in Table 2. Both the LTC3105 and LT1512 account for the majority of the entire device costs. The LTC3105 is a highly effective DC/DC converter that can harvest and regulate energy from a very minimal input voltage source.

On the other hand, the LT1512 is a 500kHz switching regulator that has been specifically designed to build a continuous-current/continuous-voltage battery charger.

Table 2
Cost calculation of the suggested method

Materials	Provider	Qty.	Price/Qty.	Subtotal
LTC3105	Analog Devices Ltd.	1	$5.30	$5.30
LT1512	Analog Devices Ltd.	1	$3.28	$3.28
Schottky Diode	Cheng Industrial Ltd.	5	$0.05	$0.25
Resistor	Cheng Industrial Ltd.	8	$0.01	$0.08
Capacitor	Cheng Industrial Ltd.	8	$0.08	$0.64
Inductor	Cheng Industrial Ltd.	3	$0.30	$0.90
			Total	**$10.45**

4. CONCLUSIONS

For this research, we built a universal ultra-low-power control circuit that can be used in a variety of harvesters. Any harvester, such as electromagnetic, piezoelectric, and others, will benefit from it. The proposed approach is more efficient than existing generally available power management circuit works. This unique circuit design results in excellent effectiveness and a quick start-up phase, making it ideal for low-energy scavenging purposes with minimum power dissipation. The highly functional energy extractor with low power regulation shown here is a suitable solution for developing a more durable and practical self-powered mechanism that can work with a wide range of ambient insufficient mechanical energy and fit into a variety of application scenarios. The proposed PMC is designed to preserve and regulate electrical energy produced without the use of an additional supply, as well as self-control capacitor charging.

Currently, the Internet of Things (IoT) is serving as an extremely essential aspect of our daily activities, grabbing worldwide attention and bringing up plenty of new opportunities. It's an exciting concept for networking equipment, where the extent of interactions between devices grows every year. With the substantial rise of IoT systems, it is also crucial to recognize sustainable, dependable, and sources of energy that are inexpensive for operating the batteries of sensors, as this research concentrates on ultra-low-power managing circuits for energy harvesters. The issues and approaches utilized to circumvent energy harvesting have been addressed in particular. The components that make up a robust energy-scavenging system are examined in this research. A full-wave bridge rectifier, a battery charging circuit, a DC-to-DC converter, and a precise energy storage system are among them. To begin, we created an AC-DC rectifier incorporating a Schottky diode, a battery charging system, and a reliable and safe voltage regulator that may deliberately reduce system expense while extending battery lifespan. A sensor is necessary to remotely monitor wave height.

To wirelessly send sensor information, a wireless sensor node is essential. The suggested ultra-low-power control circuit can be utilized to make sure that the wireless sensor node receives consistent power. When supplied power from the environmental source is unsatisfactory or unreliable to immediately turn on the electronic equipment, it is an ideal alternative for microelectronics and IoT-focused devices which are self-dependent on the intermittent functioning method.

ACKNOWLEDGEMENTS

The authors wish to express their heartfelt gratefulness to their parents for their unwavering encouragement during this research.

REFERENCES

Ababneh, M. M., Ugweje, O., & Jaesim, A. (2019). Optimized Power Management Unit for IoT Applications. *2019 15th International Conference on Electronics, Computer and Computation (ICECCO)*, 1–4. https://doi.org/10.1109/ICECCO48375.2019.9043189

Adu-Manu, K. S., Adam, N., Tapparello, C., Ayatollahi, H., & Heinzelman, W. (2018). Energy-harvesting wireless sensor networks (EH-WSNs): A review. In *ACM Transactions on Sensor Networks*. https://doi.org/10.1145/3183338

Ahmad, S., Alam, N., & Hasan, M. (2017). Robust TFET SRAM cell for ultra-low power IoT application. *EDSSC 2017 - 13th IEEE International Conference on Electron Devices and Solid-State Circuits*. https://doi.org/10.1109/EDSSC.2017.8333263

Bkheet, S. A., & Agbinya, J. I. (2021). A Review of Identity Methods of Internet of Things (IOT). *Advances in Internet of Things*. https://doi.org/10.4236/ait.2021.114011

Cabello, D., Ferro, E., Pereira-Rial, O., Martinez-Vazquez, B., Brea, V. M., Carrillo, J. M., & Lopez, P. (2020). On-Chip Solar Energy Harvester and PMU with Cold Start-Up and Regulated Output Voltage for Biomedical Applications. *IEEE Transactions on Circuits and Systems I: Regular Papers*. https://doi.org/10.1109/TCSI.2019.2944252

Fang, Y., Tang, T., Li, Y., Hou, C., Wen, F., Yang, Z., Chen, T., Sun, L., Liu, H., & Lee, C. (2021). A high-performance triboelectric-electromagnetic hybrid wind energy harvester based on rotational tapered rollers aiming at outdoor IoT applications. *IScience*. https://doi.org/10.1016/j.isci.2021.102300

Fu, X., Bu, T., Li, C., Liu, G., & Zhang, C. (2020). Overview of micro/nano-wind energy harvesters and sensors. In *Nanoscale*. https://doi.org/10.1039/d0nr06373h

Gomez-Casseres, E. A., Arbulu, S. M., Franco, R. J., Contreras, R., & Martinez, J. (2016). Comparison of passive rectifier circuits for energy harvesting applications. *Canadian Conference on Electrical and Computer Engineering*. https://doi.org/10.1109/CCECE.2016.7726840

Hu, Y., Yue, Q., Lu, S., Yang, D., Shi, S., Zhang, X., & Yu, H. (2018). An adaptable interface conditioning circuit based on Triboelectric Nanogenerators for self-powered sensors. *Micromachines*. https://doi.org/10.3390/mi9030105

Jayakumar, S., Lokesh Kumar, K., Purva Darshini, S. K., & Sanjeev, D. (2021). Traffic monitoring system using IoT and DL. *Advances in Parallel Computing*. https://doi.org/10.3233/APC210141

Kalaivaani, P. T., & Krishnamoorthi, R. (2020). Design and implementation of low power bio signal sensors for wireless body sensing network applications. *Microprocessors and Microsystems*. https://doi.org/10.1016/j.micpro.2020.103271

Kaur, N., & Sood, S. K. (2017). An Energy-Efficient Architecture for the Internet of Things (IoT). *IEEE Systems Journal*. https://doi.org/10.1109/JSYST.2015.2469676

Krishnamurthi, R., Kumar, A., Gopinathan, D., Nayyar, A., & Qureshi, B. (2020). An overview of iot sensor data processing, fusion, and analysis techniques. In *Sensors (Switzerland)*. https://doi.org/10.3390/s20216076

Leeuw, S., & Srivastava, V. M. (2021). Realization with Fabrication of Double-Gate MOSFET Based Buck Regulator. *International Journal of Electrical and Electronic Engineering & Telecommunications*, *10*(1), 66–75. https://doi.org/10.18178/ijeetc.10.1.66-75

Li, M., & Jing, X. (2021). A bistable X-structured electromagnetic wave energy converter with a novel mechanical-motion-rectifier: Design, analysis, and experimental tests. *Energy Conversion and Management*. https://doi.org/10.1016/j.enconman.2021.114466

Lin, L., Tang, Z., Tan, N., & Xiao, X. (2020). Power management in low-power MCUs for energy IoT applications. *Journal of Sensors*. https://doi.org/10.1155/2020/8819236

Marinakis, V., & Doukas, H. (2018). An Advanced IoT-based System for Intelligent Energy. *Sensors*.

Mayer, P., Magno, M., & Benini, L. (2021). Smart Power Unit—mW-to-nW Power Management and Control for Self-Sustainable IoT Devices. *IEEE Transactions on Power Electronics*, *36*(5), 5700–5710. https://doi.org/10.1109/TPEL.2020.3031697

Miglani, A., Kumar, N., Chamola, V., & Zeadally, S. (2020). Blockchain for Internet of Energy management: Review, solutions, and challenges. In *Computer Communications*. https://doi.org/10.1016/j.comcom.2020.01.014

Mishra, S., Unnikrishnan, L., Nayak, S. K., & Mohanty, S. (2019). Advances in Piezoelectric Polymer Composites for Energy Harvesting Applications: A Systematic Review. In *Macromolecular Materials and Engineering*. https://doi.org/10.1002/mame.201800463

Muhtaroğlu, A. (2017). Micro-scale energy harvesting for batteryless information technologies. In *Lecture Notes in Energy*. https://doi.org/10.1007/978-3-319-49875-1_3

Newell, D., & Duffy, M. (2019). Review of Power Conversion and Energy Management for Low-Power, Low-Voltage Energy Harvesting Powered Wireless Sensors. In *IEEE Transactions on Power Electronics*. https://doi.org/10.1109/TPEL.2019.2894465

Prasad, A., & Chawda, P. (2018). Power management factors and techniques for IoT design devices. *Proceedings - International Symposium on Quality Electronic Design, ISQED*. https://doi.org/10.1109/ISQED.2018.8357314

Priya, S., Song, H. C., Zhou, Y., Varghese, R., Chopra, A., Kim, S. G., Kanno, I., Wu, L., Ha, D. S., Ryu, J., & Polcawich, R. G. (2019). A Review on Piezoelectric Energy Harvesting: Materials, Methods, and Circuits. In *Energy Harvesting and Systems*. https://doi.org/10.1515/ehs-2016-0028

Procel, L. M., Paredes, J., & Trojman, L. (2019). Comparison of Different Technologies for Transistor Rectifiers Circuits for Micropower Energy Harvesters. *Latin American Electron Devices Conference, LAEDC 2019*. https://doi.org/10.1109/LAED.2019.8714738

Qin, H., Cheng, G., Zi, Y., Gu, G., Zhang, B., Shang, W., Yang, F., Yang, J., Du, Z., & Wang, Z. L. (2018). High Energy Storage Efficiency Triboelectric Nanogenerators with Unidirectional Switches and Passive Power Management Circuits. *Advanced Functional Materials*. https://doi.org/10.1002/adfm.201805216

Raad, H. (2020). Fundamentals of IoT and Wearable Technology Design. In *Fundamentals of IoT and Wearable Technology Design*. https://doi.org/10.1002/9781119617570

Rehmani, M. H., Reisslein, M., Rachedi, A., Erol-Kantarci, M., & Radenkovic, M. (2018). Integrating Renewable Energy Resources Into the Smart Grid: Recent Developments in Information and Communication Technologies. *IEEE Transactions on Industrial Informatics*, *14*(7), 2814–2825. https://doi.org/10.1109/TII.2018.2819169

Safwat, M., & Ibrahim, S. (2021). 91.6% efficient hybrid DC-DC buck converter with wide programmable conversion range. *Microelectronics Journal*, *114*, 105147. https://doi.org/10.1016/j.mejo.2021.105147

Samie, F., Bauer, L., & Henkel, J. (2016). IoT technologies for embedded computing: A survey. *2016 International Conference on Hardware/Software Codesign and System Synthesis, CODES+ISSS 2016*. https://doi.org/10.1145/2968456.2974004

Shi, T., Hu, G., Zou, L., Song, J., & Kwok, K. C. S. (2021). Performance of an omnidirectional piezoelectric wind energy harvester. *Wind Energy*. https://doi.org/10.1002/we.2624

Shyni, S. M., Abitha Memala, W., Bhuvaneswari, C., & Ravi Kumar, D. N. S. (2020). Iot based robot for mine and trespassers detection in defence field. *International Journal of Scientific and Technology Research*.

Siddique, A. R. M., Mahmud, S., & Heyst, B. Van. (2015). A comprehensive review on vibration based micro power generators using electromagnetic and piezoelectric transducer mechanisms. In *Energy Conversion and Management*. https://doi.org/10.1016/j.enconman.2015.09.071

Sim, S., & Choi, H. (2020). A study on the service discovery support method in the IoT environments. *The International Journal of Electrical Engineering & Education*, *57*(1), 85–96. https://doi.org/10.1177/0020720918813824

Statista. (2015). *IoT: number of connected devices worldwide 2012-2025 (in billions)*. Statista.

Tamrin, M. S., & Ahmad, M. R. (2020). Simulation of adaptive power management circuit for hybrid energy harvester and real-time sensing application. *International Journal of Power Electronics and Drive Systems (IJPEDS)*, *11*(2), 658. https://doi.org/10.11591/ijpeds.v11.i2.pp658-666

Tan, Y. K. (2017). Energy harvesting autonomous sensor systems: Design, analysis, and practical implementation. In *Energy Harvesting Autonomous Sensor Systems: Design, Analysis, and Practical Implementation*. https://doi.org/10.1201/b14572

Uchino, K. (2018). Piezoelectric Energy Harvesting Systems-Essentials to Successful Developments. In *Energy Technology*. https://doi.org/10.1002/ente.201700785

Udoh, I. S., & Kotonya, G. (2018). Developing IoT applications:

challenges and frameworks. *IET Cyber-Physical Systems: Theory & Applications*. https://doi.org/10.1049/iet-cps.2017.0068

Vanhecke, C., Assouere, L., Wang, A., Durand-Estebe, P., Caignet, F., Dilhac, J.-M., & Bafleur, M. (2015). Multisource and Battery-Free Energy Harvesting Architecture for Aeronautics Applications. *IEEE Transactions on Power Electronics*, *30*(6), 3215–3227. https://doi.org/10.1109/TPEL.2014.2331365

Villamil, S., Hernández, C., & Tarazona, G. (2020). An overview of internet of things. *Telkomnika (Telecommunication Computing Electronics and Control)*. https://doi.org/10.12928/TELKOMNIKA.v18i5.15911

Wang, L., Chen, R., Ren, L., Xia, H., & Zhang, Y. (2019). Design and experimental study of a bistable magnetoelectric vibration energy harvester with nonlinear magnetic force scavenging structure. *International Journal of Applied Electromagnetics and Mechanics*. https://doi.org/10.3233/JAE-180074

Wang, Z., He, L., Zhang, Z., Zhou, Z., Zhou, J., & Cheng, G. (2021). Research on a Piezoelectric Energy Harvester with Rotating Magnetic Excitation. *Journal of Electronic Materials*. https://doi.org/10.1007/s11664-021-08910-y

Woias, P. (2015). 5.6 - Thermoelectric Energy Harvesting from small and variable Temperature Gradients. *Tagungsband*, 83–88. https://doi.org/10.5162/12dss2015/5.6

Yan, B., Yu, N., Zhang, L., Ma, H., Wu, C., Wang, K., & Zhou, S. (2020). Scavenging vibrational energy with a novel bistable electromagnetic energy harvester. *Smart Materials and Structures*. https://doi.org/10.1088/1361-665X/ab62e1

Zeadally, S., Shaikh, F. K., Talpur, A., & Sheng, Q. Z. (2020). Design architectures for energy harvesting in the Internet of Things. In *Renewable and Sustainable Energy Reviews*. https://doi.org/10.1016/j.rser.2020.109901

Zhang, D., Shi, J., Si, Y., & Li, T. (2019). Multi-grating triboelectric nanogenerator for harvesting low-frequency ocean wave energy. *Nano Energy*. https://doi.org/10.1016/j.nanoen.2019.04.046

Zhao, C., Yang, Y., Upadrashta, D., & Zhao, L. (2021). Design, modeling and experimental validation of a low-frequency cantilever triboelectric energy harvester. *Energy*. https://doi.org/10.1016/j.energy.2020.118885

Zhao, T., Xu, M., Xiao, X., Ma, Y., Li, Z., & Wang, Z. L. (2021). Recent progress in blue energy harvesting for powering distributed sensors in ocean. In *Nano Energy*. https://doi.org/10.1016/j.nanoen.2021.106199

Zhao, Z., Liu, J., Wang, Z., Liu, Z., Zhu, W., Xia, H., Yang, T., He, F., Wu, Y., Fu, X., Peng, L. M., Wei, X., & Hu, Y. (2017). Ultrasensitive triboelectric nanogenerator for weak ambient energy with rational unipolar stacking structure and low-loss power management. *Nano Energy*. https://doi.org/10.1016/j.nanoen.2017.09.010

MIJST
MIST International Journal of Science and Technology

Physical and Strength Properties of Cements Manufactured in Bangladesh: A Case Study

Khondaker S. Ahmed[1], Mohammad F. Asef[2*], and Mahfuj Ahmed[3]

Department of Civil Engineering, Military Institute of Science and Technology (MIST), Dhaka, Bangladesh

emails: [1]*drksa@mist.ac.bd;* [2]*m.farhan.asef@gmail.com; and* [3]*mahfuj.mist@gmail.com*

ARTICLE INFO

Article History:

Received: 05th November 2021
Revised: 03rd April 2022
Accepted: 06th April 2022
Published online: 26th June 2022

Keywords:

Cement
ASTM standard
Physical properties
Fineness
Cement mortar
Concrete strength

ABSTRACT

This study investigates the physical qualities and strength properties of representative cements manufactured by different brands in Bangladesh. The physical and strength properties such as normal consistency, initial and final setting time, density, specific gravity, fineness, and compressive strength of cement mortars as well as concrete cylinders were investigated experimentally. Using CEM II/B-M type cement, a total of 300 test specimens are prepared to determine those parameters. In this case study, specimens were prepared from ten different representative cement industries of Bangladesh and tested as per ASTM specifications. The experimental result shows that the physical and strength parameters of nearly all the representative cement samples are within the ASTM recommended ranges that ultimately proofs the quality of Bangladeshi Cement. The relationship between mortar and concrete strengths from the same batch of cement has also been investigated. Besides, a regression analysis has been conducted to find relationships between the concrete strength and their age of curing. The influence of initial and final setting times on concrete strength is also investigated. This study also provides the relationships between compressive strengths, between mortar and concrete cylinders at different ages. These age dependencies of concrete strength will help to predict the actual concrete strength at the early age of curing which may ensure faster construction work.

1. INTRODUCTION

The increased demand for cement in the construction industry gains interests of researchers, engineers, and practitioners to understand their quality and standards. Several industries produce cement not only to meet the local demand but also to export cement all over the world. It is said that cement-made concrete consumption in the world is second only to the consumption of water (Goldstein, 1995). Cement is a major ingredient of concrete structures and plays a key role in the construction industry (Ali, 2010; Amin & Ali, 2009). To address the sustainability concern of any concrete structure, the quality of the raw materials of construction has to be ensured. Hence, it becomes imperative to understand the physical and mechanical properties of cement for concrete construction in real-life projects.

Concrete strength and durability are very important factors in construction which depend on various parameters including the quality of cement (Mohammed et al., 2012). Due to a huge demand for cement in concrete structures, the enormous growth of the cement industry can be noticed in the last two decades. The application of cement and its growth depends on the rate of urbanization and the number of development projects undertaken in the country. The per capita cement consumption of Bangladesh is increasing rapidly in the last decade as shown in Figure 1(a). Keeping pace with the infrastructure development of Bangladesh, the consumption of per capita cement almost doubled from 95 kg in 2011 to 187 kg in 2018 during the seven years (EBL Securities Ltd., 2017). It is observed from the figure that the cement consumption was doubled in just 7 years of span time. They have already started to export cement in many places of the world. The growth of cement export is sharply increasing as presented in Figure 1(b).

The demand is growing geometrically due to the mega projects such Dhaka Mass Rapid Transit (DMRT), Padma Multipurpose Bridge, elevated expressways in several cities, nuclear power plants, and so on. The economical effectiveness in building infrastructures depends on the

quality of the cement used in the concrete. Though high-quality cements have a higher cost, it is proved to be economical in the long term (Rafi & Nasir, 2014). To ensure the sustainability of the structure, the ingredients of the construction must meet certain qualities established by standards (Soltani et al., 2019; Hani, 2011; ASTM, 2001). These standards allow us to conduct various tests, compare the cements obtained from different manufacturers with different sets of established parameters and review the quality of the binding material (Mangi et al., 2019b; Mangi et al., 2019a). Furthermore, numerical analysis can also be applied to correlate the results to predict the quality parameters of casted concrete such as ultimate strength, porosity, etc. (Hasan & Kabir, 2011; Iffat, 2015).

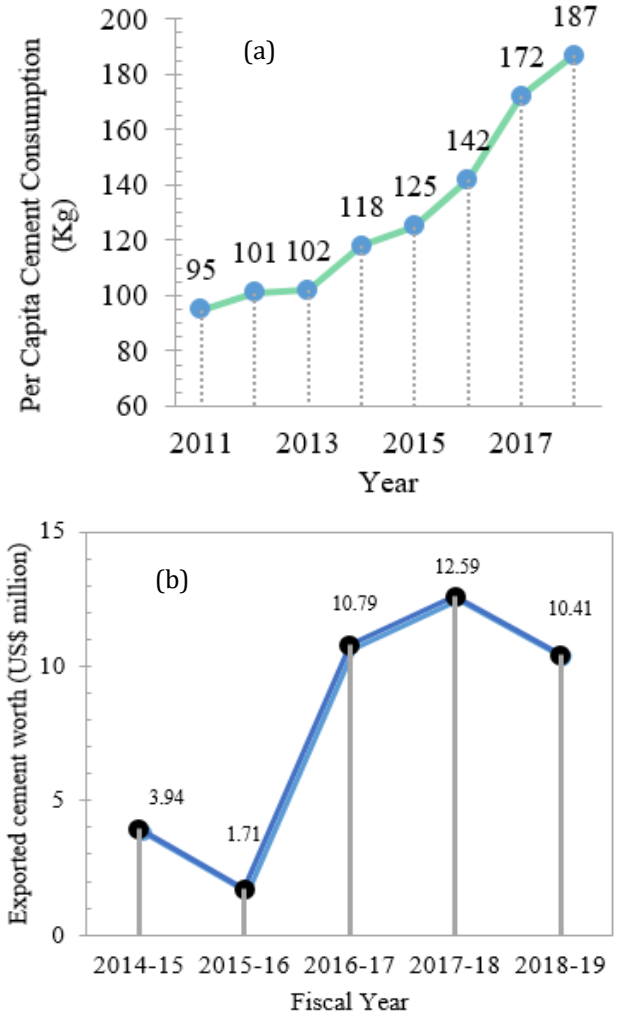

Figure 1: Overall growth of cement production in Bangladesh, (a) per capita cement consumption of Bangladesh over the past decade, (b) growth of cement export of Bangladesh (EBL Securities Ltd., 2017)

dAs most of the infrastructure development relies on locally produced cements for the construction of concrete structures, the in-depth investigation of the physical and mechanical properties of locally produces cements is of great concern. Most of these cement brands produce blended cements with a maximum of 35% admixtures mixed with clinker, which has become a global trend because of the availability of natural pozzolans and reduced environmental effects (Mohammed et al., 2011; Pourkhorshidi et al., 2010). Certain parameters such as setting time, fineness, specific gravity, and strength are largely influenced by the admixtures present in the cement (Barnett et al., 2007). Mohammed (2007) carried out research on investigation on factors related to sustainable development of concrete technology in Bangladesh. The objectives of their research work were the causes of deterioration of concrete structures, quality of cement brands, properties of concrete, recycling of demolished concrete as coarse aggregate for new construction, recycling of demolished concrete as fine aggregate for new construction.

There are 34 active different industries currently manufacturing cement in Bangladesh. However, the market is dominated by the ten to twelve leading brands because of their quality as well as cost-effectiveness. Mohammed et al. (2011), carried out research on the investigation of different cement brands commonly used in Bangladesh. They studied the common causes of deterioration of concrete structures in Bangladesh, common problems at construction sites that cause early deterioration of concrete structures in Bangladesh. However, the research was conducted more than a decade ago and important parameters like fineness and correlation between strength properties were not determined.

This case study aims to present the ASTM standard test results that can demonstrate the quality of the cements manufactured by ten of the leading industries dominating the capital market. The study also correlates different physical parameters and age dependencies to predict the concrete strength based on mentioned parameters.

2. EXPERIMENTAL INVESTIGATIONS

To determine the physical properties of cement such as normal consistency, initial and final setting time, density, specific gravity, and fineness of cement, standard tests were performed on test specimens prepared from the representative cements as per ASTM specifications. For strength properties like compressive strength of cement mortars and compressive strength (cylindrical), ASTM standards were followed in each step of the test preparation and test conduction. Based on the cement production, 10 different cement brands manufactured by 10 different industries were collected from the market to prepare 300 samples to conduct those tests. This section includes sample collection, major composition, test plan, test set-up, sample preparation, and experimental procedure.

A. Representative Sample Collection

According to Bangladesh Standard, BDS EN 197-1:2003, cements are mainly classified into five major categories according to their composition, namely CEM-I, CEM-II, CEM-III, CEM-IV, and CEM-V. CEM-II is Portland Composite Cement (PCC). CEM-II cement is sub-divided into different groups depending on the contents of mineral admixture and limestone powder, i.e., CEM II/A-M, CEM II/B-M, CEM II/A-S, CEM II/A-L. Quality assessment of CEM II/B-M type cement is justified in this analysis. Among the 34 active and recognized cement manufacturers in Bangladesh, samples of 10 major cement brands from CEM II/B-M category were collected from the market for

experimental specimen preparation. These cement industries are considered the main stakeholder of the current cement industries of Bangladesh based on the production capacities. During the collection of the samples, the manufacturing dates were observed very carefully so that the date of manufacturing for all cements were close to each other (±3 days). All cements investigated in this study were manufactured in the 13-16th June of 2019. Each cement bag was kept in an air-tight plastic bag to prevent unwanted hydration with the moisture which is normally prominent in local weather conditions.

B. Composition of Cements of Different Brands

According to Bangladesh Standard (BDS EN 197-1:2003), CEM-II is Portland Composite Cement. CEM-II is sub-divided into different groups depending on the contents of mineral admixture and limestone powder, i.e., CEM II/A-M, CEM II/B-M, CEM II/A-S, CEM II/A-L. Quality assessment of CEM II/B-M type cement is used as the sample in this case study. The composition of each representative cement sample (RCS) was recorded. The cement industries of Bangladesh that follow BDS EN 197-1:2003 and recommend that CEM II/B-M type cement contains clinker 65% - 79%, blast furnace slag, fly ash, and limestone 21% - 35%, and minor additional constituents 0% - 5%. The strength class of this cement is 42.5N. All cement bags leveled approximately the same ingredient as per BDS guideline. Since the variation of the ingredients contains a wide range, there is a chance to possess different physical properties even the different industries keep them in the range value. CEM II is widely used with any types of rebars including high strength rebars (Ahmed et al., 2021b), stainless steels (Ahmed et al., 2021a; Islam et al., 2020) and also applicable for retrofitting and strengthening of existing structures such as column jacketing (Mahmud & Ahmed, 2020).

C. Specimen preparation and test setup

A schematic view of sample preparation and test setup is presented in Figure 2. In this study, normal consistency (ASTM C187) (ASTM, 2016), initial and final setting time (ASTM C191) (ASTM, 2019), compressive strength of cement mortar (ASTM C109) (ASTM-C109, 2013), fineness of cement (ASTM C204) (Testing and Materials, 2007), density and specific gravity (ASTM C188) (Standard, 2009) and compressive strength (cylindrical) (ASTM C39) (ASTM, 2012b) were tested in the laboratory following all the designated standards. Locally obtained fine and coarse aggregates which conform to the ASTM standards were used for the preparation of cement mortar and concrete. The compressive strength of cement mortar was tested at the age of 3, 7, and 28 days and cylindrical concrete specimens were tested at 7,14, and 28 days. The number of the samples tested in this study are shown as matrix in Table 1.

Figure 2: Sample preparation and experimental setup for the tests

Table 1
Test matrix of the specimens

Designation (Representative Cement Samples)	Density & Specific Gravity	Fineness	Normal Consistency	Setting Time	Compressive strength (mortars)			Compressive strength (cylindrical)			Total Tested Sample
					3 days	7 days	28 days	7 days	14 days	28 days	
RCS-1	2	4	5	1	3	3	3	3	3	3	30
RCS-2	2	4	5	1	3	3	3	3	3	3	30
RCS-3	2	4	5	1	3	3	3	3	3	3	30
RCS-4	2	4	5	1	3	3	3	3	3	3	30
RCS-5	2	4	5	1	3	3	3	3	3	3	30
RCS-6	2	4	5	1	3	3	3	3	3	3	30
RCS-7	2	4	5	1	3	3	3	3	3	3	30
RCS-8	2	4	5	1	3	3	3	3	3	3	30
RCS-9	2	4	5	1	3	3	3	3	3	3	30
RCS-10	2	4	5	1	3	3	3	3	3	3	30
Total	20	40	50	10	30	30	30	30	30	30	300

3. RESULTS AND DISCUSSIONS

All specimens were tested following ASTM standards. All pieces of equipment used in this study were calibrated before conducting the tests. The test results of the physical properties of cement are presented as follows.

A. Density and Specific Gravity Test

The density and specific gravity of the representative cement samples (RCSs) are shown in Figures 3(a) and 3(b), respectively. The values are very close to each other varying within the range of 2.91g/cc to 3.15g/cc regarding density and 2.91 to 3.15 regarding specific gravity. Only one out of ten RCS namely RCS-3 has shown the value of specific gravity below 3. However, the range is fairly close to the commonly used value of 3.15 (ASTM C188), with the highest deviation being 7.61% in the case of RCS-3. Therefore, it can be concluded that the Bangladeshi manufacturers maintain the ASTM C 188 standard.

B. Fineness Test

The fineness test of cement samples was conducted by Blaine air permeability apparatus as per ASTM C204. Figure 4 shows the results of the fineness test which varies within the range 241-364m2/kg with a mean value of 303m2/kg. According to ASTM C150(ASTM, 2001), the standard Blaine fineness range is 260-430 m2/kg. Though 80% of RCSs concur with this standard, the fineness for RCS-1 and RCS-3 were below the lower limit of ASTM standard. However, the deviation from the lower limit of the standard is 3.8% and 7.3% respectively, which are very reasonable for this test's perspective.

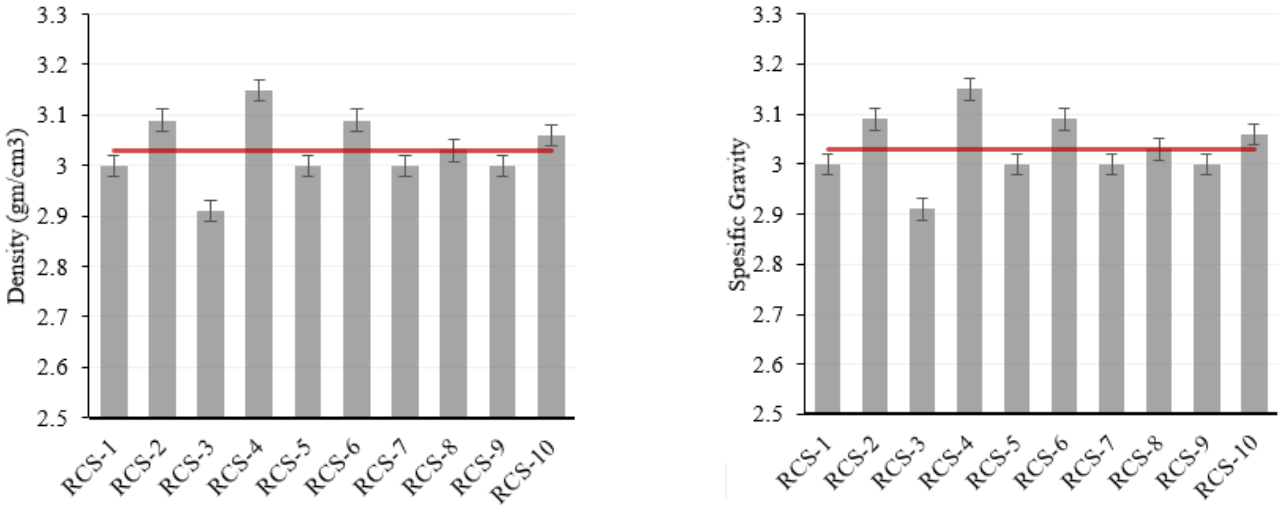

(a) (b)

Figure 3: (a) Density comparison of RCSs, (b) Specific gravity of RCSs

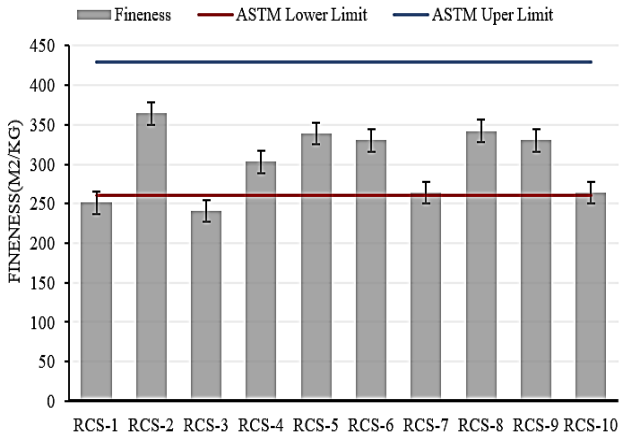

Figure 4: Fineness comparison of the RCSs

C. *Normal Consistency Test*

Figures 5a and 5b present the compiled data from the normal consistency test conducted as per ASTM C187. The relation between the percentage of water and penetration is shown in Figure 5a, whereas the normal consistency of the RCSs is shown in Figure 5b. It is observed from figure 5a that all the specimens follow a similar trend except for RCS-7. The value of normal consistency for Bangladeshi RCSs varies within 28-32% though the ASTM standard for normal consistency of cement is 22-30%.

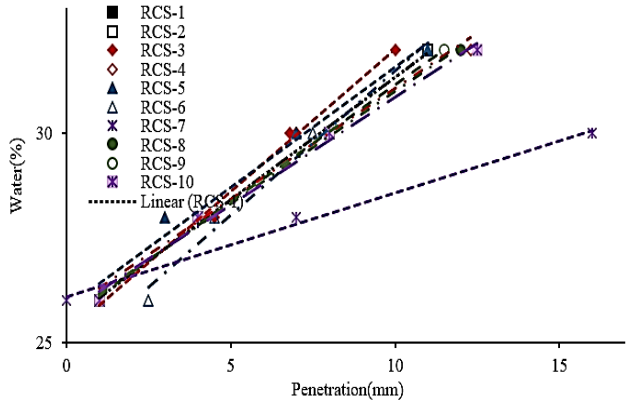

(a)

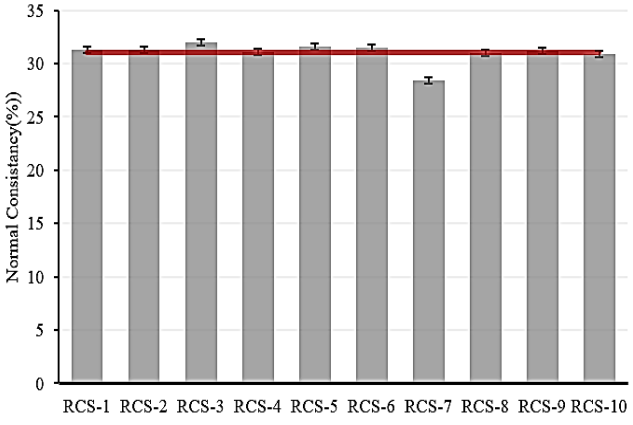

(b)

Figure 5: (a) Percentage of water vs penetration, (b) Normal Consistency of RCSs

D. *Setting Time Test*

Figure 6 shows the relationship between setting time and penetration for all RCSs. It is evident from the graph that all of the RCSs start to set within the range of 120-180 min and they reached their final setting points within 195-240mins. Figure 7 exhibits the initial and final setting times of the RCSs. As per ASTM C 150 standard, the standard requirement of initial setting time should not be less than 45 minutes and the final setting time should not be more than 375 minutes. As per ASTM Standard, all of the RCSs fall within the acceptable limit.

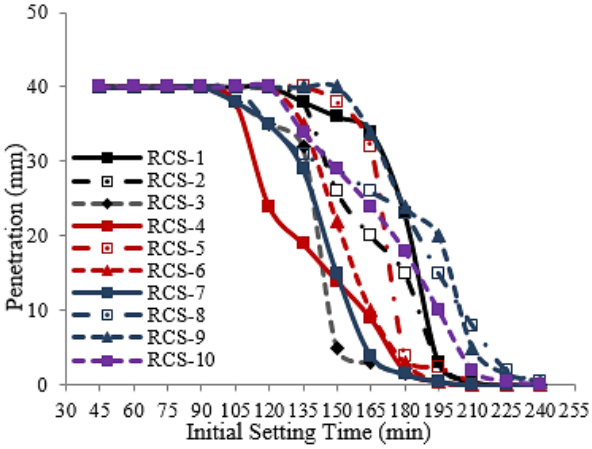

Figure 6: Penetration vs Initial setting time of RCSs

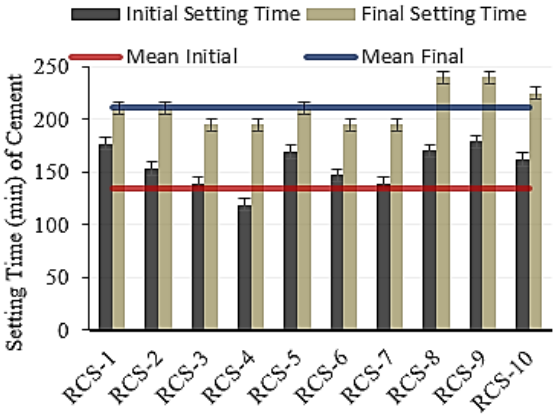

Figure 7: Initial and final setting times (min) of the RCSs

Interestingly, the RCS-7 that showed low consistency also shows relatively low setting time because consistency affects the setting time of the cement. The result also shows that the final setting time of RCS 8, 9 and 10 are comparatively higher. This can be described by the fact that those three cements hydrates slower than the others or may be due to the increased w/c ratio in the mixing process.

E. *Compressive Strength of Mortars*

A total of 90 samples were tested from 10 categories on 3 different dates (every 30 samples after 3,7 and 28 days). The test results are shown in Figure 8. According to ASTM C595-12, standard requirements of compressive strength are 13 MPa, 20 MPa and 25 MPa at 3 days, 7 days and 28

days, respectively. Among the ten RCSs, 9 meet the requirements of ASTM standard of 3 days, 6 meet the requirement of 7days and 8 specimens meet the requirement of 28 days compressive strength. The samples which do not concur with the ASTM range are also very close to the standard value. It is interesting to highlight that the compressive strength of RCS7 is lower than six other representative samples which matches well with its consistency. However, its higher than that of some cement specimens due to the low precisions in manufacturing.

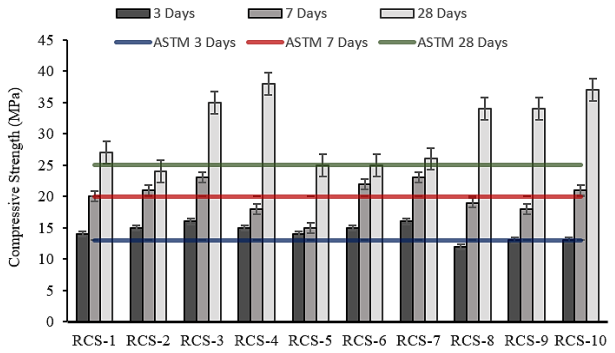

Figure 8: Compressive strength of cement mortars of RCSs at different ages

F. Regression Analysis for Compressive Strength of Mortar

Regression analysis was performed on the test results of the compressive strength test of the mortar samples to predict the strength of mortar from the data of 3days and 7days compressive strength of the mortar. For prediction of ultimate strength from 3days compressive strength, the regression equation is y = a + bx. From the regression relationship between 28-days compressive strength of cement mortar and 3-days compressive strength of cement mortar the coefficient of determination, R2 is 0.956 which is close to 1.0 that reflects a very good correlation. This implies that 95.6% of the variation in y is explained by x and 4.4% is not explained. In this case, y-intercept a= 0 and slope b= 2.102. Therefore, it can be concluded from the regression relationship between 28-days compressive strength of cement mortar and 3-days compressive strength of cement mortar that the following regression equation can be written. The regression relationship between the 28-days and 3-days compressive strength of cement mortar is shown in Figure 9 (a).

$$f'_{c\,(28d)} = 2.20 f'_{c\,(3d)} \quad (1)$$

From the regression relationship between 28-days compressive strength of cement mortar and 7-days compressive strength of cement mortar it can be understood that the coefficient of determination, R2 is 0.952. y-intercept were found to be a= 0 and slope b= 1.489. Therefore, from the regression relationship between 28-days compressive strength of cement mortar and 7-days compressive strength of cement mortar, the following regression equation can be written. The regression relationship between 28-days and 7-days compressive strength of cement mortar is shown in Figure 9(b)

$$f'_{c(28d)} = 1.49 f'_{c(7d)} \quad (2)$$

The combined regression relationship among 28-days compressive strength of cement mortar and 3 and 7-days compressive strength of cement mortar shows that adjusted R2 is 0.826. Adjusted R2 is used for multiple regression instead of R2. y-intercept a= 0 and slope or coefficient for 3-days b1= 1.489 and coefficient for 7-days b2= 0.437. Therefore, from the regression relationship between 28-days compressive strength of cement mortar and 3 & 7-days compressive strength of cement mortar, the following regression equation can be written. The regression relationship among 28-days and 3 & 7-days compressive strength of cement mortar is shown in Figure 10.

$$f'_{c(28d)} = 1.49 f'_{c(3d)} + 0.44 f'_{c(7d)} \quad (3)$$

Figure 11 represents the predicted 28-days compressive strength of cement mortar against 3-days, 7-days and a combination of 3 & 7-days compressive strength of cement mortar. From the regression relationship among f'c 28 days and f'c 3 days, f'c 28 days and f'c 7 days and fc 28 days and fc 3 & 7 days we can get the predicted 28-days compressive strength.

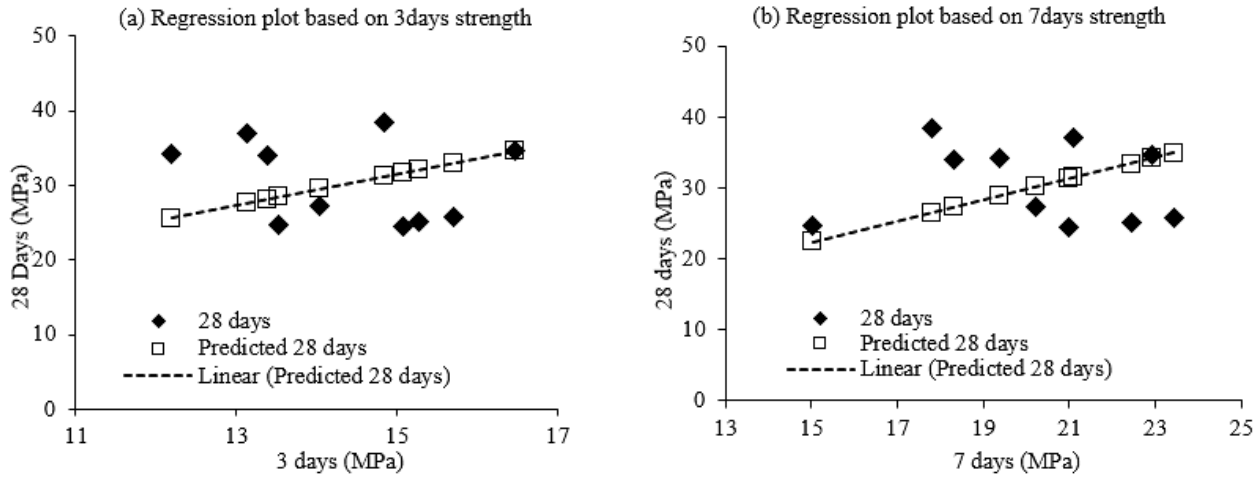

Figure 9: Regression analysis plots for the strength of cement mortar at different ages, (a) 3 days to 28 days relationship; (b) 7 days to 28 days relationship

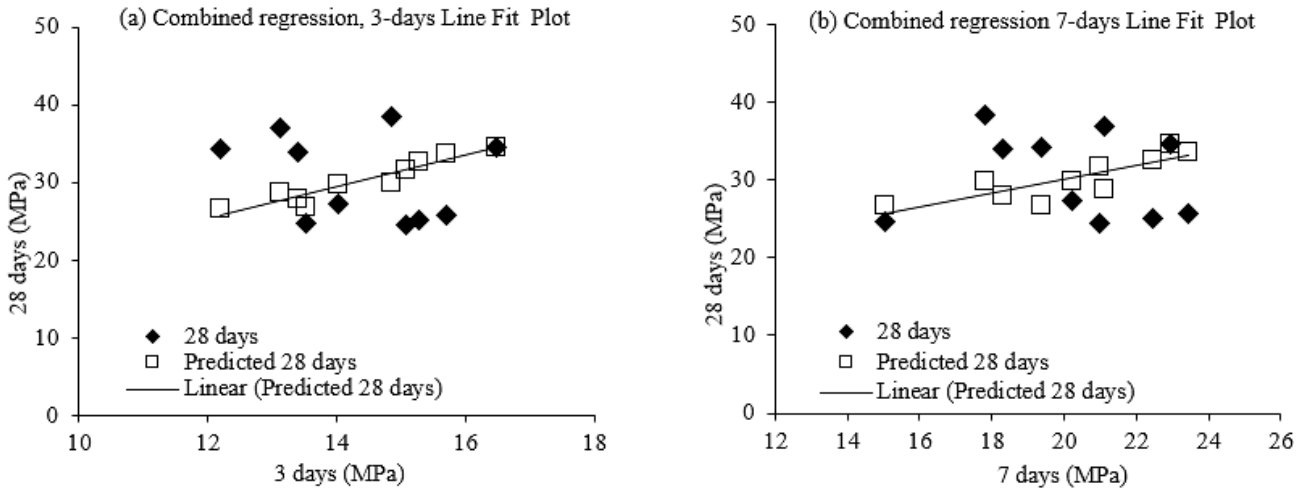

Figure 10: Concrete cylinder strength at 3 to 28 days and 7 to 28 days

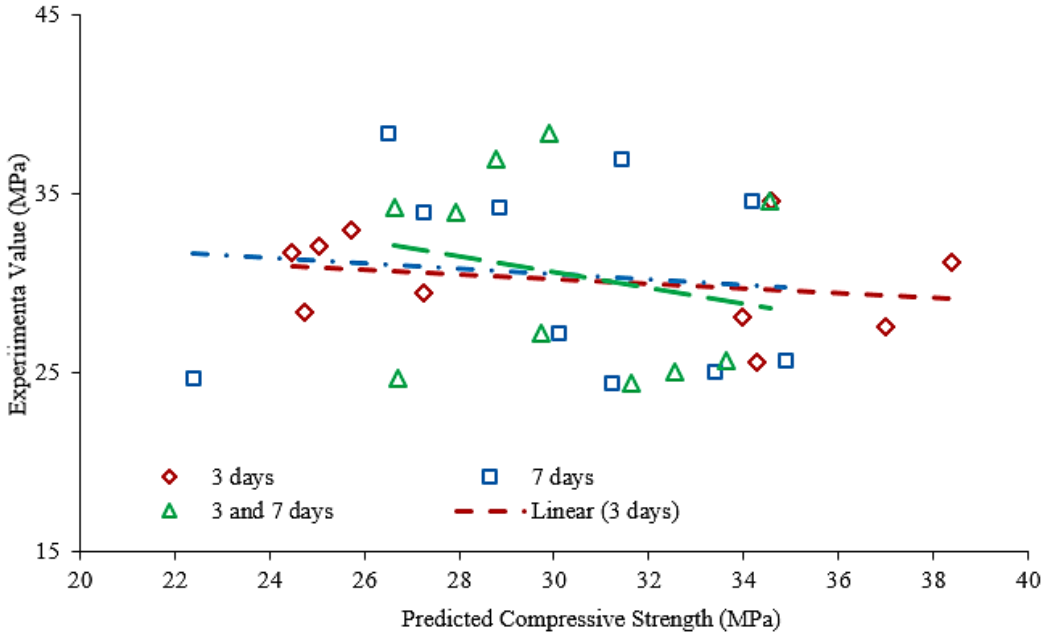

Figure 11: Experimental to predicted compressive strength of concrete at 3 days and 7 days

G. Variation of Compressive Strength of Mortar with Setting Time and Fineness

Figures 12(a) and 12(b) represent the relationship between compressive strength of mortar and initial and final setting time respectively. Though the increase in initial setting time resulted in decreased ultimate strength, the reversed trend was observed for final setting time where strength increased with the increase of final setting time. The relationship between the fineness of cement and the compressive strength of mortar is shown in Figure 13. Though all the strength values show a negative trend with the increase of fineness value of cement, the rate of decrease in strength was found to be increasing with the maturity of the mortar specimen.

H. Compressive Strength of Concrete

The variation of compressive strength of cylindrical concrete specimens is shown in Figure 14. Mix ratio for concrete was 1: 1.5: 3 and W/C ratio was 0.45. The target strength of the concrete mix was 24MPa. According to the ASTM standard, the minimum rates of strength gaining are 7 days 65%, 14 days 90%, and 28 days 99%. Compressive testing ages are 7 days, 14 days and 28 days and minimum strengths are required 15.6 MPa, 21.6 MPa and 23.76 MPa respectively. It was observed that 8 representative cement samples satisfy the 7-days requirement, only 3 representative cement samples satisfy the 14-days requirement and all representative cement samples satisfy the 28-days ASTM requirement of strength. Mean values are 17.07 MPa for 7-days, 20.8 MPa for 14-days and 36.5 MPa for 28-days. The average strength gaining rate 70.74% for 7-days, 86.26% for 14-days and 151.28% for 28-days.

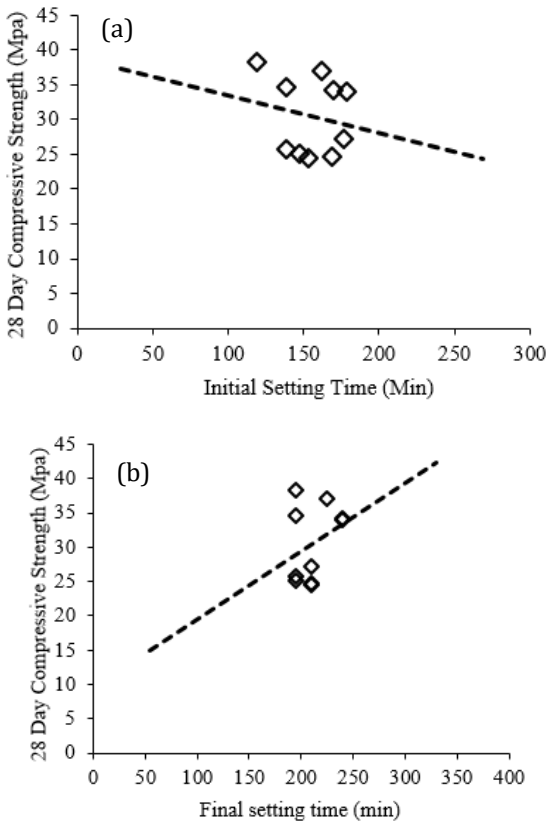

Figure 12: Variation of concrete strength with setting time

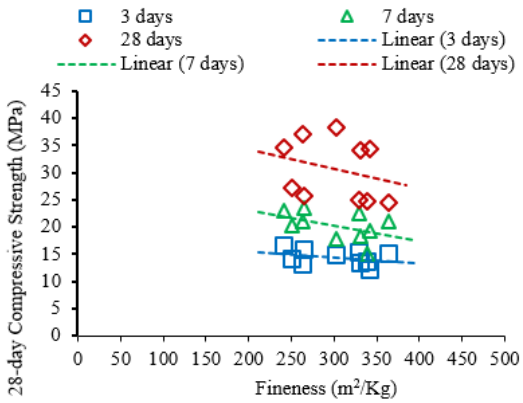

Figure 13: Relationship between the fineness of cement and compressive strength of mortar

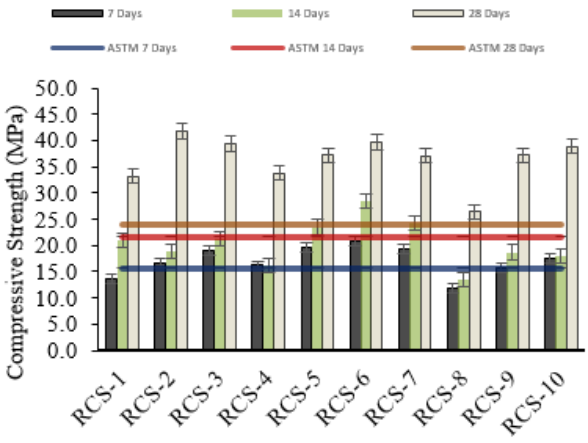

Figure 14: Compressive strength of concrete cylinder specimens at different age

I. Regression Analysis

A series of regression analysis was also performed on the test results the compressive strength test of the cylindrical specimens to predict the strength of concrete from the data of 7 days and 14 days compressive strength of the mortar. For prediction of ultimate strength from 7days compressive strength, the regression equation is $y = a + bx$. From the regression relationship between 28-days compressive strength of concrete cylinders and 7-days compressive strength of cement mortar it can be seen that the coefficient of determination, R2 is 0.989. This implies that 98.9% of the variation in y is explained by x and 1.1% is not explained. In this case, y-intercept a= 0 and slope b= 2.115. Therefore, from the regression relationship between 28-days mortar strength to that of 7-days, the regression equation can be written as presented in Eq. (4).

$$f'_{c\,(28d)} = 2.12 f'_{c\,(7d)} \quad (4)$$

The relationship obtained from the regression analysis shows that 7days strength is 47% of the 28days strength which is very much close to the ASTM recommended minimum values and also matches well with the results observed by (Hasan & Kabir, 2011).

The regression relationship between 28-days and 7-days compressive strength of cement mortar is shown in Figure 15(a). From the regression relationship between 28-days compressive strength of cement mortar and 14-days compressive strength of concrete it is evident that the coefficient of determination, R2 is 0.976. y-intercept were found to be a= 0 and slope b= 1.7138. Therefore, from the regression relationship between 28-days compressive strength of cement mortar and 14-days compressive strength of cement mortar, the regression equation can be written as presented in Eq. (5). The regression relationship between 28-days and 14-days compressive strength of cement mortar is shown in Figure 15(b)

$$f'_{c(28d)} = 1.71 f'_{c(14d)} \quad (5)$$

The relationship indicates that the strength gained in 14 days are roughly 60% of the strength gained in 28 days which is also suggested by the ASTM.

The combined regression relationship among 28-days compressive strength of concrete cylinders and 7 and 14-days compressive strength of concrete cylinders show that adjusted R2 is 0.864. Adjusted R2 is used for multiple regression instead of initial R2. y-intercept a = 0 and slope or coefficient for 7-days b1= 2.392 and coefficient for 14-days b2 = -0.227. So from the regression relationship between 28-days compressive strength of concrete cylinders and 7 & 14-days compressive strength of the specimens, the following regression equation can be written. The regression relationship among 28-days and 7 & 14-days mortar strength is shown in Figure 16.

$$f'_{c(28d)} = 2.39 f'_{c(7d)} - 0.23 f'_{c(14d)} \quad (6)$$

Figure 17 represents the predicted 28-days compressive strength of concrete against 7-days, 14-days and a combination of 7 & 14-days compressive strength of concrete. From the regression relationship among f'c 28 days and f'c 7-days, f'c 28 days and f'c 14 days and fc 28

days and fc 3 & 7 days we can get the predicted 28-days compressive strength of concrete.

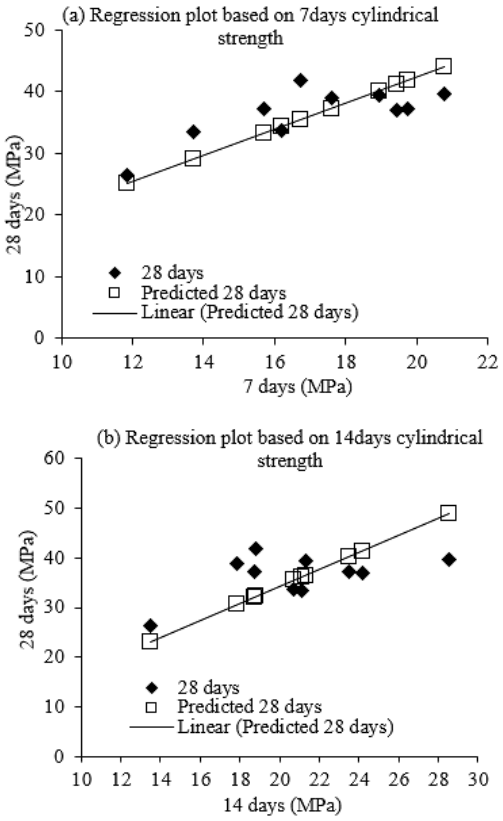

Figure 15: Regression analysis plots for concrete cylinder strength

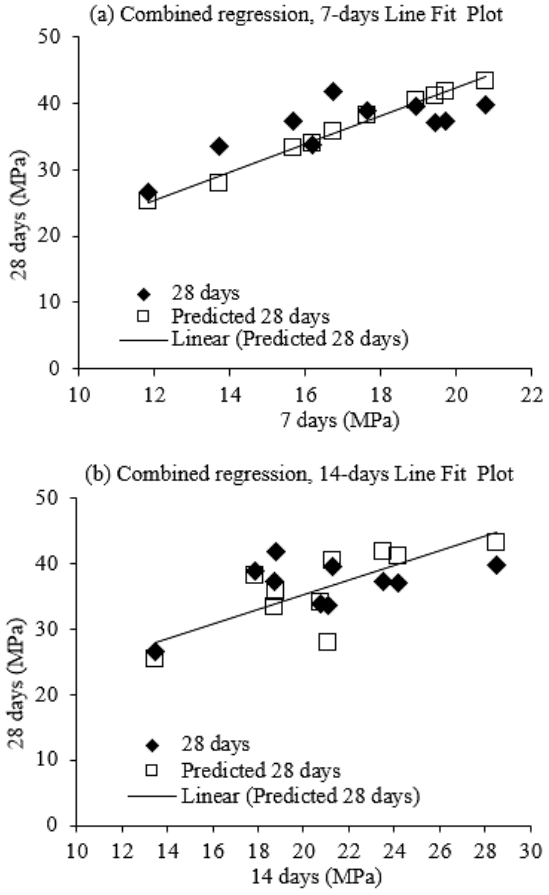

Figure 16: Combined regression analysis plots for cylindrical strength

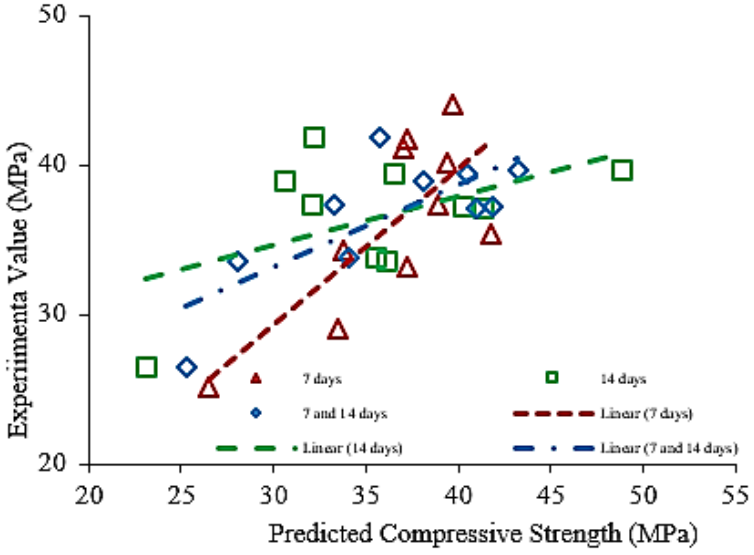

Figure 17: Experimental result to predicted compressive strength

4. CONCLUSIONS

In Bangladesh, the demand for cement is increasing day by day due to the ongoing extensive construction work and mega projects. Besides national demand, local industries are exporting cement to other countries. In a view to understanding the cement quality, this study investigates the physical and strength properties of concrete by performing a total of 300 tests on 10 different representative cement brands of Bangladesh. The key findings of this study are presented as follows.

The experimental results on density and specific gravity showed that the mean density of all tested samples is 3.023

whereas the ASTM range of specific gravity of such type cement varies in the range of 3.12-3.19. Since the mean value is very close to the ASTM range, it can be concluded that the specific gravity of Bangladeshi cements follows the guideline quite accurately.

The experimental result showed that the fineness of more than 80% of the tested cement samples is in the ASTM recommended range (2600-4300 m2/kg). The mean value of fineness of all the samples is 3028 m2/kg that satisfies the ASTM standard.

As per ASTM C187, the standard for normal consistency of cement is 22~30%. However, the Bangladeshi cements showed a bit higher consistency than the ASTM range. 90% of the representative cement samples showed quite similar behavior. All the samples showed consistency in the range of 28.0~32% rather (22-30%) with a mean value of normal consistency as 31 %.

All representative cement samples satisfy the ASTM C 595-12(ASTM, 2012a) requirements of the limit of initial setting time and final setting time. It is found that there is a tendency of achieving lower strength for the representative cement samples with a longer initial setting time and a higher level of strength for the cement with a longer final setting time.

The result showed that the compressive strength of cement increases with age as expected. According to ASTM C 595-12, the standard requirements of compressive strength of cement mortars are 13 MPa in 3 days, 20 MPa in 7 days, and 25 MPa in 28 days. It is found that 90% of representative cement samples satisfy the 3-days requirement, 60% of representative cement samples satisfy the 7-days requirement and 80% of representative cement samples satisfy the 28-days requirement. Mean values of compressive strength at different ages satisfy the ASTM requirements.

According to the ASTM standard of compressive strength of cylindrical concrete specimens, the minimum rates of strength gaining are 3 days 40%, 7 days 65%, 14 days 90%, and 28 days 99%. The test results indicated that they conform with the guideline with very few exceptions.

Based on regression analysis of the experimental results the following relations were derived to predict both the ultimate strength of the cement mortar and cylindrical strength. For mortar samples predicted 28-days strength from 3- and 7-days strength is formulated by,

$f'_{c(28d)} = 1.49f'_{c(3d)} + 0.44f'_{c(7d)}$, where R2=0.826

For cylindrical samples predicted 28-days strength from 3- and 7-days strength is formulated by,

$f'_{c(28d)} = 2.39f'_{c(7d)} - 0.23f'_{c(14d)}$, where R2=0.864

The values of the coefficient of determination reflect that the proposed equations are quite accurate to predict the concrete strengths at 28 days. Those correlations may be used to predict the 28 days concrete strength at the early age of concrete. Therefore, the construction industries may take the benefit in decision making and plan accordingly to ensure faster construction.

ACKNOWLEDGEMENTS

The authors gratefully acknowledge the support provided by the technical staff of the Concrete Laboratory of the Civil Engineering Department of Military Institute of Science and Technology (MIST) during the sample preparation, curing, and testing. The authors also acknowledge the partial financial support provided by MIST.

REFERENCES

Ahmed, K. S., Habib, M. A. & Asef, M. F. (2021a). Flexural response of stainless steel reinforced concrete beam. *Structures*, 34**,** 589-603.

Ahmed, K. S., Shahjalal, M., Siddique, T. A. & Keng, A. K. (2021b). Bond strength of post-installed high strength deformed rebar in concrete. *Case Studies in Construction Materials***,** e00581.

Ali, K. (2010). Chemical Analysis and Comparison of Ordinary Portland Cement of Khyber Pakhtoon Khwa Pakistan. *Chemical Engineering Research Bulletin*, 14**,** 45-49.

Amin, N. U. & Ali, K. (2009). Recycling of bagasse ash in cement manufacturing and its impact on clinker potential and environmental pollution. *Journal of the Chemical Society of Pakistan*, 31**,** 357-361.

ASTM-C109 (2013). C109/C109M-13 Standard Test Method for Compressive Strength of Hydraulic Cement Mortars (Using 2-in. or [50-mm] Cube Specimens).

ASTM (2001). ASTM C150: Standard specification for Portland cement. ASTM Philadelphia^ ePA PA.

ASTM (2012a). ASTM C595 / C595M-12, Standard Specification for Blended Hydraulic Cements, ASTM International, West Conshohocken, PA www.astm.org.

ASTM (2012b). Standard test method for compressive strength of cylindrical concrete specimens. *ASTM, C39M-12*.

ASTM (2016). ASTM C-187,Standard test method for normal consistency of hydraulic cement.: American Society of Testing Materials USA.

ASTM (2019). ASTM C191-19, Standard Test Methods for Time of Setting of Hydraulic Cement by Vicat Needle, ASTM International, West Conshohocken, PA, www.astm.org.

Barnett, S. J., Soutsos, M. N., Bungey, J. H. & Millard, S. G. (2007). Fast-track construction with slag cement concrete: adiabatic strength development and strength prediction. *ACI materials journal*, 104**,** 388.

EBL Securities Ltd. (2017). A Comprehensive Review on Bangladesh Cement Industry. Dhaka, Bangladesh.

Goldstein, H. (1995). Not your father's concrete. *Journal of Civil Engineering*, 65**,** 60.

Hani, F. F. B. (2011). Chemical analysis of ordinary portland cement of Jordan, Assiut Univ. *Bull. Environ. Res*, 14**,** 1-8.

Hasan, M. M. & Kabir, A. (2011). Prediction of compressive strength of concrete from early age test result. 4th Annual Paper Meet and 1st Civil Engineering Congress. 978-984.

Iffat, S. (2015). Relation between density and compressive strength of hardened concrete. *Concrete Research Letters*, 6**,** 182-189.

Islam, K., Billah, A. M., Chowdhury, M. M. I. & Ahmed, K. S. (2020). Exploratory study on bond behavior of plain and sand coated stainless steel rebars in concrete. *Structures*, 27**,** 2365-2378.

Mahmud, R. & Ahmed, K. S. (2020). Interface dependency of reinforced concrete jacketing for column strengthening. *Proceedings of the Institution of Civil Engineers–Structures Buildings*, 173**,** 31-41.

Mangi, S. A., Jamaluddin, N. B., Siddiqui, Z., Memon, S. A. & Ibrahim, M. H. B. W. (2019a). Utilization of sawdust in concrete masonry blocks: A review. *Mehran University*

Research Journal of Engineering & Applied Technology, 38**,** 487–494.

Mangi, S. A., Wan Ibrahim, M. H., Jamaluddin, N., Arshad, M. F. & Putra JAYA, R. (2019b). Short-term effects of sulphate and chloride on the concrete containing coal bottom ash as supplementary cementitious material. *Engineering Science and Technology, an International Journal*, 22**,** 515-522.

Mohammed, T., Hasnat, A., Sarwar, N., DAS, H., Miah, J. & Awal, M. (2011). Sustainable Development of Construction Works in Bangladesh. EACEF-International Conference of Civil Engineering. 057-057.

Mohammed, T. U., Hasan, P., Islam, B., Hasnat, A. & Sharkia, S. (2012). Investigation on Different Cement Brands Commonly Used in Bangladesh. Third International Conference on Construction In Developing Countries (ICCIDC–III)"Advancing and Integrating Construction Education, Research & Practice", Bangkok, Thailand.

Pourkhorshidi, A. R., Najimi, M., Parhizkar, T., Jafarpour, F. & Hillemeier, B. (2010). Applicability of the standard specifications of ASTM C618 for evaluation of natural pozzolans. *Cement and Concrete Composites*, 32**,** 794-800.

Rafi, M. & Nasir, M. (2014). Experimental Investigation of Chemical and Physical Properties of Cements Manufactured in Pakistan. *Journal of Testing and Evaluation*, 42**,** 774-786.

Soltani, A., Khoso, S., Keerio, M. A. & Formisano, A. (2019). Assessment of Physical and Mechanical Properties of Concrete Produced from Various Portland Cement Brands *Open Journal of Composite Materials*, Vol.09No.04**,** 11.

STANDARD, A. (2009). Annual Book of ASTM Standards. *C188: Standard Test Method for Density of Hydraulic Cement.*

TESTING, A. S. F. & MATERIALS. (2007) ASTM C 204: Standard Test Methods for Fineness of Hydraulic Cement by Air-Permeability Apparatus. 2007. ASTM Philadelphia.

CALL FOR PAPERS

MIJST invites to submit Unpublished, Original, and Innovative research works from any branch of Engineering, applied sciences, and related areas.

Submitted manuscripts will undergo a double-blind peer-review process. For submission of Manuscript template and authors' instructions, please visit journal website at: ***https://mijst.mist.ac.bd/mijst/index.php/mijst/***

MIJST offers a faster peer-review process. There will be no charges for Registration, Online submission, Publication of manuscripts, and access to the published articles. Best selected papers will also be awarded by MIJST.

ABOUT MIJST

MIST International Journal of Science and Technology (MIJST), published biannually (June and December), is a peer-reviewed open-access journal of the Military Institute of Science and Technology (MIST). This journal is a continuation of the 'MIST Journal of Science and Technology', published by MIST, under ISSN 1999-2009 from 2009 to 2011, ISSN 2224-2007 from 2012 to 2019, & E-ISSN 2707-7365 since 2020.

MIJST publishes original research findings as regular papers, review papers (by invitation). The Journal provides a platform for Engineers, Researchers, Academicians, and Practitioners who are highly motivated in contributing to the Engineering, Science, and Technology and Applied Sciences disciplines. MIJST welcomes contributions that address solutions to the specific challenges of the developing world.

The Journal is now indexed in the "DOI Crossref", "ISSN Portal", "BaglaJOL", "Creative Common", "Microsoft Academic Search", "Publons", "Semantic Scholar", "ScienceGate" and "Open Journal System" databases and is accessible through the Google Scholar. The journal is also planned to be registered under the Asian Citation Indexing, Directory of Open Access Journals (DOAJ), SCOPUS, and Emerging Source Citation Indexing (ESCI) in course of time. The Journal aims to be one of the leading journals of the Country and the Region for its contributions in the advancement of Science and Technology. Unpublished innovative world-class research papers under the following subject areas are invited. Contributions from other areas of Engineering and Applied Sciences are also welcome.

SUBJECT AREAS:

- **AEROSPACE AND AVIONICS ENGINEERING**
- **APPLIED PHYSICS & SCIENCE**
- **ARCHITECTURE**
- **BIOMEDICAL ENGINEERING**
- **CHEMISTRY**
- **CIVIL ENGINEERING**
- **COMPUTER SCIENCE AND ENGINEERING**
- **ELECTRICAL, ELECTRONIC AND COMMUNICATION ENGINEERING**
- **ENVIRONMENTAL, WATER RESOURCES, AND COASTAL ENGINEERING**
- **INDUSTRIAL AND PRODUCTION ENGINEERING**
- **MATERIALS SCIENCE & ENGINEERING**
- **MECHANICAL ENGINEERING**
- **NAVAL ARCHITECTURE AND MARINE ENGINEERING**
- **NUCLEAR SCIENCE & ENGINEERING**
- **PETROLEUM AND MINING ENGINEERING**

E-ISSN: 2707-7365

Journal URL